

THESIS

QUANTITATIVELY DISTINGUISHING BETWEEN BONE SURFACE MODIFICATIONS  
USING CONFOCAL MICROSCOPY AND SCALE-SENSITIVE FRACTAL ANALYSIS

Submitted by

Ross M. Campbell

Department of Anthropology and Geography

In partial fulfillment of the requirements

For the Degree of Master of Arts

Colorado State University

Fort Collins, Colorado

Spring 2023

Master's Committee:

Advisor: Michael C. Pante

Co-Advisor: Andrew Du

Diego Krapf

Copyright by Ross M. Campbell 2023

All Rights Reserved

## ABSTRACT

### QUANTITATIVELY DISTINGUISHING BETWEEN BONE SURFACE MODIFICATIONS USING CONFOCAL MICROSCOPY AND SCALE-SENSITIVE FRACTAL ANALYSIS

The damage found on fossilized bone surfaces resulting from the feeding behavior of various prehistoric taphonomic actors (hominins, carnivores, raptors, etc.) in archaeological assemblages is a crucial piece of evidence that provides an inferential framework within which archaeologists can reconstruct the ecological and behavioral contexts of our hominins ancestors. However, these reconstructions are only useful if the bone surface modifications (BSM) can be inferentially linked to the specific taphonomic actor which created the mark. The inability to do so in a standardized and replicable manner has sparked multidecade-long debates over the actors responsible for individual marks and has resulted in drastically different interpretations of site formation processes and hominin behavioral ecology.

Therefore, the goal of this study is to determine whether variations in within-mark fractal variables, paired with the micromorphological variables presented in Pante et al. (2017), can aid in quantitatively distinguishing between four different taphonomic agents (cut, trample, tooth, and percussion marks). To achieve this goal, a sample of 100 experimentally - produced BSM were sampled from the existing collection in the 3D imaging and analysis laboratory at Colorado State University. Scans of individual marks were acquired using Sensofar's S-neox 3D scanner, while 3D models of the marks were analyzed with the Digital Surf® software. Quadratic discriminant and complimentary random forest models were created to identify relationships between the measured fractal variables and the taphonomic agents creating BSM.

The results of the quadratic discriminant and random forest models classifying all 4 BSM agents result in low classification accuracies between 52% - 58%, thereby indicating the micromorphological and fractal variables could not be used to accurately identify taphonomic agents by their within-mark surface complexity/roughness measurements. However, sub - grouping the dataset into models discriminating between only pairs of BSM types (i.e., cutmark vs trample mark) increases the classification accuracy of the QDA and random forest models to the 60% - 86% range, thereby indicating the micromorphological variables presented in Pante et al. (2017), when paired with the fractal variables Smooth – Rough Crossover (SRC), Area Scale Fractal Complexity (Asfc) and the Scale of Max Fractal Complexity (Smfc), can discriminate between the known taphonomic agents in the sample with relative accuracy. This study is beneficial to the study of archaeological BSM as it aids in our understanding of hominin subsistence behavior in prehistoric contexts by continuing the development of an objective and standardized method of differentiating feeding traces which provides a platform for more scientific, i.e. *testable* inferences about hominin behavior in archeological sites.

## ACKNOWLEDGEMENTS

I would like to sincerely thank my advisor, Dr. Michael Pante, for his guidance and patience throughout this project, for offering opportunities to learn and grow as a writer, researcher, and person. I would like to thank my committee members Dr. Andrew Du and Dr. Diego Krapf for their assistance and encouragement throughout the many stages of this project. In particular, I would like to thank Dr. Andrew Du for his honest and much appreciated advise for improving my writing and statistical analysis skills. Thank you, Dr. Diego Krapf, for advising me on fractals and for your tireless work on editing this study. I am of course very grateful to Colorado State University for partially funding my master's degree studies.

This thesis would not have been possible without the undying support of my family and friends. My father Andy and mother Alison have always shown love, support, and encouragement for all that I do. I would especially like to thank my mom Alison, who is not alive to see the completion of this project, but who I know is very pleased to see it finally completed. I will endlessly thank my partner Morgan Myers, who has always been there when I needed emotional or editing support, without her love and kindness, this project would have not been completed. My good friends Morgan Lundy, Alex Pelissaro and Wyatt Benson offered the friendship, academic advice and camaraderie necessary to maintain mental sanity and complete this study. Thank you, Katya, for editing many of my papers over the course of my class work. Lastly, I thank my lifelong friend Robert Vose for offering me an oasis of comfort during a time of immense familial and academic stress. Ultimately, my success in completing this thesis is the product of the love and support of all these people.

DEDICATION

*For Alison*

## TABLE OF CONTENTS

|                                                                         |    |
|-------------------------------------------------------------------------|----|
| ABSTRACT.....                                                           | ii |
| ACKNOWLEDGEMENTS.....                                                   | iv |
| DEDICATION.....                                                         | v  |
| LIST OF TABLES.....                                                     | ix |
| LIST OF FIGURES .....                                                   | xi |
| CHAPTER 1 INTRODUCTION.....                                             | 1  |
| 1.1 Research Problem .....                                              | 1  |
| 1.2 Goals and Objectives of Study .....                                 | 5  |
| 1.3 Research Question .....                                             | 6  |
| 1.4 Research Hypothesis .....                                           | 7  |
| CHAPTER 2 THEORETICAL BACKGROUND AND LITERATURE REVIEW .....            | 8  |
| 2.1 Theoretical Background .....                                        | 8  |
| 2.2 History of BSM Studies .....                                        | 11 |
| 2.3 History of Approaches for BSM Identification.....                   | 15 |
| 2.3.1 Scanning Electronic Microscope .....                              | 16 |
| 2.3.2 Digital Micro-photogrammetry .....                                | 17 |
| 2.3.3 3D Optical Profilometry .....                                     | 18 |
| 2.4 A History of Fractals and Archaeology .....                         | 21 |
| 2.5 Scale – Sensitive Fractal Analysis .....                            | 23 |
| 2.5.1 SSFA of Use-Wear on Stone Tools.....                              | 25 |
| 2.5.2 SSFA and Tooth – Microwear Studies .....                          | 27 |
| CHAPTER 3 METHODS AND MATERIALS .....                                   | 31 |
| 3.1 Experimental Sample .....                                           | 31 |
| 3.2 Surface Molding .....                                               | 33 |
| 3.3 3D Optical Metrology .....                                          | 33 |
| 3.4 Processing of 3D BSM Scans .....                                    | 34 |
| 3.5 Measurements of 3D BSM Models .....                                 | 36 |
| 3.6 Statistical Analysis .....                                          | 39 |
| 3.6.1 Data Exploration .....                                            | 39 |
| 3.6.2 Multivariate Analysis- Quadratic Discriminate Analysis .....      | 42 |
| 3.6.3 Analysis Using Machine Learning: Random Forest .....              | 43 |
| CHAPTER 4 RESULTS .....                                                 | 45 |
| 4.1 Data Normalization: Histograms .....                                | 45 |
| 4.2 Correlation Matrix .....                                            | 45 |
| 4.3 Variable Selection: Predictor Screening Test .....                  | 47 |
| 4.4 Multivariate Analyses Results .....                                 | 48 |
| 4.5 Random Forest Analysis Results .....                                | 52 |
| CHAPTER 5 DISCUSSION .....                                              | 58 |
| 5.1 Interpretation of Results: Multivariate Discriminant Analysis ..... | 58 |
| 5.2 Random Forest Analysis .....                                        | 63 |
| 5.3 Limitations of Study .....                                          | 65 |
| 5.4 Future Research Prospects .....                                     | 68 |

|                                                                  |    |
|------------------------------------------------------------------|----|
| CHAPTER 6 CONCLUSION .....                                       | 70 |
| REFERENCES .....                                                 | 73 |
| Appendix A- TABLE OF EXPERIMENTAL BSM SAMPLE .....               | 84 |
| Appendix B - HISTOGRAM DISTRIBUTIONS OF UNIVARIATE BSM DATA..... | 87 |

## LIST OF TABLES

|                                                                                                                           |    |
|---------------------------------------------------------------------------------------------------------------------------|----|
| Table 1: Height, Spatial and Functional Parameters .....                                                                  | 36 |
| Table 2: Scale-Sensitive Fractal Analysis Parameters .....                                                                | 37 |
| Table 3: Volume of a Hole Parameters .....                                                                                | 39 |
| Table 4: Table displaying the strength of the correlation between each variable in relation to Das and SRC Threshold..... | 46 |
| Table 5: Classification accuracy of all QDA models.....                                                                   | 49 |
| Table 6: Confusion matrix for quadratic discriminant analysis between all 4 BSM types .....                               | 52 |
| Table 7: Confusion matrix for quadratic discriminant analysis between cut and trample marks..                             | 52 |
| Table 8: Confusion matrix for quadratic discriminant analysis between cut and toothmarks.....                             | 52 |
| Table 9: Confusion matrix for quadratic discriminant analysis between cut and percussion marks.<br>.....                  | 52 |
| Table 10: Confusion matrix for quadratic discriminant analysis between trample and toothmarks<br>.....                    | 52 |
| Table 11: Confusion matrix for quadratic discriminant analysis between trample and percussion<br>marks .....              | 52 |
| Table 12: Confusion matrix for quadratic discriminant analysis between tooth and percussion<br>marks .....                | 52 |
| Table 13: Table showing the out-of-bag (OOB) error estimate for each random forest model.<br>.....                        | 53 |
| Table 14: : Confusion matrix for random forest analysis between all 4 BSM types .....                                     | 57 |
| Table 15: Confusion matrix for random analysis between cut and trample marks.....                                         | 57 |
| Table 16: Confusion matrix for random forest analysis between cut and toothmarks .....                                    | 57 |
| Table 17: Confusion matrix for random forest analysis between cut and percussion marks.....                               | 57 |
| Table 18: Confusion matrix for random analysis between trample and toothmarks .....                                       | 57 |
| Table 19: Confusion matrix for random forest analysis between trample and percussion marks<br>.....                       | 57 |
| Table 20: Confusion matrix for random forest analysis between tooth and percussion marks .....                            | 57 |

## LIST OF FIGURES

|                                                                                                                                                                                                                                                                                                                                                            |    |
|------------------------------------------------------------------------------------------------------------------------------------------------------------------------------------------------------------------------------------------------------------------------------------------------------------------------------------------------------------|----|
| Figure 1 – Example of BSM circled on bone surface before scanning .....                                                                                                                                                                                                                                                                                    | 32 |
| Figure 2: Top Left image shows a 3D cut mark model after initially importing it into the Digital Surf® software. The top right image shows the same 3D model after “remove form”. Bottom left image shows the mark after being rotated to a vertical position. The bottom right image shows the final product of the 3D process, an extracted cutmark..... | 35 |
| Figure 3: Scatter Plots displaying the non-linear relationships and outliers between variables.....                                                                                                                                                                                                                                                        | 41 |
| Figure 4: Correlation Matrix of all 28 measured variables .....                                                                                                                                                                                                                                                                                            | 46 |
| Figure 5: Predictor Screening Table for “BSM Type”. The table visualizes the proportion of the variation in the response attributed to each variable.....                                                                                                                                                                                                  | 48 |
| Figure 6: QDA Canonical plot showing classification of all 4 BSM types .....                                                                                                                                                                                                                                                                               | 50 |
| Figure 7: Plot indicating the percentage of error in classification for all four different BSM types and out-of-bag sample average over the course of the 500 decision trees in the random forest model.....                                                                                                                                               | 54 |

## CHAPTER I INTRODUCTION

### 1.1) Research Problem

Due to cutmarks conspicuous preservation on fossilized bone surfaces, archaeologists have studied and used them to infer a wide variety of characteristics and behaviors of our Pleistocene ancestors. For instance, the placement, orientation and internal morphology of cutmarks on fossilized bone surfaces has been used to infer the relative timing of hominin and carnivore access to carcasses (Binford 1981, Blumenschine et al. 1988b, Blumenschine 1995; Lupo and O'Connell 2002, Domínguez-Rodrigo and Barba 2007); what kinds of nutrients (within or outside bone) remained at the time of carcass access (Pobiner et al. 2015; 2018), tool-use strategies (Merritt, 2016), and in the interpretation of burial practices (Fernandez-Jalvo and Andrews, 2011). Therefore, due to cutmarks being a direct result of past behavior by hominins, they are foundational components of taphonomic inferential hierarchies used by archaeologists to understand hominin behavioral ecology (Blumenschine et al. 1988, Gifford Gonzalez 1991, Blumenschine et al. 1994; 1996, Pante et al. 2012; 2014, Merrit et al. 2019).

However, similarities in appearance between hominin - induced cutmarks and the bone surface modifications (BSM) left by other taphonomic forces on fossilized bone surfaces has sparked a multidecade-long debate over the actors (carnivore or hominin) responsible for individual marks (Binford, 1981; Bunn, 1981, Bunn and Kroll 1986, Njau and Blumenschine 2006, James and Thompson 2014, Harris et al 2017). Disagreement over the actors responsible for fossilized BSM has led to drastically different interpretations of site formation and hominin behavioral ecology (Gifford-Gonzalez 1991, James and Thompson 2014). A popular example of this disagreement can be found at Olduvai Gorge, Tanzania. Where, after half a century of

research there is still no general agreement regarding the involvement of different taphonomic actors in the accumulation and modification of the fossil assemblage at FLK *Zinjanthropus* (Binford 1981, Behrensmeier et al. 1989, Blumenschine 1995, Domínguez-Rodrigo and Barba 2007, Pante et al. 2012; 2014).

These disagreements greatly decrease the inferential potential of BSM by throwing serious doubt on our ability to accurately identify the actor responsible for generating the force required to produce the BSM, as well as the effector (tooth, stone tool edge, hoof etc.) which directly contacts and modifies the surface of the bone. Likewise, Blumenschine et al. (1996) noted, if zooarchaeologists cannot come to agreement on the process of identifying BSM, then doubt is shed on any results that draw from this method. Indeed, the inability to have confident actor/effector identification raises the possibility of an incorrect BSM identification going unnoticed in archaeological studies. If such inconsistencies become entrenched within the literature, then what we believe we know about hominin evolution may rest upon instances of poor, yet unchallenged interpretations (James and Thompson 2014). Therefore, misdiagnosis of the cause of fossilized BSM has major implications for the interpretation of the ecological context of hominin behavior (Domínguez-Rodrigo et al. 2012, Pante et al. 2011; 2014, Pobiner et al. 2015; 2018, Pobiner 2020). Consequently, it is imperative to develop new quantitative and objective strategies for distinguishing between the actors and effectors that produce BSM (Bello and Soligo 2008, Bello et al. 2009; Bello 2011, Pante et al. 2017, Benito-Calvo 2017).

Until a few decades ago, methods of identification were largely subjective, relying on categorical diagnosis based on the knowledge of individual experts working with fossil and experimental collections (Blumenschine et al., 1996). However, it has become increasingly clear that such subjective approaches are problematic in cases where mark morphologies have

ambiguous characteristics. This issue regarding researcher subjectivity has been addressed through the use of confocal microscopy (Archer and Braun, 2013; Pante et al., 2017; Otárola-Castillo et al. 2017; Gümrukçu and Pante, 2018) and statistical approaches capable of differentiating between BSM actors based on standardized ‘archetype’ marks by using 3D scanning equipment, and the statistical evaluation of overlap between mark types using 3D morphometrics (Bello et al 2008; 2009; 2011, Boschini and Crezzini 2012, Pante et al. 2017, Yravedra et al 2018, Francisco et al. 2018, Meijer et al. 2019). 3D reconstructions of BSM use quantification of the internal mark morphology produced by *known* actors and effectors to identify diagnostic criteria to be applied to the taphonomic interpretation of bone assemblages. These approaches provide replicable, quantitative comparison of the shape of individual BSM by way of comparison with the archetypes (statistical average) of marks made by different processes. This creates a key for identifying BSM by its effector which is less influenced by the bias of individual analysts and enables researchers to assign probabilities to the “the goodness of fit” between a given mark and its inferred cause.

Indeed, many 3D micromorphometric methods have found success distinguishing between cases where the potential for mimicry is high, i.e., where human and non-human processes create similar mark morphology on bone surfaces (Bello 2008; 2011, Pante 2017, Courtenay et al. 2017; 2019; 2020, Keevil 2018, Yravedra et al., 2018, Meijer et al. 2018, Francisco et al 2018). Additionally, researchers have used 3D morphometric methods to identify the raw material and type of stone tools used in butchering activities (Mwakyoma 2021). With this success in discrimination between BSM actors, researchers continue to search for measurable parameters which can increase the accuracy of inferential links between the physical properties of effectors and the micromorphology of the resultant marks (James and Thompson

2014, Thompson et al. 2017, Harris et al. 2017). Toward this end, we investigate fractal parameters, as described by Brown et al. 2018, as a new method for characterizing and distinguishing BSM through the measurement of within-mark surface complexity and roughness.

Fractals were developed by mathematician Benoit Mandelbrot as a new branch of mathematics able to describe complex forms in nature. He states fractals are a group of irregular, complex shapes which occur naturally, but which possess the characteristics of self-similarity and scale invariance (Mandelbrot 1977, 1982). Self-similarity here is defined as a shapes ability to be broken down into smaller pieces of itself (therefore decreasing in size and scale) and still retain its shape. Fractal shapes are scale-invariant because, unlike Euclidean shapes, fractals have no natural size. Therefore, Fractals are mathematically and visually the same at all scales. Due to fractals scale-invariant and self-similar properties, there is a statistical equivalence between small-scale and large-scale changes in fractal patterns. Likewise, Benoit noted the description of fractal shapes and patterns allows for the measurement of complex surfaces at multiple scales (where statistical measures are preserved across scales). Indeed, the fractal dimension has been found to be a useful parameter to describe physical surfaces, and furthermore, that eroding processes in nature generate surfaces with fractal properties (Unger et al. 2003, Scott et al. 2005, Brown 2005, Brown et al. 2018).

This ability to mathematically describe and document irregular shapes at multiple scales can be of great value to archaeologists studying the surfaces of archaeological materials.

Archaeologists have applied the concept of fractals and the use of fractal dimension measurements to understand complex, non-linear relationships in the past. For example, Scale-Sensitive Fractal Analysis (SSFA) has been used to successfully document different kinds of

worn surfaces on stone and bone tools (Stemp et al 2008, Stemp et al. 2009, Stemp et al. 2010, Stemp et al. 2014, Evans and Donahue 2008, Lesnik 2011, Watson and Gleason 2016), as well as document dietary habits from teeth microwear (Ungar et al. 2003; Scott et al 2005, Krueger 2015, Ranjitkar et al. 2017, Unger and Berger 2018). The results of these studies make clear SSFA provides measurement of topological phenomena like surface complexity, i.e. an object's surface irregularity which changes with the size of the scale being measured. Importantly, surface complexity is considered a scale that is useful for differentiating surface types (Brown 2005, Brown et al. 2018). Therefore, due to the characteristics of fractals, they are appropriate to mathematically describe and document the complexity of BSM - damaged bone surfaces because bone microtopography necessitates quantitative descriptors well-suited to irregular surfaces. Fractal geometry is employed in this study as a means to accurately capture and distinguish the complex surfaces of experimentally generated BSM.

## **1.2) Goals and Objectives of Study**

The goal of this thesis is to use high-resolution 3D scanning and SSFA to aid in identification and classification of various taphonomic agents by discriminating with measurable statistical confidence between the 3D morphologies and surface complexity measurements of experimentally generated BSMs. Specifically, we use subtle differences in surface complexity between cut, trample, tooth and percussion marks to establish stronger causal links between the micromorphological characteristics of BSMs and hominin butchery behaviors in the past. Understanding how and when early *homo* used stone tools for meat procurement has been argued to be significant in understanding the early evolution of our genus. Indeed, inferred dietary shifts in fossil hominins have been hailed by paleoanthropologists as key milestones in human evolution. For instance, the consumption of meat and marrow from mammal carcasses is

argued to have possibly enabled the emergence of adaptations associated with our genus. These include: an increase in average brain and body size, heightened social group cohesion and organization, wider geographical range, and smaller teeth and jaws (Aiello and Wells 2002, Milton 1999; 2003, Antón and Snodgrass 2012, Wrangham 2017). Therefore, to make more accurate inferences when investigating hominin subsistence behavior, this study has the following objectives.

The objective of this study is to apply discriminate modeling and SSFA to an experimentally generated BSM sample in order to better classify BSM agents and more accurately differentiate between them. This is accomplished by applying quadratic discriminate analysis (QDA) on the experimental BSM sample. Here, QDA uses variation in the surface roughness and complexity of the mark to discriminate (classify) between four different taphonomic agents (cutmark, trample, toothmark, percussion) in the dataset. The surface texture variables considered are: smooth-rough crossover (src), area-scale fractal complexity (Asfc), and scale of max complexity (smfc). The variable for fractal complexity (Asfc) is probably most informative in this study because it measures how the surface roughness changes with the changing scale of observation and is a variable unique to SSFA. It is hoped this provides a method for surface characterization appropriate for assessing BSM effector-related differences in mark surface roughness (surface complexity). Since the sample is of known actors and agents, results from this study will help in diagnosing hominin and non-hominin activity with future application to archaeological contexts.

### **1.3) Research Question**

To achieve the objective, this study seeks to answer the following question: Which, if any of the fractal parameters diagnosed from 3D optical metrology can be used to classify

experimentally - produced BSM by taphonomic effector (cut, trample, tooth and percussion marks)? This question can be investigated by looking at quantitative properties of the BSM in this study and by removing highly correlated variables until only the uncorrelated, fractal variables describing surface roughness and complexity remain for analysis. Next, the use of QDA provides information regarding the ability of the fractal variables to describe and differentiate between the four BSM groupings.

#### **1.4) Research Hypothesis**

Based on the posed research questions, the study therefore hypothesizes (H1), that fractal measurements of mark surface roughness diagnosed from 3D optical profilometry are reflective of the taphonomic agents creating BSM and therefore, SSFA can be used to discriminate between BSM types. This means that for (H1) to be validated, this study must refute alternate hypothesis (Ho) that the fractal measurements diagnosed from 3D optical profilometer are not reflective of the known BSM agents and therefore are not useful in BSM agent discrimination.

## **CHAPTER 2 THEORETICAL BACKGROUND & LITERATURE REVIEW**

This study aims to enhance our understanding of prehistoric hominin butchery by studying the relationship between the taphonomic actors (carnivore, hominin, herding mammals) creating bone surface modification (BSM) and the fractal dimensions of the marks they inflict upon bone surfaces. The acronym BSM is used here to refer to the damage found on bone surfaces that are inflicted by either anthropogenic or nonanthropogenic actors. This thesis uses uniformitarianism and middle-range theoretical approaches to accomplish its stated goals (both terms are defined below).

This chapter provides an overview of the theoretical assumptions underlying the study, a history of methods used for BSM identification and interpretation, and the applications of using Scale-Sensitive Fractal Analysis (SSFA) combined with Laser Scanning Confocal Microscopy (LSCM) to identify and classify worn surfaces from archaeological contexts.

### **2.1) THEORETICAL BACKGROUND**

This thesis is grounded in the theoretical principles of uniformitarianism. As defined by Charles Lyell (1830), uniformitarianism assumes that the physical laws governing natural processes (erosion, gravity, etc.) remain the same regardless of temporal or spatial context. The permanence of physical processes implies that the past and present causes of events are similar and produce the same observable effects. This stability of cause and effect allows geologists and archaeologists to feel justified in their claims that prehistoric phenomena can be explained through the past operation of presently observable processes (Gould 1965). Uniformitarian assumptions are supported by many examples in which the past-present inferential link appears to be strong (Gifford-Gonzalez 1991). For example, when a volcano erupts, it spews out lava which turns into basalt after cooling. Assuming geological processes have been relatively the

same throughout space and time, we can conclude that every time basalt is present in geologic strata, it is formed from the cooling of lava (Philpotts and Ague 2009). Therefore, the assumption of uniformitarianism is crucial to the generation of knowledge in the historical sciences (Wylie 1985). Indeed, zooarchaeologists and taphonomists have long acknowledged that their work rests on the assumption that bone and other animal tissues have responded to stresses the same in the past as today. However, there is a real danger of misapplication of uniformitarian assumptions and analogies (Wylie 1985). The most common cited mistake is the use of substantive uniformitarianism instead of methodological uniformitarianism.

Substantive uniformitarianism assumes phenomena *change at constant rates* throughout time: i.e. change is usually gradual and there are no great fluctuations in the rate of natural processes. Secondly, substantive uniformitarianism assumes a *uniformity of state* across time and space where change is evenly distributed throughout the universe. This assumption implies that physical processes on earth and elsewhere are always working at the same speeds (Gould 1965). However, this assumption was discredited by Stephen Jay Gould's, in his 1965 work, *Is Uniformitarianism Necessary?*. In it, he argues the assumption of a constant rate of change is an unwarranted constraint on scientific inquiry because it restricts physical processes in the past to those of the present. Indeed, substantive uniformitarian assumptions have often been found to be false.

Conversely, methodological uniformitarianism assumes only a *uniformity of natural law* where natural and geological processes have behaved similarly in all temporal and spatial contexts. This constancy of natural laws is a necessary assumption for all scientists to meaningfully study the unobservable past. Secondly, methodological uniformitarianism assumes the *uniformity of process* across time and space. This means the natural processes at work today

are at work in all spatial and temporal contexts. For that reason, the past is best explained by processes currently at work, but the rate of those processes can fluctuate (Gould 1965).

Therefore, this study uses methodological uniformitarianism as a baseline assumption so that observations of physical processes in the present can be used as analogies for similar events in the past. Since this study uses experimentally - created samples by Muttart et al. (2017), Keevil et al. (2018), Orlikoff et al. (2018) and Tolley et al. (2018), we therefore assume the processes used in the present to create these experimental BSM samples are justifiably similar to the contexts which created cutmarks in archaeological assemblages. These assumptions allow us to create a foundation for identifying and isolating the behaviors of prehistoric hominins in the archaeological record. However, these hominin behavioral and environmental reconstructions are often restricted due to the difficulty in assigning a single behavior to the resulting mark morphology (Gifford Gonzalez, 1991).

Consequently, the aim of this thesis is to identify replicable, causal connections between BSM surface complexity and taphonomic agents by using a middle-range theoretical framework. The middle-range theoretical approach relies on the creation of analogies between observations of current phenomena and similar behaviors in the past (Binford 1981, Gifford-Gonzalez 1991). Here, analogies are used to make inferential relationships more comprehensible by comparing them to something more familiar and better understood. The relationship between past and present phenomena is tested through experimental archaeology, where direct cause and effect connections between a particular behavior and its resulting trace in the archaeological record are tested (Binford 1981). For instance, we observe phenomena like BSM on fossilized bone surfaces. Using the middle-range theoretical approach, we can try to recreate these marks in the present day in the hope that understanding the context of mark creation will shed light on their

creation in the past. Therefore, based on our knowledge of the present-day world, we chose a modern counterpart to use as an analogy for prehistoric phenomena. A comparison of the experimental and archaeological BSM either does or does not support the analogous relationship between past and present mark creation contexts.

Taking this a step further, Gifford-Gonzalez (1991) developed a hierarchical system of relational analogies which use experimentally tested causal relationships to inferentially connect a trace to its causal actor. The effector (carnivore tooth, stone tool edge, hoof) is connected to the causal agent (immediate physical causes like stone tool grinding on bone surface), then the actor creating the trace (carnivore, hominin, raptor) and finally to its broader behavioral and ecological contexts (Gifford-Gonzalez, 1991). This relational approach provides a logical chain connecting a mark to the behavioral context within which it was created. Most importantly, this approach limits the possibility of creating unsupported interpretations of prehistoric hominin behavior by misinterpreting trace marks. This study utilizes these perspectives by modeling the measurable fractal features of BSM experimentally created by known actors in the present to shed light on prehistoric hominin butchery.

## **2.2) History of BSM Studies**

The study of diet as a causal force of adaptation in hominin evolution has long been a core research area in archaeology and paleoanthropology. This makes sense considering diet is a fundamental aspect of any organism's ecological niche. What animals eat has been found to underly many of the behavioral and ecological differences observed in living species, including, but not excluded to, group size and structure, locomotion and mating strategies (Fleagle, 1999, Unger and Sponheimer 2011). Diet is, therefore, important for understanding the physical adaptations and evolutionary history of any organism. BSM on fossilized bone surfaces are the

most direct method in use to understand the diet of our hominin ancestors. Anthropogenic BSMs include; cutmarks from hominins butchering animals (Bunn 1981, Blumenschine et al. 1996) and hammerstone percussion marks (Blumenschine and Selvagio 1988) while non-anthropogenic BSMs include carnivore toothmarks (Blumenschine 1988, Blumenschine 1995), trampling marks (Dominguez-Rodrigo et al. 2009, Courtney et al. 2019; 2020), bioerosion marks (Dominguez-Rodrigo & Barba 2006, Blumenschine et al. 2006), and fluvial erosion (Griffith et al. 2016, Gumruku and Pante 2018).

Due to the preservation of anthropogenic BSMs (mainly cutmarks) on fossilized bone surfaces, archaeologists have studied and used them to infer a wide variety of characteristics and behaviors of our Pleistocene ancestors. Cutmarks on fossilized bone surfaces can indicate the defleshing, skinning, or disarticulation of a mammal which serves as direct evidence of carcass access and processing by hominins (Blumenschine et al. 1994, Blumenschine et al. 1996). The location and frequency of cutmarks on different skeletal parts have been used to make inferences regarding hominin timing and access to carcasses nutrients (Bunn 1981, Shipman & Rose, 1983a; 1983b, Bunn and Kroll 1986, Blumenschine 1988;1995). For example, a fossilized bone with a higher cutmark frequency (and with marks located on prime meat locations) relative to carnivore toothmarks is argued to indicate that hominins had earlier access than carnivores to that particular carcass. Whereas lower frequencies of cutmark to carnivore toothmarks may indicate hominins had late access to carcasses and were mostly acquiring meat scraps and bone marrow after carnivores consumed the meatiest portions (Blumenschine 1995, Dominguez Rodrigo & Barba 2006, Dominguez-Rodrigo et al. 2010).

Archaeologists have used BSM to understand past hominin butchery behavior for more than 150 years. Early comparisons of experimental and fossil collection BSM were made by

Lartet (1860) and Desnoyers (1863a). In these cases, BSM was mainly studied as evidence of human cohabitation with now-extinct animals, thereby challenging the established narrative of biblical literalism which had been used to explain human history. While Lartet and Desnoyers were mainly concerned with comparisons between experimental and fossil cutmarks, Henri-Martin (1907) attempted to differentiate between anthropogenic and non-anthropogenic processes creating BSM. Following these pioneering efforts, archaeologists began basing their inferences concerning past butchery strategies on archaeological skeletal part representation, completeness, and the presence or absence of BSM (James and Thompson 2014). Additionally, ethnographic observations of animal butchery by contemporary indigenous peoples came into use as a basis for inferring different butchery activities, (i.e. defleshing, dismembering, and carcass part preference) from cutmark anatomical distribution on fossilized bones (Brain 1967, Binford 1981), however, the use of indigenous peoples as an analog for the behavior of extinct hominins has since been understood as both ethically problematic and misleading (Lupo & O'Connell 2002).

It wasn't until the latter half of the 20<sup>th</sup> century that archaeologists began to explore the mechanical principles employed by hominins and other taphonomic actors in modifying bone surfaces. Emphasis shifted toward trying to understand how marks get onto bones and the different processes that affect mark morphology. During the 1980s and 90s, BSMs began to be used to gauge the extent to which different taphonomic actors contributed to site formation in archaeological fossil assemblages (Bunn 1981, Binford 1981, Brain 1983, Blumenschine 1995). This period of investigation led to a critical reevaluation of how to identify the actors (the biological or nonbiological origin of the mark) and effectors (carnivore tooth, stone tool edge, hoove) creating surface marks (Potts and Shipman 1981; Shipman 1984; Gifford-Gonzalez 1991,

James and Thompson 2014). Indeed, through the use of both naturalistic and experimental observations complemented with statistical modeling, specialists realized many archaeological BSM thought to be anthropogenic were instead caused by carnivore teeth, suggesting a high level of carnivore involvement in archaeological assemblages (Binford 1981, Blumenschine 1988, Blumenschine and Silvagio 1988). This discovery cast serious doubt on earlier interpretations of fossilized cutmarks as evidence for hominins hunting (and gaining early access to carcass nutrients) on African landscapes. Instead, many argued for inferring late access (scavenging) by hominins (Binford 1981, Blumenschine 1988; 1995) in which small-bodied, pre-*H. erectus* hominins were not able to hunt large ungulates and instead gained access to ungulate carcasses after the larger carnivores had their fill. Another important perspective was added through the analysis and characterization of cutmarks themselves. This process of classifying BSM by taphonomic actors led to specialists taking into consideration the possible cutmark mimicry produced by non-anthropogenic phenomena such as mammal herd trampling, animal gnawing or the distorting effects of diagenesis (Binford 1981; Shipman 1981; 1984, Domínguez-Rodrigo et al. 2009, James and Thompson 2014).

Indeed, the increased importance of BSMs and the knowledge of cutmark mimicry has led to the realization that problems could arise if marks are misidentified (Behrensmeier et al. 1989, Gifford-Gonzalez 1991, Blumenschine et al. 1996). This potential for misinterpretation has cast doubt on many archaeological sites being of anthropogenic origin because what is being called butchery marks could actually be caused by natural processes. This uncertainty has sparked debates about the appropriate methodology for identifying anthropogenic marks and how to differentiate them from non-anthropogenic marks (Gifford Gonzalez 1991). These concerns have also prompted an even more intensive shift toward actualistic and experimental

approaches in understanding how BSMs are created (Blumenschine and Selvaggio 1988, Blumenschine 1995, Blumenschine et al. 1996). These more experimental approaches focus on inferentially linking the morphologies of marks created by different actor–effector–trace combinations (Gifford-Gonzalez 1991). Unfortunately, the large quantity of experimental research over the past few decades has been unable to bring about a consensus regarding how to differentiate anthropogenic from non-anthropogenic BSM. However, it should come as no surprise that BSM causes such contention among experts. BSM on fossilized bone surfaces are frequently subjected to multiple taphonomic processes following initial burial and abandonment (Olsen and Shipman 1988; Blumenschine et al. 2006, Domínguez-Rodrigo et al. 2009, Pante et al. 2012). Additionally, marks on bone surfaces are one of the most morphologically variable traces in the archaeological record. In any given fossil assemblage with BSM there are always some marks that overlap in morphology with a mark made by hominins (Domínguez Rodrigo et al. 2009). Sometimes this mimicry can make analysis challenging, and at other times completely impossible.

### **2.3) History of Approaches for BSM Identification and Differentiation**

Consequently, due to the significance of cutmarks to our understanding of hominin evolution and diet, it is of the utmost importance to develop new quantitative and reproducible strategies for distinguishing between the actors and effectors which produce BSM (Bello and Soligo 2008, Bello et al. 2009; Bello et al. 2011, Pante et al. 2017, Benito-Calvo 2017). Toward this end, researchers have developed a variety of methods and technologies to characterize BSM. These methods range from the use of the naked eye and expert knowledge (Bunn 1981, Blumenschine et al. 1996), 3D micro photogrammetry (Mate-Gonzalez et al. 2015, Courtney et

al. 2018) to 3D confocal microscopy (Bello et al. 2008; 2011, Braun et al. 2016; Pante et al. 2017, Courtenay et al. 2019; 2020).

Until a few decades ago, methods of identification were largely subjective, relying on categorical diagnosis based on the knowledge of individual experts working with fossil and experimental collections (Blumenschine et al. 1996, James and Thompson 2014). This method entails using handheld lenses and low-power microscopes to look for qualitative traits related to mark morphology which distinguishes BSM by taphonomic actor (Potts & Shipman, 1981, Shipman & Rose 1984, Blumenschine 1995, Blumenschine et al. 1996). For example, the cross section of a cutmark visually appears ‘V-shaped’ while carnivore toothmarks are described as looking more ‘U-shaped’. Blumenschine et al. (1996) demonstrated the accuracy of this method by performing blind tests of inter-analyst accuracy. The results showed experts correctly differentiated taphonomic actors by BSM morphology in 99% of cases and even students with fewer than three hours of training can correctly differentiate between experimentally generated BSM at rates greater than 86%. However, there has been a distinct lack of agreement among experts regarding how to macroscopically identify BSM. Thereby limiting the replicability and comparability of results between studies using this method (James and Thompson 2014). Indeed, macroscopic examination coupled with expert knowledge has been criticized for its inadequacies in solving issues where mark morphologies have ambiguous characteristics.

### 2.3.1) Scanning Electron Microscope (SEM)

Starting in the early 1980`s many researchers used Scanning Electron Microscopes (SEM) to overcome the limitations of macroscopic trace mark analysis. SEM provides high-resolution images of surface topography and texture, thereby allowing microscopic analysis of BSM morphology (Potts and Shipman 1981; Shipman 1981; Shipman and Rose 1983a). The use

of SEM has led to the discovery of qualitative differences between BSM types, for example, Potts and Shipman (1981) noted that cutmarks tend to have internal striations while carnivore toothmarks tend to lack these striations. Olsen and Shipman (1988) used SEM to successfully investigate and develop micromorphological criteria to distinguish stone from metal tools in prehistoric contexts. Indeed, SEM does provide benefits in BSM identification over macroanalysis, namely continuous magnification over a large range, high-resolution images, and the capability to make high-quality microphotographs of marks (Fisher 1995). However, SEM also has several downsides when analyzing BSM, including only being able to analyze 3D BSM using 2-D images, is destructive for artifacts, high operating costs (expensive equipment), the time needed to set up and take each photo and tends to have high interobserver inaccuracy (Bello and Soligo, Bello et al. 2008, Bello et al. 2011, Boschini and Crezzini 2012). These issues have prompted analysts to look for other methods that have less interobserver error and are better able to measure quantitative characteristics of trace marks.

### 2.3.2) Digital Micro-photogrammetry

Micro-photogrammetry is a relatively recent technique used by researchers trying to quantitatively relate the micromorphological features of BSM to the taphonomic actor responsible for its creation (Maté-González et al. 2015; 2016, Yravedra et al. 2018). Micro-photogrammetry is a more cost-effective alternative to SEM, providing a quicker method of capturing and characterizing the morphology of trace marks (Courtney et al. 2018). This method analyzes BSM by first capturing a large number of photographs of a mark from multiple angles in order to produce a high-resolution 3D model of the BSM. Once the photographs are compiled into a 3D reconstruction, quantifiable measurements, such as mark width, opening angle of mark, opening, mark depth and angle of the tool impact can be recorded (Maté-González et al. 2015;

2016). These measurements are analyzed and classified by taphonomic actor using statistical methods involving the use of experimental datasets, where variations in the measurements of BSM micromorphology are used to discriminate cutmarks from the trace marks of other taphonomic actors. Mate-Gonzalez et al. 2016 successfully used this method to differentiate between the cutmarks left by stone tools made from flint, copper and quartzite with roughly 70% accuracy.

However, micro photogrammetry has been shown to have a number of issues when modeling BSM micromorphology. Like SEM, photogrammetry has been criticized for a lack of inter-observer studies testing the replicability of micro-photogrammetric measurements and results. The problem of reproducibility is magnified by the need to take numerous inexact measurements, which introduces bias into the analysis because different researchers can measure the same mark but have different results due to the imprecision of the data collection process (Maté-Gonzalez et al. 2015). Additionally, research has shown that profile measurements can vary between multiple cross-sections of single mark depending on the position in the mark where the researcher decides to take the profile (Maté-González et al. 2015, Keevil et al. 2018). Furthermore, the average time used to analyze a single cutmark is roughly an hour, much longer compared to the methodological alternatives. Consequently, more objective and reproducible methods of capturing and classifying BSM are needed.

### 2.3.3) 3D Optical Profilometry

SEM and photogrammetry have recently been complemented by BSM studies using white-light non-contact confocal profilometers. This technology provides high-resolution 3D images of bone surfaces where micro-topographic features can be quantitatively measured, which was unobtainable using SEM. The 3D reconstructions of BSM use quantification of the

internal mark morphology produced by *known* actors and effectors to identify diagnostic criteria to be applied to the taphonomic interpretation of bone assemblages. Indeed, 3D Optical Profilometry provides replicable, quantitative comparisons of the shape of individual BSM by way of comparison with the archetypes (statistical average) of marks made by different processes. This creates a key for identifying BSM by its effector which is less influenced by the bias of individual analysts and enables researchers to assign probabilities to the “the goodness of fit” between a given mark and its inferred cause (Bello et al. 2008; 2009; 2011). This approach is argued to be better at BSM identification than the other methods listed above, especially considering 2D approaches exclude vast portions of bone mark morphologies (Otárola-Castillo et al. 2018).

Likewise, many 3D micro morphometric studies have found success distinguishing between cases where anthropogenic and non-human processes create similar mark morphology on bone surfaces (Bello 2008; 2011, Pante 2017, Courtenay et al. 2017; 2019; 2020, Keevil 2018, Yravedra et al., 2018, Meijer et al. 2018, Fransisco et al 2020). Bello & Soligo (2008) were the first to produce 3D reconstructions of cutmark micromorphology. They developed their methodology to discriminate between experimentally created cutmarks based on tool type (effectors) through the use of measurements of cutmark cross-sectional shape, shoulder heights along mark, sharpness and depth of the mark (Bello & Soligo 2008). Next, Bello et al. (2009) applied this approach to archaeological butchery marks made by handaxes and to cutmarks on human teeth. Their analysis revealed that differences in the micromorphological characteristics of cutmarks can be attributed to different butchery activities (dismembering or filleting). Additionally, they found differences between experimental and fossil cutmarks. Fossil marks are generally broader and deeper, which the authors suggest is an indication of the greater muscle

strength of archaic hominins relative to anatomically modern humans. Boschin & Crezzini (2012) built upon this previous work by conducting a 3D microscopic analysis of BSM using morphometric measurements taken from the mark (depth, breadth, angles) as quantitative criteria for identifying the effector tools used to create cutmarks. Additionally, they tested the archaeological value of 3D microscopy experiments by also using cutmarks found on pigs from an Iron Age archaeological site alongside their experimental sample. Their analysis of these metrological measurements showed 83% accuracy in determining tool type for experimental marks and 59% accuracy of fossil cutmarks. Their results imply that fossilized cutmarks may be harder to classify due to post-depositional changes caused by diagenesis. Yravedra et al. 2018 used 3D confocal microscopy to differentiate percussion marks produced with modified hammerstones and carnivore tooth pits. They found that 70% of their sample of percussion marks could be statistically differentiated from carnivore toothmarks. However, they also found that 30% of the percussion marks were likely to be mistaken for carnivore toothmarks, thereby demonstrating that more work is needed for higher accuracy rates. Courtney et al. 2019 and Courtney et al. 2020 use 3D digital microscopy to provide a detailed characterization of trampling marks through their micro-morphology. Through this methodology, they defined two new categories of trample marks that they called scratch and graze trampling marks. These studies demonstrate the effectiveness of 3D confocal microscopy in classifying BSM by taphonomic actor and providing a greater degree of quantitative comparison and reproducibility which other methods of BSM characterization lack.

However, critics of 3D profilometric microscopy have raised concerns regarding reproducibility between analysts, because while many specialists use the same equipment, they used different variables to characterize BSM. This lack of standardized methodology prevents

any meaningful patterns in the micromorphological characteristics of BSM from being identified. Fortunately, Pante et al. (2017) overcame the replicability issue by creating a standardized approach using measurement of the micromorphological features (such as surface area, volume, depth, length, etc.) for diagnosing BSM actors and effectors. The replicability of this method was demonstrated through inter-observer experiments where there was no inter-observer error among analysts (Pante et al. 2017, Keevil et al. 2018). Additionally, this protocol can distinguish cutmark from carnivore toothmarks with 97.5% accuracy (Pante et al. 2017), toothmarks can be classified by carnivore taxa (Muttart et al. 2017), the effects of fluvial abrasion on cutmark micromorphology has been described (Gumrukcu & Pante, 2018), and cutmarks have been successfully classified by raw material and tool type used in butchery (Keevil 2018, Mwakyoma 2021). With this success in discrimination between BSM actors, researchers continue to search for measurable parameters which can increase the accuracy of inferential links between the physical properties of effectors and the micromorphology of the resultant marks (James and Thompson 2014, Thompson et al. 2017, Harris et al. 2017). Toward this end, we investigate fractal parameters, as described by Brown et al. 2018, as a new method for characterizing and distinguishing BSM through the measurement of within-mark surface complexity.

#### 2.4) A History of Fractals and Archaeology

To study the complex surfaces of BSMs, we turn to fractal analysis to better identify and differentiate actors. Fractals were developed by mathematician Benoit Mandelbrot as a new branch of mathematics able to describe complex, rough forms in nature. Mandelbrot states fractals are a group of irregular, complex shapes or patterns which occur naturally, but which possess the characteristics of self-similarity and scale invariance (Mandelbrot 1977, 1982). Self-similarity means a fractal shape looks the same visually and mathematically at any scale. For

example, a fern is composed of branches that look like smaller versions of the larger tree and those branches in turn are made of smaller but structurally identical leaves. Fractal shapes are scale-invariant because, unlike regular, euclidean shapes, fractals have no natural size. And can be, at least mathematically, visually the same at any scale. In other words, if a fractal shape is examined at any scale it will resemble the whole in a statistical sense; therefore, there is a statistical equivalence between small-scale and large-scale changes in fractal patterns and this allows for the measurement of complex surfaces at multiple scales. Therefore, measuring the fractal dimension of a surface is a measure of its geometric complexity with changing of scale, which is calculated as the number of fractal shapes we observe as the size of observation decreases, therefore, the more geometric shapes, the more complex a surface is. Therefore, due to its self-similar and scale invariant characteristics, the fractal dimension is a useful parameter to distinguish different eroding processes on various surfaces, because effectors (stone tool, tooth, hoove) are made of different materials, which generate surfaces with distinguishable surface complexities.

However, it is important to note that fractals can only be used as models for natural shapes because natural objects usually lack several characteristics that define fractals (i.e. infinite length and self-similarity at all scales). Additionally, although ideal mathematical fractals have the property of scale-invariance over all possible scales, real-world fractals are usually scale-free over only a finite range of scales (Jelenik et al. 2005). How large this range needs to be so that an object can be called a fractal is a matter of debate (Brown 2005).

The third important aspect of fractals is the “fractal dimension”, commonly symbolized as “D” and mathematically described as:  $a = 1 \text{ sD}$ . The fractal dimension quantifies the complexity (variation in length, area, volume and height) with changes in the size of the

measuring scale (Brown 2005). In the equation above, “a” is the number of self-similar “pieces,” s is the scaling factor of the pieces to the whole, and “D” is the dimension that we want to calculate (Jelenik et al. 2005). This equation can be better visualized by returning to the fern example, as the size of the ferns branches shrinks, the number of fractals or self-similar pieces, “a”, increases. The fractal dimension, “D”, tells us how many new branches we will observe as the size of the branches get smaller.

In contrast to Euclidean dimensions which are measured as integers (0= point, 1 = a line, 2 = a plane etc.), most fractals are measured as fractions. The larger the fractal dimension, the more a fractal object fills up the space surrounding it. For example, a fern with a fractal dimension of 2.1 is a sparse tree with a few thin branches which isn't taking up much space. However, a fern with a fractal dimension of 2.5 is much denser and has many more branches. A fern with a fractal dimension of 2.9 has a large number of dense branches filling up space and capturing sunlight.

## **2.5) Scale-Sensitive Fractal Analysis**

Therefore, the fractal dimension “D” tells us important information about the type of processes that generate patterns on metrological surfaces. Likewise, Benoit noted the description of fractal shapes and patterns allows for the measurement of complex surfaces at multiple scales (where statistical measures are preserved across scales). Indeed, the fractal dimension has been found to be a useful parameter to describe physical surfaces, and furthermore, eroding processes in nature generate surfaces with fractal properties (Unger et al. 2003, Scott et al. 2005, Brown 2005, Brown et al. 2018). This ability to mathematically describe and document irregular surfaces at multiple scales is extremely valuable for a number of different fields, including Archaeology, Tribology, Engineering and Electrochemistry. Additionally, and importantly for

this study, many archaeological phenomena have fractal characteristics. This is to be expected because fractal patterns have been shown to be common in many kinds of natural, cultural, and social data (Brown 2005, Brown et al. 2018).

Scale Sensitive Fractal Analysis (SSFA) calculates the fractal dimension from the slope of a log-log plot where a geometric property is measured versus the scale used for measurement. The topography of the surface is considered fractal with respect to the scale when the slope of the graph varies (Brown et al. 2018). SSFA also provides a number of informative parameters which characterize the surface being studied. In this thesis we use the fractal parameters SRC (smooth-rough crossover),  $Asfc$  (Area scale fractal complexity) and  $smfc$  (max complexity). The SRC is the point at which the surface that appears Euclidean and smooth at larger scales, becomes rough at smaller scales and is best described using fractal geometry. The SRC has been shown to vary between different topographies (Hyde et al 2014) and can discriminate wear patterns generated by different abrasive forces on a statistical basis. The  $Asfc$  is calculated in the section of the log-log plot that has the greatest complexity, i.e. corresponding to the two orders of magnitude in scale where the negative slope is the steepest (Brown et al. 2018).  $Asfc$  uses repeated area measurements of constructed triangular tiles on the surface at different scales and makes them “relative” by dividing those totaled areas against the scan area. The logs of relative area measurements are plotted against the log of the scale used, and the value for the steepest part of the curve (multiplied by  $-1,000$ ) is calculated.  $Asfc$  is therefore a good indicator of surface complexity, with higher values generally indicating greater degrees of pitting and peaks in a surface.

### 2.5.1) Scale Sensitive Fractal Analysis of Use-Wear on Stone Tools

Archaeologists have used the concept of fractals and fractal dimension measurements to successfully document different kinds of worn surfaces on stone and bone tools (Stemp et al 2008, Stemp et al. 2009, Stemp et al. 2010, Lesnik 2011, Stemp et al. 2014, Evans and Donahue 2008, Watson and Gleason 2016). The use of SSFA for discrimination between use-wear patterns on stone tools is a product of microscopic use-wear analysis which was developed in the mid-twentieth century to identify the used portions of tools and the types of materials being worked upon by the tool edge. Use wear is the microscopic scratches, pits and polish found on stone tool surfaces after repeated use (Keeley 1980). Like BSM studies, the identification of use-wear on stone tool edges in archaeological contexts is based on middle-range theory, where tools created in experimental contexts are used for identification and wear classification in archaeological contexts. Also, like BSM studies, there have been issues regarding the lack of reliability of optical microscopy combined with expert knowledge for identifying and classifying wear on tool edges (Stemp et al. 2008). Furthermore, discriminating use-wear with expert analysis relies upon various qualitative approaches by different analysts which lack reproducibility and objectivity (Keeley, 1980). This has led archaeologists to devise other, less qualitative methods to study stone tool use wear. The most successful of these methods has been the characterization of tool edges using SSFA.

The first experiment using SSFA to quantify stone tool use-wear was performed by Stemp and Stemp (2001). Profiles of used and unused chert and obsidian stone tools were measured using a laser profilometer. Discrimination of used and unused surfaces occurred at different scales of measurement. Next, Stemp and Stemp (2003) used SSFA and laser profilometry to differentiate chalk flakes used to saw different materials (pottery and wood) from

the same surfaces before use. Following the encouraging results of these experiments, they performed additional tests trying to discriminate more chalk flakes used on even more materials (shell, wood, hide and antler). The chalk flakes were classified using the fractal variable Relative Area. ReIA calculates the change in area with respect to the scale measured. Likewise, Álvarez et al. (2012) used SSFA to differentiate between use-wear on experimental stone flakes used to scrape bone, hide, and wood. Stemp et al. (2013) increased the accuracy of this methodology using the parameter  $Asfc$  (area scale fractal complexity) to classify the used and unused regions of four Mistassini quartzite scrapers by their surface complexity. Through the use of  $Asfc$ , they accurately classified the worn surfaces above the 95% confidence level at coarse scales. These experiments show the effectiveness of SSFA in classifying worn surfaces from unused surfaces and allows diagnosis of the effectors used by people in the past.

Lesnik (2011) was among the first to use SSFA and laser scanning confocal microscopy to study worn surfaces of bone tools from archaeological contexts. She used artifacts excavated from Swartkrans, South Africa (1.8–1.0 million years old), to determine their potential use by early hominins for digging into termite mounds for food. Lesnik (2011) found that  $Asfc$  demonstrated significant statistical differences in surface complexity between bone tools used for different digging tasks. Additionally, they found significant differences between the Swartskrans artifacts and the experimentally created stone tools in variation of  $Asfc$ , with the experimental tools having lower complexity values. These experiments demonstrate the potential application of SSFA to mathematically describe and discriminate surface wear on stone and bone tools to determine tool function and support inferences regarding past hominin subsistence behavior.

### 2.5.2) Scale Sensitive Fractal Analysis and Tooth-Microwear Studies

Similar to use-wear and BSM studies, microwear on teeth has been used to infer prehistoric hominin behavior, and researchers have been using SSFA to create more empirical, reproducible dietary classifications (Ungar et al. 2003, Scott et al. 2005, Krueger 2015, Ranjitkar et al. 2017, Unger and Berger 2018). As defined by Schmidt (2010), dental wear is the loss of hard tissue on the enamel surface to abrasion from ingested food. Microwear are the scratches and pits which can only be detected microscopically and numerous studies of microwear on primate teeth have been conducted (Grine 1981, Teaford and Walker 1984; Ungar and Grine 1991). Microwear is universal across animal species whether the comparisons are between primates that masticate tough versus hard foods, or between carnivores that specialize on meat. For example, the orangutan, which generally uses its incisors to prepare food before consumption, shows more scratches on its incisors than does the gibbon which does not use its incisors as much (Ungar 1994). Knowledge of microwear analysis has greatly benefited studies of extinct hominin diet and have been refined through controlled experimental studies on live animals, where diets can be monitored to observe the relationship between diet and microwear on teeth surfaces. Such studies have documented the rate of microwear formation as well as elucidate the potential role of non-food items in producing wear.

Early microwear studies were qualitative in nature, researchers mainly used their expert knowledge and light microscopy to make inferences regarding diet (Merceron 2010). In the late 1970`s, analysts began using SEM which produces high - resolution images with a depth of field more appropriate for microwear analysis (Walker et al. 1978). Walker (1980) and Grine (1981) used SEM to show there is a range of microwear patterns present in both living and fossil species. However, as mentioned above, SEM suffers from disadvantages. There is information

loss when representing a 3D surface in two dimensions. Additionally, there is high interobserver error (5-10%) due to differences in the angle needed between the electron beam and tooth surface, so researchers scanning a tooth at even slightly different orientations get different measurements from the SEM images (Grine 2002). These issues have prompted researchers to use SSFA to quantitatively characterize tooth surfaces. Indeed, recent interdisciplinary research has led to the realization that teeth function at multiple scales and therefore should be studied from multiple scales. This realization has in turn led to the development of combining laser scanning confocal microscopy (LSCM) with SSFA to perform dental topographic analysis. This approach has proven more effective than SEM at quantifying and classifying microwear, being free of observer error and based on the automated quantification of 3D surfaces (Merceron 2010).

Dental microwear texture analysis (DMTA) uses confocal white-light profiler and SSFA to generate large samples of microwear surfaces and repeatable measurements (Scott et al. 2005, Merceron et al. 2010). This method relies on three-dimensional coordinates collected at high resolution from microwear surfaces identified by the investigator together with quantitative variables describing surface textures using principles from fractal geometry (Scott et al. 2006). Therefore, it increases the power to resolve and classify differences in microwear between species and allows for direct comparisons of results between observers. Indeed, metrological techniques provide more precise and repeatable ways of characterizing microwear surfaces than counting and measuring individual scratches and pits.

Ungar et al. (2003) were the first to pair scanning confocal microscopy with SSFA to measure tooth surface anisotropy and area scale fractal complexity ( $A_{sfc}$ ) to differentiate between grazer and browser diets. Grazers were found to have high anisotropy values, while

browsers exhibited high values for asfc. Scott et al. 2005 improved upon previous research by using dental microwear texture parameters (asfc, epLsar, heterogeneity of asfc and texture fill volume) to study differences in dental microwear texture and diet between hominins and other primates. They found that dental microwear textures vary significantly with diet. Additionally, they found that Asfc describes the fractal complexity of microwear surfaces and has been associated with food hardness. Years later, Scott et al. 2012 would cement the advantages of this strategy by using SSFA to discern differences in dietary and behavioral strategies of fossil. Their microwear texture analysis indicates that *Australopithecus africanus* microwear is more anisotropic (directional patterns in the enamel surface), but also has a less complex surface than the contemporaneous *Paranthropus robustus*. This latter species has more complex and variable microwear surfaces than *A. africanus*. This suggests that *A. africanus* ate more tough foods and *P. robustus* consumed more hard and brittle items, but that both had variable and overlapping diets. Scott et al. (2012) demonstrate SSFA combined with LSCM does not suffer from the low repeatability and observer biases of SEM. Namely, scanners are easier to use and cost less than SEMs. Additionally, SSFA ensures both accurate characterization of microwear surface texture, and repeatability in quantification.

These case studies demonstrate the effectiveness of the combining LSCM and SSFA in distinguishing experimental and archaeological tooth wear by diet and making testable inferences regarding the behavior of our hominin ancestors. The results of these studies make clear SSFA is an appropriate methodology for BSM differentiation by identifying which measured variables of a surface, and at what scales, are the most relevant at telling topographies apart (Brown 2005, Brown et al. 2018). Therefore, due to the characteristics of fractals, they are appropriate to mathematically describe and document the complexity of BSM - damaged bone

surfaces because bone microtopography necessitates quantitative descriptors well-suited to irregular surfaces.

## CHAPTER 3 METHODS & MATERIALS

This study uses 3D-optical metrology protocols described by Pante et al. (2017) for the systematic collection and processing of micro-morphological data. This data is an experimentally created sample of 100 Bone Surface Modifications (BSM) consisting of 25 cut, trample, tooth and percussion marks respectively. This sample was generated to test the viability of Scale-Sensitive Fractal Analysis (SSFA) as a means to accurately capture and distinguish between BSM types based on measurements of within-mark surface complexity. This research hopes to aid in the identification of butchery activity on fossilized bone surfaces from archaeological contexts.

### 3.1) Experimental Sample

To test whether SSFA can classify BSM type based on measurements of within-mark surface complexity, a sample of 100 experimentally produced BSM were sampled from the existing collection in the 3D imaging and analysis laboratory at Colorado State University. Bones with BSM of known taphonomic actors were used from several past projects; cutmarks were taken from Keevil et al. (2018), trample marks from Orlikoff et al. (2018), toothmarks from Muttart et al. (2017) and percussion marks from Tolley et al. (2018). Keevil et al. 2018 created their experimental cutmark sample by designing a cutting machine that allowed for the control of the applied force and impact angle relative to the bone surfaces. All bones in their sample were cut on a maximum of 2 useable surfaces 5 times per bone (Keevil et al. 2018). Orlikoff et al. (2018) created the trample marked bone sample by directing cattle to walk over long bone fragments scattered in sandy sediment within a confined area. Muttart et al. 2017 created the experimental toothmark sample by conducting feeding observations of grey wolves (*Canis*

*lupus*) at a rehabilitation sanctuary for wolves in Colorado, USA. The Grey Wolves were fed moderately fleshed bones twice a week on days of fasting. The bones were collected 20-24 hours after initial feeding. Tolley et al. (2018) produced the experimental percussion-marked bones using a hammerstone-on-anvil technique and controlled for animal species, bone type and hammerstone raw material.

Individual marks were circled on photographs of the complete bones (see figure 1 below). Marks that were scanned from the same mold were labeled with the same ID name and number but with unique mark letters “A, B, C”. For example, a mold comprising of three scanned marks would be labeled as CM1 Mark A, CM1 Mark B, and CM1 Mark C. This signifies that each mark is from the same scanned surface but should be measured separately (see Appendix A). No more than three marks were taken from a single mold to limit the bias of a single lab specimen.

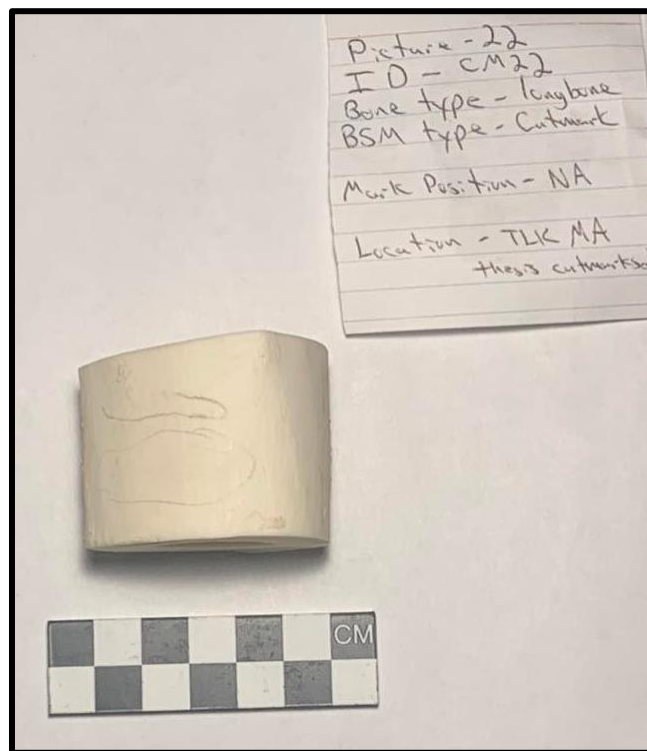


Figure 1: Example image of how BSM were identified and catalogued in the experimental sample. Here, the toothmark is circled on the anterior surface of the rib in order to more easily locate the mark during scanning.

### **3.2) Surface Molding**

After initial identification and cataloguing, each bone specimen would be lightly rinsed under a running water faucet to remove any debris on the surface. All 100 marks were molded using AccuTrans® silicone red and white mold to accurately copy the bone surface topography and BSM morphology. Due to the red mold leaving residue on bone surfaces, I switched to only using white mold for this study. It is highly recommended that all future studies using AccuTrans® molding and 3D confocal microscopy use the white mold as it has higher reflectivity which expedites the scanning process and does not leave mold residue on the bone surface which hinders future research. The finished molds were closely examined using a Sensofar s-neox white-light confocal profilometer to determine the quality of the molded surface. If the mold was found to accurately copy the bone surface and modifications without bubbles or other surface defects, then it would be scanned for marks. However, if a mold was found to contain defects, then the molding process would be repeated until the mold was found to accurately copy the bone surface without defects.

### **3.3) 3D Optical Metrology**

A total of 100 cut, trample, tooth and percussion marks from 61 experimentally damaged bones were scanned following Pante et al's. (2017) protocol for BSM diagnosis. This detailed methodology makes the data in this study replicable and comparable to other BSM studies using similar methodology. All 3D data was collected using a Sensofar s-neox white-light confocal profilometer equipped with a 5x objective.

First, a molded mark is placed in a position that aligns the mark with its longest axis perpendicular to the axis of the scanner. All molds were manually oriented and levelled in the x, y and z axes using foam bone holders and “puddy sand” to make the marks flat underneath the objective. Once a mark was located with the optical lens and scanned, then each subsequent mark was chosen based on proximity to the previous mark. In many instances, multiple marks were scanned together on a single mold. In these cases, the longest mark was oriented perpendicular to the x-axis, however the orientation of other marks on the mold were often slanted in relation to the direction at which profiles were collected.

### **3.4) Processing of 3D BSM Scans**

Once scanning was completed, the 3D BSM models would be exported from the Sensoview® software to Digital Surf® software to take metrological measurements of the 3D scans. The first step for processing the 3D models in the Digital Surf® software is to use the ‘operator’ tab called “Remove Outliers” (see fig. 2 below). The ‘Remove Outliers’ function removes outlying peaks or holes in the 3D model to create a “topographic layer”. Next, the operator called “Fill in Non-Measured Points” was applied to the BSM studiabiles. This algorithm fills any missing points that were not captured during the scanning process. This function was only used in rare cases where data points were not captured due to side wall angles being greater than 87 degrees. Next, the 3D model was mirrored on its z-axis to better replicate the original surface. This is necessary because molds copy a reverse image of the original bone surface, and therefore to mirror the scanned mold surface on the z-axis provides an accurate right-side up 3D Model. The operator named “remove form” was used next to take out the influence of the shape of the bone on the actual shape of the mark. The “remove form” operator excludes the mark itself from the levelling algorithm which produces a 3D studiable containing a

flat and unmodified BSM. The operator “threshold” is then applied which defines the height and depth of the mark’s profile. Then, the 3D models are manually rotated on the y-axis to a vertical position to ensure accuracy of measurements. This was done because slanted marks have been shown to reduce the accuracy of metrological measurements (Pante et al. 2017). Lastly, the area of the mark was extracted from the vertically positioned 3D studiable by closely tracing the BSM on the 3D model using an operator named “extract area”. The marks were carefully outlined by tracing the edge identified by the first change in color signifying a change in depth leading into the mark.

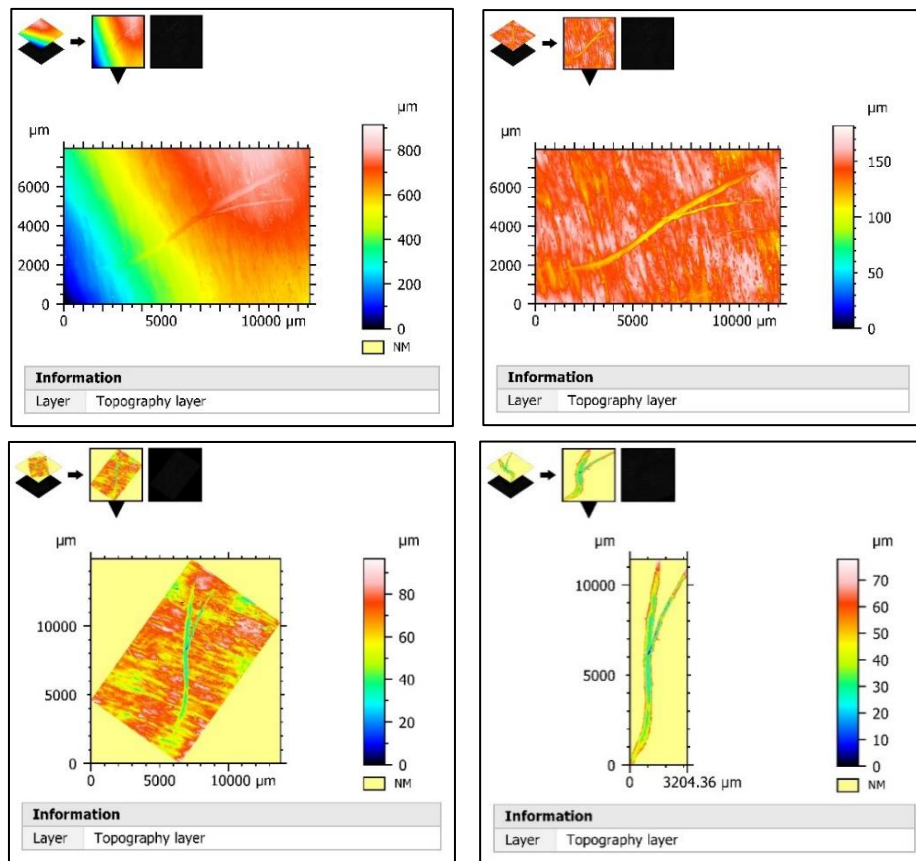


Figure 2: Top Left image shows a 3D cut mark model after initially importing it into the Digital Surf® software. The top right image shows the same 3D model after “remove form”. Bottom left image shows the mark after being rotated to a vertical position. The bottom right image shows the final product of the 3D process, an extracted cutmark. The color scales on right of both images indicate depths. The color white indicating a shallow surface and black indicating a deep surface.

### 3.5) Measurements of the 3D BSM Models

The detailed outline by Pante et al. (2017) was used to digitally analyze all scanned BSM models. Marks were processed and measured using Digital Surf Software ®. After processing the 3D mark models in Digital Surf ®, the software collects height, spatial and functional measurements from each mark which are displayed in a parameter table (see table 1 below).

Table 1: Height, Spatial and Functional Parameters: ISO 25178-2: 2012.

| Parameter Name                                                              | Symbol | Definition                                                                                                                                                                                                                                                                                                                            |
|-----------------------------------------------------------------------------|--------|---------------------------------------------------------------------------------------------------------------------------------------------------------------------------------------------------------------------------------------------------------------------------------------------------------------------------------------|
| The Root Mean Square Height                                                 | Sq     | The value of the ordinate datapoints (how up or down a data point is) within a scale-defined area. Is equivalent to the standard deviation of heights.                                                                                                                                                                                |
| Skewness                                                                    | Ssk    | A measurement of the asymmetry of the height distribution on a bell curve. The sign <b>Ssk</b> indicates the presence of many of peaks ( <b>Ssk</b> > 0) or many pits ( <b>Ssk</b> < 0) on the surface.                                                                                                                               |
| Kurtosis                                                                    | Sku    | Indicates whether or not there are very high peaks and deep valleys on a surface. The Sku sign indicates the presence ( <b>Sku</b> >3.00) or absence ( <b>Sku</b> <3.00) of peaks and valleys making up the texture. If the surface heights are normally distributed (on a bell curve) then <b>Ssk</b> is 0.00 and <b>Sku</b> is 3.00 |
| The Maximum Peak Height                                                     | Sp     | The highest peak height within a defined surface area.                                                                                                                                                                                                                                                                                |
| The Maximum Pit Height                                                      | Sv     | Absolute value of the height of the largest pit within the defined area.                                                                                                                                                                                                                                                              |
| The maximum height                                                          | Sz     | A variable quantifying the sum of the tallest peak height and the deepest pit depth within the area of measurement.                                                                                                                                                                                                                   |
| Arithmetical Mean Height (Average Roughness of Surface within Defined Area) | Sa     | This variable measures the absolute value of the difference in height of each point on a surface compared to the arithmetical mean of heights on that surface. Is often used to measure surface roughness.                                                                                                                            |
| Texture Direction of the Scale-Limited Surface                              | Std    | A measure of the angular direction of the dominant texture pattern on a surface and the orientation of that pattern. <b>Std</b> is defined relative to the Y axis. Therefore, a surface with a dominant texture pattern oriented along the Y axis has a <b>Std</b> of 0 deg.                                                          |
| Peak Extreme Height                                                         | Sxp    | Quantifies the difference in height between the average surface height and the peaks on a surface after outliers are removed.                                                                                                                                                                                                         |
| Material Volume                                                             | Vm     | An indication of the volume of material comprising a surface. Is measured from a height corresponding to the material ratio to the highest peak on the surface.                                                                                                                                                                       |
| Void Volume                                                                 | Vv     | The volume of space on a surface at a height corresponding to an arbitrary material ratio (between 0-100%) and the lowest pit.                                                                                                                                                                                                        |
| Peak Material Volume of the Scale-Limited Surface                           | Vmp    | The volume of space on a surface at a height corresponding to an arbitrary material ratio (between 0-100%) and the highest peak.                                                                                                                                                                                                      |

|                                                   |                 |                                                                                                                                                                                                                              |
|---------------------------------------------------|-----------------|------------------------------------------------------------------------------------------------------------------------------------------------------------------------------------------------------------------------------|
| Core Material Volume of the Scale-Limited Surface | V <sub>mc</sub> | The difference in volume of material comprising the surface between heights corresponding to the arbitrary material ratio values of “p” and “q”.                                                                             |
| Core Void Volume of the Scale-Limited Surface     | V <sub>vc</sub> | The volume of space bounded by the texture at heights corresponding to the material ratio values of “10%” and “80%”.                                                                                                         |
| Dale Void Volume of the Scale-Limited Surface     | V <sub>vv</sub> | The volume of space on a surface from a plane at a height corresponding to an arbitrary material ratio to the lowest pit. This valley is called a “dale” or the region around a pit where all downward paths end at the pit. |

Next, fractal measurements were taken using the “Scale Sensitive Fractal Analysis” operator in the “studies” function in Digital Surf®. This operation provides measurements of each individual marks fractal complexity (asfc), scale of max complexity (smfc), fractal dimension (das) and smooth-rough crossover (src) (see table 2 below for definitions).

Table 2: Scale-Sensitive Fractal Analysis Parameters: ISO 25178-2:2012

| Parameter Name                                     | Symbol         | Definition                                                                                                                                                                                                                                                                                                                                                                                                                                                                                                                                         |
|----------------------------------------------------|----------------|----------------------------------------------------------------------------------------------------------------------------------------------------------------------------------------------------------------------------------------------------------------------------------------------------------------------------------------------------------------------------------------------------------------------------------------------------------------------------------------------------------------------------------------------------|
| Smooth-Rough Crossover Threshold                   | SRC threshold  | Value of relative area or volume used to determine the smooth-rough crossover scale. Starting from the largest scales, working towards the smallest, the first relative area or volume to exceed the threshold is used to determine the SRC.                                                                                                                                                                                                                                                                                                       |
| Smooth-Rough Crossover                             | SRC            | The scale encountered going from relatively larger scales where the surface appears to be smooth to smaller scales where the surface appears to be rough. When the scales used for observation are large and the surface appears smooth, the fractal dimension will measure similar to the Euclidean dimension. However, when the scales used for measurements are sufficiently small and the surface appears rough, the fractal dimension exceeds the Euclidian dimension. SRC is often used in studies determining surface friction and contact. |
| Regression Coefficient                             | R <sup>2</sup> | This variable is used to gauge the accuracy of the fractal complexity value. A high value means the fractal complexity value is accurate while a low value indicates an inaccurate complexity value.                                                                                                                                                                                                                                                                                                                                               |
| Area-Scale Fractal Complexity (Fractal Complexity) | Asfc           | A measure of self-similarity at each scale of observation. Is measured as a function of the slope of the relative lengths or areas over some portion of the scale of analysis, or as one minus the slope of the length- scale plot. Large asfc values are an indication of higher complexity or roughness of the surface at scales somewhere below the SRC.                                                                                                                                                                                        |

|                         |      |                                                                                                                                                                                                                                                                                                                                                                                                                                                                                                                                                                                       |
|-------------------------|------|---------------------------------------------------------------------------------------------------------------------------------------------------------------------------------------------------------------------------------------------------------------------------------------------------------------------------------------------------------------------------------------------------------------------------------------------------------------------------------------------------------------------------------------------------------------------------------------|
| Fractal Dimension       | Das  | This variable provides a statistical index of surface complexity comparing how detail in a fractal pattern changes with the scale at which it is measured. The fractal dimension is an indication for how a fractal pattern scales differently from the topographical space around it. In Scale-Sensitive Fractal Analysis, the fractal dimension is calculated from the slope of a log-log graph calculating geometric property versus scale. The fractal dimension usually exceeds the Euclidian dimension and is measured as a fraction between the numbers 2 and 3 for a surface. |
| Scale of Max Complexity | Smfc | The scale at which the surface exhibits its highest complexity. After the scale with the surface complexity is reached, then the complexity declines. A high Smfc value indicates a surface dominated by high peaks and deep valleys at small scales.                                                                                                                                                                                                                                                                                                                                 |

To improve classification accuracy, more measurements were collected from the processed studiables following the protocol set forth by Pante et al. 2017. These measurements include the projected surface area of the mark, maximum depth of the mark, mean depth of the mark, volume of the mark and maximum length and width of the mark (see table 3 below for definitions). Maximum length and maximum width of the marks were recorded using the “distance” tool in the Digital Surf ® software. Maximum length is measured as the distance from each end on the longest part of the mark. Likewise, maximum width is measured as the distance between ends on the widest part of the mark. If the mark was curved in shape, then the length and width could be measured in incremental segments. These segments are drawn and then added together to get the total length or width measurement. Next, volume of the mark, projected surface area, maximum depth and mean depth are recorded using the “volume of a hole” function in the Digital Surf ® software. To acquire these measurements, the processed marks are traced along the edge which can be identified by a change in color indicating a change in depth leading into the mark. Once tracing the outline of the mark is completed, the measurements are automatically provided by the software.

Table 3: Volume of a Hole Parameters: Pante et al. 2017

| Parameter              | Definition                                                                         |
|------------------------|------------------------------------------------------------------------------------|
| Projected Surface Area | A 2-D measurement providing the size of the mark                                   |
| Maximum Depth          | Measures the deepest part of the mark relative to the defined plane.               |
| Mean Depth             | 3D measurement of the average depth across the mark relative to the defined plane. |
| Volume of Hole         | A 3-D measurement providing the amount of bone displaced by the mark               |
| Maximum Length         | The distance from end-to-end on the longest part of the mark.                      |
| Maximum Width          | The distance from end-to-end of the widest part of the mark.                       |

### 3.6) Statistical Analysis

Statistical analyses were performed using Microsoft Excel, R Studio version 4.0.2 and JMP statistical software v13, as well as R packages (MASS), (caret), (corrplot), (rstatix) and (randomForest).

#### 3.6.1) Data Exploration

The experimentally created BSM used in this analysis were grouped into four categories (cutmark, trample, toothmark, percussion) based on the taphonomic agent that created each mark. Histograms were used to identify whether each recorded variable was normally distributed for all BSM groups. These histograms were created using the hist() function in R Studio version 4.0.2 statistical software. The histograms of almost all measured variables indicated non-normal distributions. The only variable with a normal distribution across all BSM types was ssk (see Appendix B). Therefore, when distribution normality was an assumption of analysis all non-normally distributed variables were log - transformed to normal distributions using the log() function in rstudio. Logarithm transformations remove the skewness present in data so that statistical analysis results are not misleading due to non-normal distribution in the dataset (Metcalf and Casey 2016).

Next, a correlation matrix was created to ensure the variables were not highly correlated and reporting an incorrect accuracy in discriminant analysis. Correlation refers to the degree of

linear dependence between any two random variables in a dataset. Researchers usually want to remove correlated variables from analysis because they are redundant and can be better expressed with less correlated parameters. A correlation matrix is a table of correlation coefficients for a dataset which determines whether a linear relationship exists between the variables. The relationship is provided by the coefficients, which indicates the direction (positive vs negative) and the strength of the relationship between variables in the dataset. This relationship is expressed as a range of values between the values of -1 and 1. The value -1 indicates a non-linear (negative) relationship, whereas 1 is a positive linear relationship and 0 is in-between neither positive nor negative linear interdependency. However, a value of 0 does not mean the variables are completely independent of one another (Ferré 2009). Two variables, SRC Threshold and Das, were removed from analysis due to their complete collinearity with other variables.

This study uses Spearman correlation instead of Pearson correlation due to the outliers present in the dataset and the lack of linear relationship between variables (see figure. 3 below), which go against the assumptions of Pearson correlation (Myers and Well 2003). Pearson and Spearman correlation measure different aspects of variable relationships. Pearson correlation evaluates the linear relationship between two variables while Spearman analyzes how variables increase or decrease together (Rebekić et al. 2015).

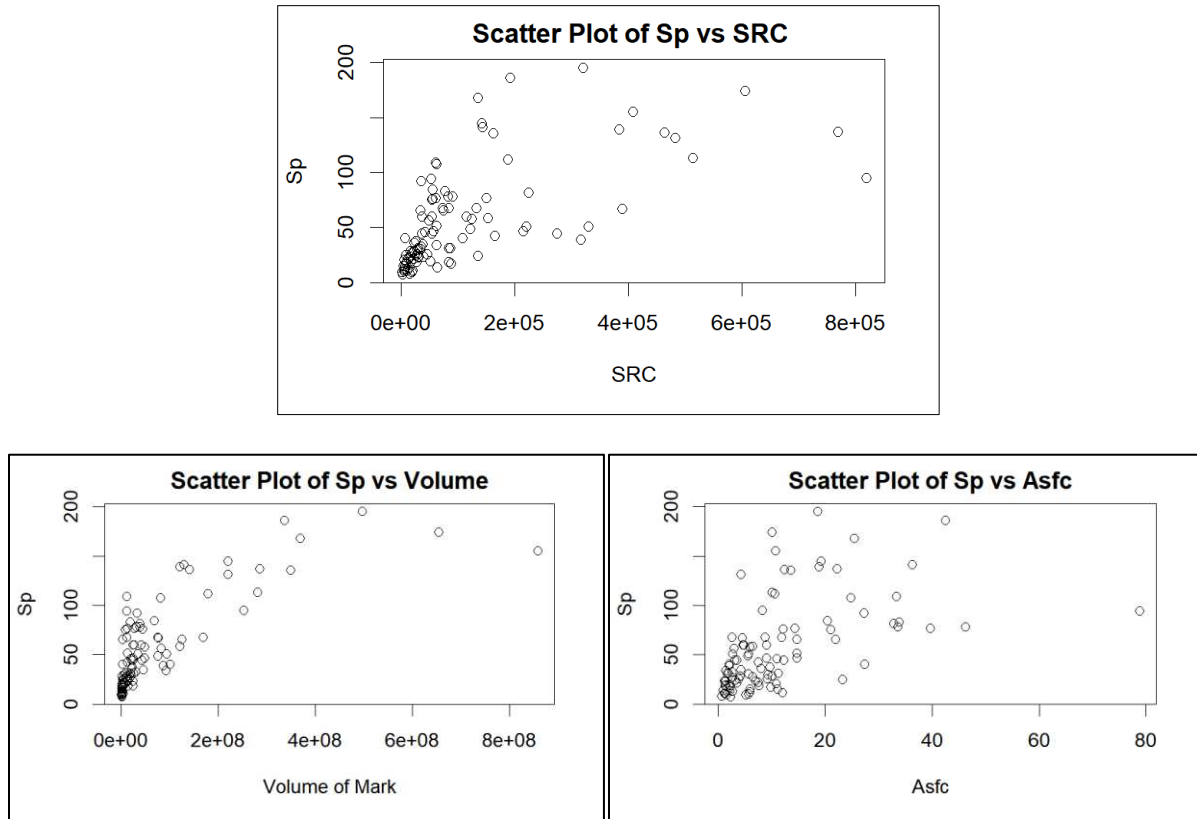


Figure 3: Scatter Plots displaying the non-linear relationships and outliers between variables. Due to the non-linear relationship visualized in the plots above this study uses the nonparametric Spearman correlation for assessing relationships between variables.

Next, variables were selected for discriminant analysis by performing a predictor screening test in JMP statistical software v13. Predictor screening analysis examines the contribution of each variable for classifying BSM types. The predictor screening test does this by using a bootstrap forest model of 100 decision trees to select potentially important variables for distinguishing and classifying the 4 BSM types (cutmark, trample, toothmark, percussion). The contributions of each variable to the bootstrap forest model are then ranked from highest to lowest. The predictor variables with higher contributions are likely to be important for BSM group prediction, while those with low contribution are likely not useful. The resulting table visualizes the proportion of the variation in the response attributed to each variable. However, the predictor screening test involves a degree of randomness, so variable contributions can be

differ slightly every time the test is rerun (SAS Institute 2016). Interestingly, the predictor screening test shows the fractal variable *asfc* as one of the top 3 most important variables for differentiating BSM types. However, other fractal variables such as *smfc* and *SRC* are less important for BSM classification according to the predictor test. Prior to performing the predictor screening test the variables *y-max* and  $R^2$  were removed from analysis due to being insignificant in classification of BSM types. Additionally, the variables *std* and *ssk* were removed from analysis due to their lack of utility in classifying BSM types. The decision to remove *std* and *ssk* was made after observing classification power increase when either variable was excluded from discriminant analysis.

### 3.6.2) Multivariate Analysis- Quadratic Discriminate Analysis

This study uses multivariate QDA models to identify and classify the taphonomic agents creating BSM using variations in cut mark micromorphology and surface complexity. QDA models the likelihood of each class of variables as normal distribution and uses the posterior probabilities to assign the class of each datapoint (Srivastava et al. 2007). QDA was the preferred statistical method because there is a lack of homogenous covariance across groups within this dataset and QDA explicitly works with classification problems where equal covariance is not assumed in the data. Unequal covariance matrices can be assumed due to well-known fact that the various kinds of BSM types vary differently with regards to their morphological characteristics (length, width etc.). For example, the length of cutmarks varies more than the length of toothmarks due to the manner of mark creation and the prevalence of meat on the bone at time of butchery. Therefore, we could assume unequal covariance matrices between BSM types and use QDA for BSM classification. Data analyses in this study was performed using the “qda” function in RStudio v4.0.2. Seven QDA models were created from this analysis. These

consist of one model categorizing all four BSM types together and the other six models classify between only two BSM types, i.e. “cutmark vs toothmark”, “trample vs percussion” etc.

After creating the QDA models, Leave One Out Cross-Validation (LOOCV) was performed to test each model's ability to predict new data that was not used in its creation. LOOCV is used in studies where the goal is prediction, and one wants to estimate how accurately a predictive model performs in practice with “real world” data. This helps identify problems regarding overfitting or selection bias and gives insight into how well the model classifies with an independent dataset of unknown data. LOOCV uses all but one of the observations vectors in the sample to decide the function for classification. Then, that classification function is used to predict the omitted observation’s vectors group membership. This process is repeated for each datapoint so that each observation is classified by a function of the other observations (Molinero et al. 2005). To perform LOOCV in RStudio, the command `CV=TRUE` was coded into the `qda()` function. The command `CV=TRUE` automatically returns results for the models cross-validation by LOOCV.

### 3.6.3) Analysis Using Machine Learning: Random Forest

Next, Random Forest Machine Learning was performed to better identify classificatory patterns in the data. This method was preferred because machine learning uses statistical learning to identify boundaries between groups and therefore classify them. Random Forest creates multiple decision trees. Decision trees look at one variable at a time using if-then statements (forks) to define the patterns in the data. Forks split the data tree into two branches based on a value called the split point. The forest assigns each datapoint a BSM classification based on which taphonomic category received the most votes. The random forest outputs an out-of-bag

(OOB) error estimate for each random forest model. OOB is an estimate of the error rate that the random forest uses for new data from the same distribution. The estimate of error is calculated as the number of misclassified marks in the model divided by the total number of classifications (Genuer, & Poggi 2020).

The resulting output in R Studio provides the number of trees constructed (500), the percentage of trees that correctly classified the data sampled (error rate) and a confusion matrix visualizing how accurately the tree managed to categorize by BSM type based on the measured variables. To perform Random Forest in RStudio, the package (randomForest) was installed and the “randomForest()” function is used. As with QDA, a total of seven models were created. One model categorizes all four BSM types together and the other six classify between only two BSM types, i.e. “cutmark vs toothmark”). Cross-validation was not performed for the random forest models as there is no need for cross-validation to get an unbiased estimate of the training set error. This estimate is performed automatically by the random forest algorithm since each tree is created with the unused out-of-bag sample from the original data and checked against these data points not used in the creation of the decision trees (Genuer, & Poggi 2020).

## CHAPTER 4 RESULTS

### 4.1) Data Normalization: Histograms

Histograms were created to identify whether each of the 28 recorded variables were normally distributed across all BSM groups. Assessing distribution skewness is important because many types of statistical analyses require normally distributed data (data points clustered around the mean) to provide accurate results. These histograms were created using the `hist()` function in R Studio version 4.0.2 statistical software. The histograms of almost all measured variables indicated non-normal distributions. The only variable with a normal distribution across all BSM types is `ssk` (see Appendix B). Therefore, when distribution normality was an assumption of analysis all non-normally distributed variables were log - transformed to normal distributions using the `log()` function in RStudio.

### 4.2) Correlation Matrix

Next, a correlation matrix of the dataset was created to remove all highly correlated variables. The correlation matrix created for all measured variables indicates complete interdependence between variables `Das` and `Asfc`, as well as between `SRC Threshold` and `Y-max` (see figure 4 below). The collinearity between `Das` and `Asfc` is logical considering `Asfc` is calculated on the same log-log plot as the fractal dimension and `Asfc` is the section of the slope that has the greatest fractal complexity (Brown et al. 2018). Therefore, due to their complete codependence with other fractal variables, `SRC threshold` and `Das` were removed from analysis (see table 4 below).

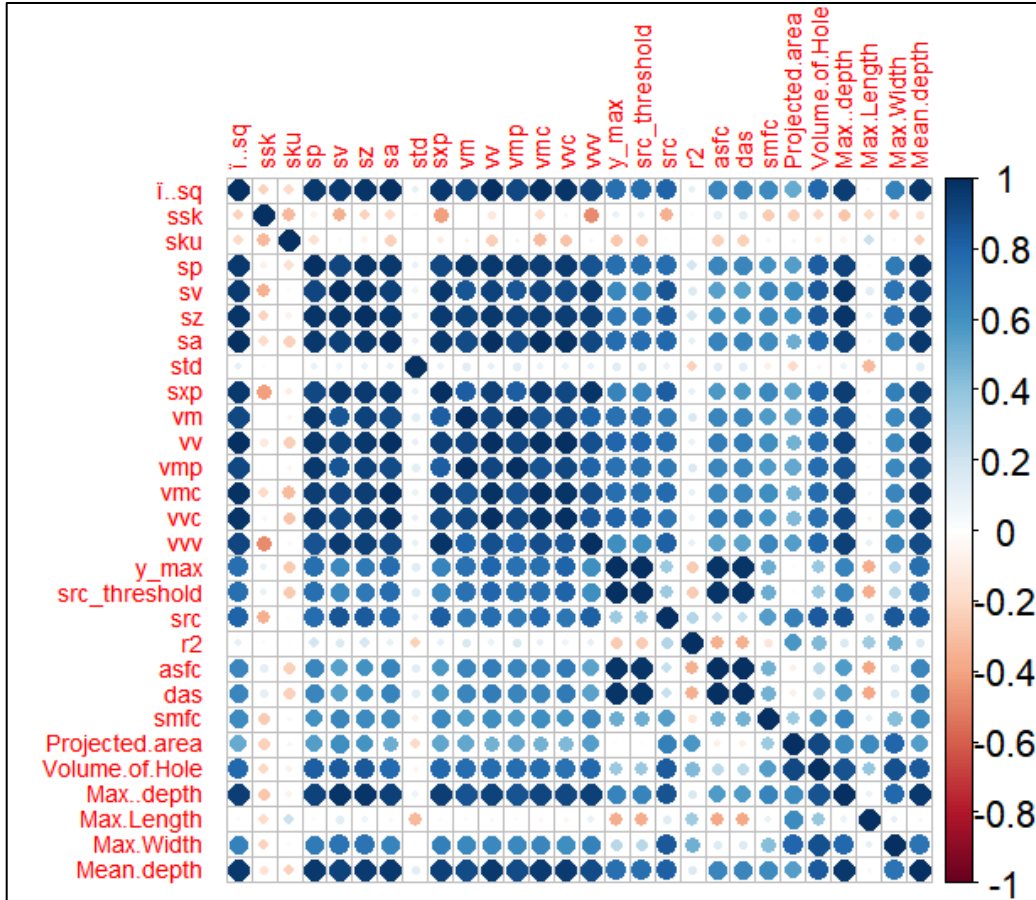


Figure 4: Correlation Matrix of all measured variables. The scale shows the relationship between the colors and the degree of correlation between variables. Blue circles indicate a positive collinear relationship and red circles a negative relationship. The darker the circle color, the stronger the collinearity.

Table 4: This table displays the strength of the correlation between each variable in relation to Das and SRC Threshold. The instances of 100% correlation between variables are highlighted.

| Variable | Das         | SRC Threshold |
|----------|-------------|---------------|
| Sq       | 0.65570957  | 0.75440744    |
| Ssk      | 0.11452745  | 0.09304530    |
| Sku      | -0.23643564 | -0.26966697   |
| Sp       | 0.65960996  | 0.75764776    |
| Sv       | 0.54250225  | 0.64231623    |
| Sz       | 0.60981698  | 0.71030303    |
| Sa       | 0.66601860  | 0.76400840    |
| Std      | 0.12010801  | 0.13438944    |
| Sxp      | 0.57501350  | 0.66843084    |
| Vm       | 0.65554155  | 0.74280228    |
| Vv       | 0.69478548  | 0.79024302    |
| Vmp      | 0.65554155  | 0.74280228    |
| Vmc      | 0.65406541  | 0.75402340    |

|                |             |             |
|----------------|-------------|-------------|
| Vvc            | 0.70923492  | 0.80314431  |
| Vvv            | 0.53846985  | 0.61827783  |
| Y_Max          | 0.97875788  | 1.00000000  |
| SRC Threshold  | 0.97875788  | 1.00000000  |
| SRC            | 0.23087909  | 0.36592859  |
| R <sup>2</sup> | -0.35673567 | -0.25900990 |
| Asfc           | 1.00000000  | 0.97875788  |
| Das            | 1.00000000  | 0.97875788  |
| Smfc           | 0.47661109  | 0.49519501  |
| Surface Area   | -0.08523252 | 0.01572157  |
| Volume of Mark | 0.26457846  | 0.37662166  |
| Maximum Depth  | 0.56585659  | 0.66809481  |
| Maximum Length | -0.38085809 | -0.36747675 |
| Maximum Width  | 0.14555056  | 0.27721572  |
| Mean Depth     | 0.65356136  | 0.75452745  |

#### 4.3) Variable Selection: Predictor Screening Test

After removing redundant variables, a predictor screening test was performed to assess the importance of each variable for classifying the 4 BSM types (cutmark, trample, toothmark, percussion). However, before screening the predictors, the variables y-max, R<sup>2</sup>, std and ssk were removed from analysis due to their lack of utility in classification of the BSM types. Once those variables were removed, the remaining 22 measurements were further reduced to 11 for discriminant analysis by performing predictor screening test in the JMP statistical software. Predictor screening analysis examines the contribution of each variable for classifying the BSM types. The predictor variables with higher contributions are likely to be important for BSM group prediction, while those with low contributions are likely not useful. The resulting table visualizes the proportion of the variation in the response attributed to each variable (see figure 5 below). Using the proportion of variance as a guide for classification importance, the top 11 variables were chosen for discriminant analysis: Maximum Width, Maximum Length, Sp, Asfc, Vmc,

Surface Area, Sku, Smfc, Sq, Volume of the mark and SRC. Together these variables make up 83% of the proportion of variation present in the BSM type groupings.

| bsm_type      |              |         |  |      |
|---------------|--------------|---------|--|------|
| Predictor     | Contribution | Portion |  | Rank |
| Max W Log     | 24.3916      | 0.1887  |  | 1    |
| Max L Log     | 15.9591      | 0.1235  |  | 2    |
| Sp log        | 15.5977      | 0.1207  |  | 3    |
| Asfc Log      | 12.0094      | 0.0929  |  | 4    |
| Vmc Log       | 8.9603       | 0.0693  |  | 5    |
| Surf Area Log | 6.9342       | 0.0537  |  | 6    |
| Sku log       | 6.6165       | 0.0512  |  | 7    |
| Smfc Log      | 4.6080       | 0.0357  |  | 8    |
| Sq log        | 4.5857       | 0.0355  |  | 9    |
| Volume Log    | 4.4475       | 0.0344  |  | 10   |
| SRC Log       | 3.2678       | 0.0253  |  | 11   |
| Vm Log        | 3.1024       | 0.0240  |  | 12   |
| Sz Log        | 2.9196       | 0.0226  |  | 13   |
| Mean D Log    | 2.8370       | 0.0220  |  | 14   |
| Sv log        | 2.8163       | 0.0218  |  | 15   |
| Vv Log        | 1.9914       | 0.0154  |  | 16   |
| Max D Log     | 1.7223       | 0.0133  |  | 17   |
| Vvc Log       | 1.6571       | 0.0128  |  | 18   |
| Vvv Log       | 1.3998       | 0.0108  |  | 19   |
| Sxp Log       | 1.3297       | 0.0103  |  | 20   |
| Vmp Log       | 1.1482       | 0.0089  |  | 21   |
| Sa Log        | 0.9379       | 0.0073  |  | 22   |

Figure 5: Predictor Screening Table for “BSM Type”. The table visualizes the proportion of the variation in the response attributed to each variable.

#### 4.4) Multivariate Analyses Results: Quadratic Discriminant Analyses (QDA)

Seven different quadratic discriminant models were made using Rstudio v4.0.2. These models were created by categorizing the scanned BSM data points into various sub - groupings, based on the mark agent (cutmark, trample, toothmark, percussion). Of the seven models created, one model discriminates between all four BSM types together and the other six models test the discriminatory accuracy between two BSM types each, i.e. “cutmark vs toothmark”, “trample vs percussion”, etc. Posterior probabilities are the resulting discriminant scores indicating the probability of classifying each mark into one of 4 BSM types based on the variable’s

measurements. The BSM type with the largest discriminant score will be the prediction for a given mark (Srivastava et al. 2007).

The results of the LOOCV for all QDA models are displayed below. The accuracy percentages indicate the effectiveness of the models in classifying new data not present in the original dataset (Molinaro et al. 2005). The confusion matrices created by these seven discriminant models recorded a wide range of classification accuracies, depending on how the BSM data was subcategorized. Using the fractal and surface roughness variables, discriminant model accuracies ranged between 58% when all 4 BSM types are compared to 86% classification accuracy when comparing cutmark vs toothmarks and cutmarks vs percussion (see table 5 below).

Table 5: Classification accuracy of all QDA models.

| Model                   | Percent Accurate Classification |
|-------------------------|---------------------------------|
| All 4 BSM Types         | 58%                             |
| Cutmark vs Trample      | 78%                             |
| Cutmark vs Toothmark    | 86%                             |
| Cutmark vs Percussion   | 86%                             |
| Trample vs Toothmark    | 74%                             |
| Trample vs Percussion   | 76%                             |
| Toothmark vs Percussion | 60%                             |

Discriminant Method: Quadratic

Classification: BSM Type

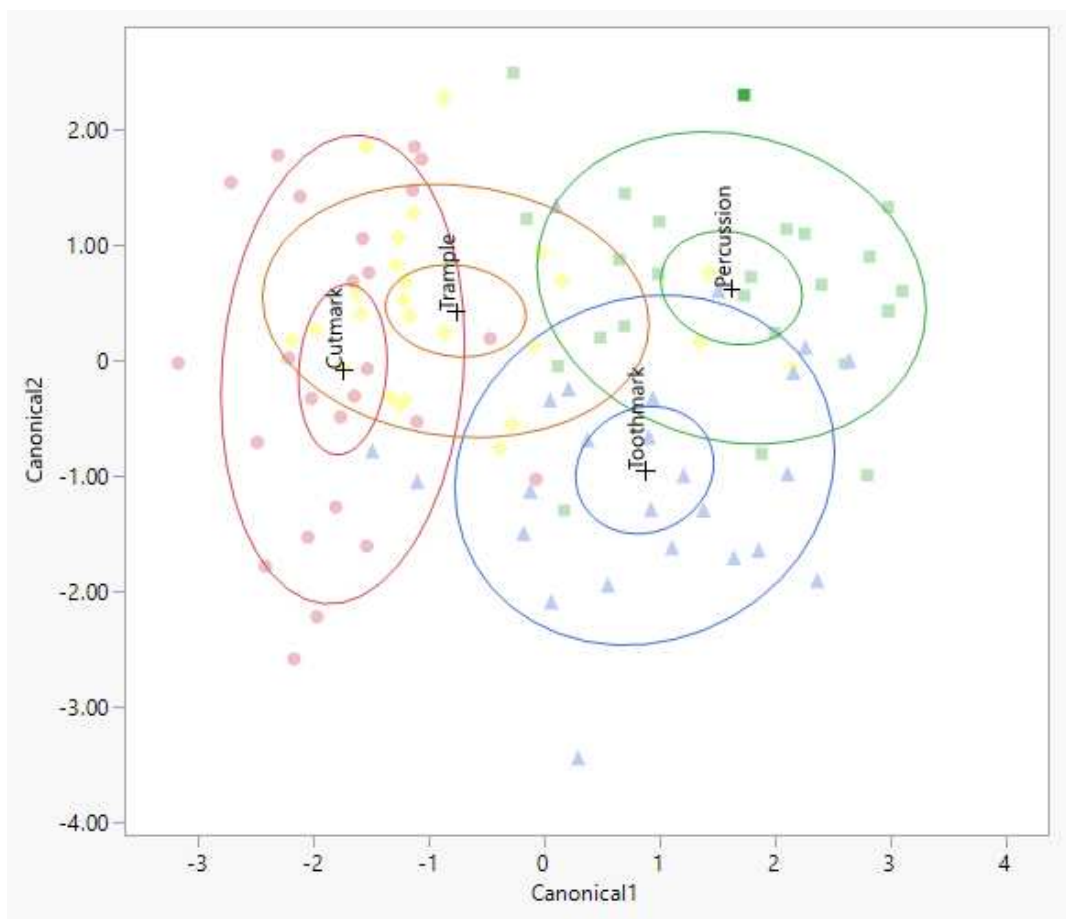


Figure 6: QDA Canonical plot showing classification of the 4 BSM types (cutmarks, trample, toothmarks, percussion)

The largest QDA model classifying the scanned BSM of all four taphonomic agents together (cutmark, trample, toothmark and percussion) has 58% accuracy in correctly classifying the scanned marks by the measured variables with a mean posterior probability of 89.59%. Cutmarks have the highest classification accuracy in this model. A majority of the misclassified cutmarks were identified as toothmarks while a smaller amount were misclassified as trample. Similar to cutmarks, the incorrectly categorized trample marks were mainly categorized as

toothmarks, however, similar numbers of trample marks were also misclassified as percussion and cutmarks. The model struggled to differentiate tooth from percussion marks, with a vast majority of toothmark misclassifications attributed to percussion marks. Likewise, a large majority of misclassified percussion marks were labeled as toothmarks. Therefore, it appears this model struggles to differentiate tooth and percussion marks based on the measured variables (see table 6 below).

Next, the QDA model classifying scanned BSM of cutmarks and trample marks has an accuracy of 78% in correctly classifying scanned marks by their measured variables with a mean posterior probability of 95.86% (see table 7 below). Thirdly, the QDA model classifying cut and toothmarks has the highest classification accuracy of 86% with a mean posterior probability of 96.78%. Interestingly, this model was able to correctly classify all 25 toothmarks when compared to trample marks (see table 8 below). The fourth QDA model classifies cutmarks and percussion marks also has an accuracy of 86% with a mean posterior probability of 97.4% for correct classifications. Very few of either BSM type were misclassified (see table 9 below). The fifth QDA model classifying trample and toothmarks has an accuracy of 74% in correctly classifying scanned marks by their measured variables and has a mean posterior probability of 91.7% for correct classifications. While many trample marks were misclassified as toothmarks in this model, toothmarks were rarely misclassified as trample marks (see table 10 below). The sixth QDA model classifying scanned BSM of trample and percussion marks has a classification accuracy of 76% with a mean posterior probability of 96.7 for correct classifications (see table 11 below). The final QDA model classifies the scanned BSM of tooth and percussion marks with an accuracy of 60% and a mean posterior probability of 93.6 for correct classifications. This

model has a lower classification accuracy due to the inability of any of the measured variables, except asfc, to differentiate between tooth and percussion marks (see table 12 below).

Table 6: All BSM Types Compared

| <b>Actual</b>   | <b>Predicted Count</b> |                |                  |                   |
|-----------------|------------------------|----------------|------------------|-------------------|
| <b>BSM Type</b> | <b>Cutmark</b>         | <b>Trample</b> | <b>Toothmark</b> | <b>Percussion</b> |
| Cut             | 17                     | 3              | 5                | 0                 |
| Trample         | 3                      | 13             | 5                | 4                 |
| Tooth Mark      | 0                      | 3              | 15               | 7                 |
| Percussion      | 0                      | 5              | 7                | 13                |

Table 7: Cutmark vs Trample

| <b>Actual</b>   | <b>Predicted Count</b> |                |
|-----------------|------------------------|----------------|
| <b>BSM Type</b> | <b>Cutmark</b>         | <b>Trample</b> |
| Cutmark         | 20                     | 5              |
| Trample         | 6                      | 19             |

Table 8: Cutmark vs Tooth Mark

| <b>Actual</b>   | <b>Predicted Count</b> |                  |
|-----------------|------------------------|------------------|
| <b>BSM Type</b> | <b>Cutmark</b>         | <b>Toothmark</b> |
| Cutmark         | 18                     | 7                |
| Toothmark       | 0                      | 25               |

Table 9: Cutmark vs Percussion Marks

| <b>Actual</b>   | <b>Predicted Count</b> |                   |
|-----------------|------------------------|-------------------|
| <b>BSM Type</b> | <b>Cutmark</b>         | <b>Percussion</b> |
| Cutmark         | 20                     | 5                 |
| Percussion      | 2                      | 23                |

Table 10: Trample vs Tooth Marks

| <b>Actual</b>   | <b>Predicted Count</b> |                  |
|-----------------|------------------------|------------------|
| <b>BSM Type</b> | <b>Trample</b>         | <b>Toothmark</b> |
| Trample         | 16                     | 9                |
| Toothmark       | 4                      | 21               |

Table 11: Trample vs Percussion

| <b>Actual</b>   | <b>Predicted Count</b> |                   |
|-----------------|------------------------|-------------------|
| <b>BSM Type</b> | <b>Trample</b>         | <b>Percussion</b> |
| Trample         | 20                     | 5                 |
| Percussion      | 7                      | 18                |

Table 12: Toothmarks vs Percussion

| <b>Actual</b>   | <b>Predicted Count</b> |                   |
|-----------------|------------------------|-------------------|
| <b>BSM Type</b> | <b>Toothmark</b>       | <b>Percussion</b> |
| Toothmark       | 17                     | 8                 |
| Percussion      | 12                     | 13                |

#### 4.5) Random Forest Analysis Results

Next, seven random forest models were created to compliment the QDA results and better discriminate between the BSM by their surface complexity and roughness measurements. As with QDA, the random forest models were developed by categorizing the scanned BSM data points into sub - groupings based on different combinations of the four taphonomic agents

(cutmarks, trample, toothmarks, percussion). The confusion matrices created by these seven random forest models record a wide range of classification accuracies, depending on how the BSM data was subcategorized. Random Forest model error rates ranged from 48% when all 4 BSM types are compared to 14% classification accuracy when discriminating between cutmarks and percussion as well as between trample and percussion marks (see table 13 below).

Table 13: This table shows the out-of-bag (OOB) error estimate for each random forest model. OOB is an estimate of the error rate that this training approach uses for new data from the same distribution. The estimate of error is calculated as the number of misclassified marks in the model divided by the total number of classifications (Genuer, & Poggi 2020).

| Model                   | OOB Estimate Of Error Rate |
|-------------------------|----------------------------|
| All BSM Types           | 48%                        |
| Cutmark vs Trample      | 42%                        |
| Cutmark vs Toothmark    | 20%                        |
| Cutmark vs Percussion   | 14%                        |
| Trample vs Toothmark    | 26%                        |
| Trample vs Percussion   | 14%                        |
| Toothmark vs Percussion | 28%                        |

The largest random forest model classifying the scanned BSM of all four taphonomic agents (cutmark, trample, toothmark and percussion) has 48% classification error in classifying the scanned marks by their measured variables. The model performed poorly classifying cutmarks, being unable to differentiate trample and cutmarks. Conversely, this random forest model was able to accurately classify most percussion marks. Similar to the QDA results, the model struggles to differentiate percussion and toothmarks, with toothmarks being the BSM type most confused for percussion. Likewise, the model misclassified toothmarks as percussion

marks more than any other BSM type. Lastly, of the trample marks misclassified by this model, a majority were incorrectly identified as cutmarks (see table 14 below). Indeed, cut and trample marks have been shown to be difficult to differentiate in other similar studies.

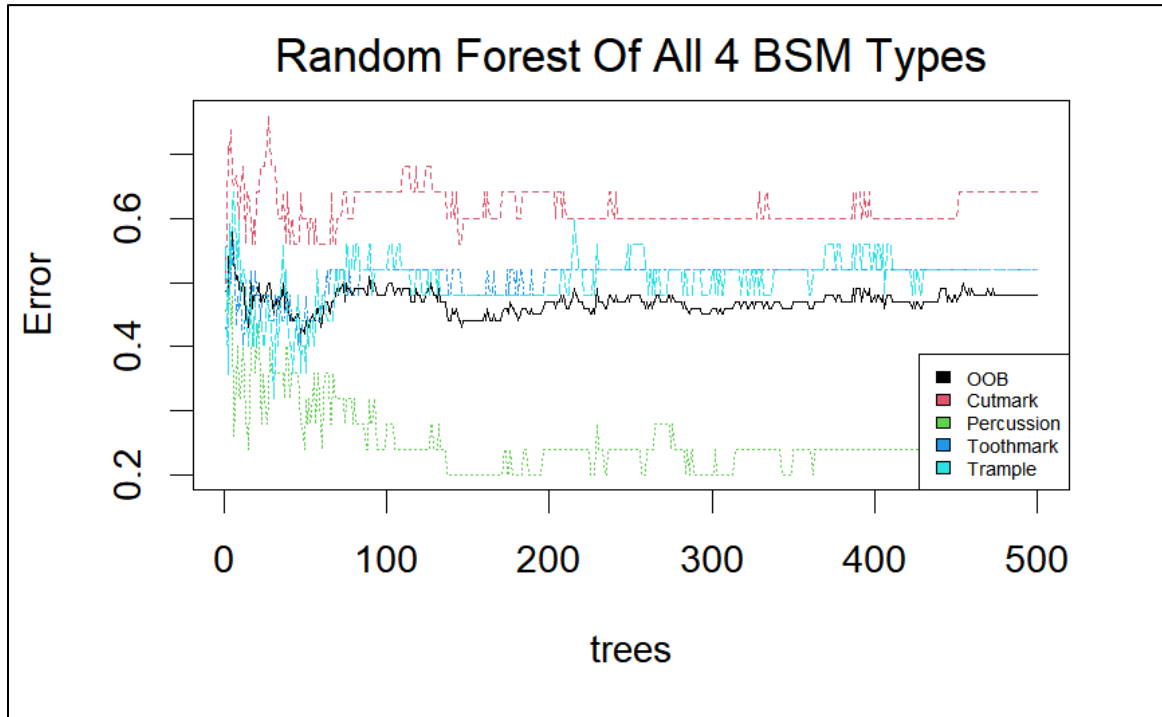


Figure 7: This plot indicates the percentage of error in classification for all four different BSM types (colored) and out-of-bag sample average (black) over the course of the 500 decision trees in the random forest model.

Next, the relative importance of each variable in classifying the data in the random forest is evaluated using the `importance()` function of the `randomForest` package in R studio. The `importance()` function results in the mean decrease in Gini coefficient. This is a measure of how each variable contributes to the uniformity of the decision trees in the random forests. The higher the value of the mean decrease Gini score (MDG), the higher the importance of the variable in the model (Genuer, & Poggi 2020). For example, in this random forest model, the variable `sp` is the most important in classification (MDG = 9.01), followed by Maximum Length (MDG = 8.86), then the fractal variable `asfc` is ranked third in importance (MDG = 8.60), then maximum

width (MDG = 8.34), vmc (MDG = 7.07), surface area (MDG = 6.01), sq (MDG = 5.89), volume of the mark (MDG = 5.58), sku (MDG = 5.29), smfc (MDG = 5.16) and src in last with a Mean Gini Decrease of 4.42.

Secondly, the random Forest model classifying the scanned BSM of cut and trample marks has a classification error rate of 42% in classifying the scanned marks by their measured variables (see table 15 below). Therefore, this random forest model is 20% less accurate than the QDA in distinguishing between cut and trample marks. For the cutmark vs trample random forest model, the variable maximum length is the most important in classification (MDG =3.27), followed closely by asfc (MDG = 3.21), then sp (MDG = 2.84), smfc (MDG = 2.17), Maximum Width (MDG = 2.13), sku (MDG = 2.03), sq (MDG = 1.96), Volume of mark (MDG = 1.92), surface area (MDG = 1.89), vmc (MDG = 1.78) and the least important variable in classification being SRC (MDG = 1.28).

Thirdly, the random forest model classifying scanned BSM of cut and toothmarks has a low classification error rate of 20% in correctly classifying scanned marks by their measured variables (see table 16 below). Therefore, this random forest model provides a very similar classification accuracy to that provided by the QDA model classifying cut and toothmarks. For the cutmark vs toothmark random forest model, the variable maximum width is by far the most important in classification (MDG =7.18), followed by sq (MDG = 2.58), then Maximum Length (MDG = 2.57), vmc (MDG = 2.28), SRC (MDG = 2.19), sp (MDG = 1.71), Volume of the mark (MDG = 1.66), surface area (MDG = 1.29), asfc (MDG = 1.20), smfc (MDG = 0.97) and the least important variable in classification being sku (MDG = 0.85).

Fourthly, the random forest model classifying cut and percussion marks has the lowest average classification error of 14%. Therefore, this random forest model provides the exact same

classification accuracy as the cutmark vs percussion QDA model. For the cutmark vs percussion random forest model, the variable maximum length is the most important in classification (MDG =4.90), followed by sp (MDG = 3.54), then vmc (MDG = 3.51), sq (MDG = 2.69), maximum width (MDG = 2.48), asfc (MDG = 2.12), SRC (MDG = 1.78), surface area (MDG = 0.96), smfc (MDG = 0.95), volume of the mark (MDG = 0.91) and the least important variable in classification being sku (MDG = 0.67).

The fifth random forest model classifies between trample and toothmarks and has an average classification error rate of 26% in correctly classifying scanned marks by their measured variables (see table 18 below). Yet again, this QDA model provides the exact same results as its QDA counterpart (see above). For the trample vs toothmark random forest model, the variable volume of the mark is the most important in classification (MDG =4.41), followed by maximum width (MDG = 3.91), then vmc (MDG = 2.66), surface area (MDG = 2.54), sq (MDG = 2), sp (MDG = 1.92), asfc (MDG = 1.90), maximum length (MDG = 1.39), smfc (MDG = 1.364), sku (MDG = 1.360) and the least important variable in classification being SRC (MDG = 1.07).

Next, random forest model differentiating between trample and percussion marks has an accuracy error rate of 14% (see table 19 below). Therefore, this random forest model provides a 10% increase in classification accuracy compared to the trample vs percussion mark QDA model. For the trample vs percussion random forest model, the variable sp is the most important in classification (MDG =5.58), followed by asfc (MDG = 3.50), then vmc (MDG = 3.28), sq (MDG = 2.57), maximum width (MDG = 2.13), maximum length (MDG = 1.69), sku (MDG = 1.59), volume of the mark (MDG = 1.27), SRC (MDG = 1.11), smfc (MDG = 0.93) and the least important variable in classification being surface area (MDG = 0.86).

Lastly, the random forest model classifying between tooth and percussion marks has an error rate of 28% in correctly classifying scanned marks by the 11 variable measurements (see table 20 below). Therefore, this random forest model provides a 12% increase in classification accuracy compared to the toothmark vs percussion mark QDA model. This result is remarkable considering the difficulty usually encountered with distinguishing between tooth and percussion marks. For the toothmark vs percussion random forest model, the fractal variable asfc is by far the most important in classification (MDG = 5.09), followed by maximum length (MDG = 3.66), then surface area (MDG = 2.69), sp (MDG = 2.41), SRC (MDG = 2.01), smfc (MDG = 1.61), maximum width (MDG = 1.60), volume of the mark (MDG = 1.59), sq (MDG = 1.43), vmc (MDG = 1.21) and the least important variable in classification being sku (MDG = 1.20).

Table 14: Random Forest Model: All BSM Types Compared

| BSM Type   | Cutmark | Percussion | Toothmark | Trample | Error% |
|------------|---------|------------|-----------|---------|--------|
| Cutmark    | 9       | 2          | 4         | 10      | 0.64   |
| Percussion | 2       | 19         | 3         | 1       | 0.24   |
| Toothmark  | 3       | 6          | 12        | 4       | 0.52   |
| Trample    | 7       | 4          | 2         | 12      | 0.52   |

Table 15: Cutmark vs Trample

| BSM Type | Cutmark | Trample | Error% |
|----------|---------|---------|--------|
| Cutmark  | 14      | 11      | 0.44   |
| Trample  | 10      | 15      | 0.40   |

Table 16: Cutmark vs Toothmark

| BSM Type  | Cutmark | Tooth | Error% |
|-----------|---------|-------|--------|
| Cutmark   | 22      | 3     | 0.12   |
| Toothmark | 7       | 18    | 0.28   |

Table 17: Cutmark vs Percussion

| BSM Type   | Cutmark | Percussion | Error% |
|------------|---------|------------|--------|
| Cutmark    | 21      | 4          | 0.16   |
| Percussion | 3       | 22         | 0.12   |

Table 18: Trample vs Toothmarks

| BSM Type | Trample | Tooth | Error% |
|----------|---------|-------|--------|
| Trample  | 18      | 7     | 0.28   |
| Tooth    | 6       | 19    | 0.24   |

Table 19: Trample vs Percussion

| BSM Type   | Trample | Percussion | Error% |
|------------|---------|------------|--------|
| Trample    | 21      | 4          | 0.16   |
| Percussion | 3       | 22         | 0.12   |

Table 20: Toothmarks vs Percussion

| BSM Type   | Tooth | Percussion | Error% |
|------------|-------|------------|--------|
| Toothmark  | 19    | 6          | 0.24   |
| Percussion | 8     | 17         | 0.32   |

## CHAPTER 5 DISCUSSION

Our ability to inferentially link feeding traces found on fossil bones to specific taphonomic actors is critical to reconstructing the ecological and behavioral contexts of hominins in archaeological sites (Domínguez-Rodrigo et al. 2012, Pante et al. 2012; 2014, Pobiner et al. 2015; 2018, Pobiner 2020). The use of optical profilometry and high-resolution 3D scanning provides a reliable method for identifying the presence of specific taphonomic actors from their feeding traces. This thesis seeks to contribute to this body of work by building upon the replicable protocol for collecting and processing metrological data set forth by Pante et al. (2017) to identify within-mark fractal characteristics of BSM with which to discriminate between taphonomic agents. Future research building upon this dataset could further enhance our reconstructions of hominin behavioral ecology during the early Pleistocene when the introduction of butchered meat into the hominin diet probably caused biological and behavioral adaptations in the genus *Homo* (Aiello and Wells 2002, Milton 1999; 2003, Antón and Snodgrass 2012, Wrangham 2017).

### **5.1) Interpretation of Results: Multivariate Discriminant Analysis**

The relationship between the fractal parameters and the taphonomic agents creating BSM was tested by computing the 100 scanned marks into a QDA model and classifying each mark into one of the 4 taphonomic groupings (cutmark, trample, toothmark, percussion) based on the 11 measured variables. This quadratic discriminant model can classify the BSM type of the experimental marks with 58% accuracy. With this low classification accuracy, the results of the discriminant model classifying all 4 BSM types do not support H1, which states the fractal measurements of mark surface complexity are reflective of the agents creating BSM. Therefore,

the “All 4” QDA model supports the null hypothesis (H<sub>0</sub>), which states the fractal variables are *not* reflective of the known BSM agents and therefore are *not* useful in BSM agent classification.

Examination of the confusion matrix for the discriminate model comparing all 4 BSM types (table 4 in the previous chapter) indicates the model struggles to differentiate trample, tooth, and percussion marks, but can adeptly distinguish between cut and percussion marks.

Most of the incorrect classifications for each BSM grouping are attributed to toothmarks. The significant overlap between the Grey Wolf and Lion toothmarks with the other 3 taphonomic agents could indicate a high degree of variability in the micromorphology and fractal measurements of sampled toothmarks. It is possible the Grey Wolf and Lion toothmarks have a large degree of overlap with other taphonomic agents because they produce small tooth pits and scratches that can be easily misclassified as percussion and trample marks.

Sub - grouping the dataset into models discriminating between only pairs of BSM types effectively increases the 58% accuracy of the “All 4” QDA model to the 60% - 86% range. The increased classification accuracy with the smaller sub - grouped models is probably a result of the relative ease of discriminating between only 2 BSM types compared to 4. Additionally, the improved classification accuracy of the paired BSM models may indicate the fractal variables are best used for BSM discrimination when comparing only two BSM types at a time. Nevertheless, the higher accuracies resulting from sub - grouped discriminate models do indicate that the metrological measurements used in Pante et al. (2017), when paired with the 3 fractal variables *Asfc*, *SRC* and *Smfc* can distinguish between BSM types with average levels of accuracy. Therefore, when sub - grouped into pairs, the results support H<sub>1</sub>.

The sub - grouped QDA model comparing cut and trample marks by their fractal and micromorphological variables provides a classification accuracy of 78%. While not an

impressive degree of accuracy, this result is promising when considering these two BSM types have been difficult to distinguish in previous studies. In fact, this result is complementary to those of Orlikoff et al. (2018), who used 3D microscopy paired with multivariate discriminate analysis to acquire an 80% classification accuracy between trample and cutmarks. Conversely, while sub - grouping BSM agents to pairwise comparisons does provide a much higher level of accuracy compared to the “All 4” model, the data still shows a degree of overlap between cut and trample marks (see table 5 in the previous chapter). Examination of the confusion matrix for the cut vs trample mark QDA model in the previous chapter indicates the misclassifications could be due to the inherent difficulty in differentiating cut from trample marks as both taphonomic agents produce long striations on bone surfaces.

Thirdly, the sub - grouped QDA model comparing cutmarks and carnivore toothmarks by their fractal and micromorphological variables provides a classification accuracy of 86% (see table 6 in previous chapter). This is an excellent result. As the ability to distinguish between these two taphonomic agents by their feeding traces is crucial to understanding hominin behavior and carcass acquisition sequences in archaeological sites (Blumenschine & Pobiner 2007). However, the results of the cutmark vs toothmark discriminant model are relatively low compared to the results of Pante et al. (2017). They use 3D profilometric methods and multivariate analyses to discriminate between cutmarks and mammalian carnivore toothmarks with 97.5% accuracy. The 11.5% drop in classification accuracy between this thesis and Pante et al. (2017) could be due to several factors. Namely, this study did not use the mark profile measurements used by Pante et al. (2017) and subsequent studies (Muttart 2017, Keevil 2018, Mwakyoma 2021). The profile measurements measure the deepest part of the mark because it reflects the greatest amount of force applied to the bone surface, which correlates with

taphonomic actor. Most importantly, the profile measurements provide even more useful variables with which to distinguish BSM types, including mark depth, area, width, roughness (Ra), opening angle and floor radius (Pante et al. 2017). Therefore, it is possible that overall classification accuracies could be improved with the inclusion of the profile measurements.

The sub - grouped QDA model comparing cutmarks and hammerstone percussion marks also provides a classification accuracy of 86%. This is another excellent result. Indeed, examination of the confusion matrix for the cutmark vs percussion mark model (see table 7 in previous chapter) indicates the discriminant model is very adept at classifying between these two BSM types. This adequate classification accuracy may be due to the drastic differences in morphology between cut and percussion marks. Percussion marks usually occur as pits or grooves pressed into a bone's surface by protrusions on the hammerstone's surface (Blumenschine 1988). Whereas cutmarks are usually longer, thin striations running across the bone surface. Given the presence of prehistoric hammerstone breakage of long bones in archaeological contexts, the high degree of separation between cut and percussion marks is crucial for accurately identifying the biological agents responsible for bone modifications.

The 5<sup>th</sup> and 6<sup>th</sup> QDA models compare trample to toothmarks and trample to percussion marks by their fractal and micromorphological variables. Both discriminant models produce relatively average classification accuracies of 74% and 76% respectively (see tables 8 & 9 in the previous chapter). The similarity of these results, as well as the similar classification accuracy acquired in the cutmark vs trample model (78%) indicate the 11 variables are able to distinguish trample marks from other 3 BSM types an average of 76% of the time when sub - grouped. The ~24% overlap between trample marks and cut, tooth and percussion marks may be due to the inherent variation of trample marks in their fractal and micromorphological measurements. This

overlap could be mitigated with a larger sample size capturing the wider range of variation inherent to each BSM type, thereby aiding in the diagnostic identification and classification of each BSM type.

Lastly, the QDA model comparing toothmarks and hammerstone percussion marks by their fractal and micromorphological variables has the lowest classification accuracy of any of the sub - grouped discriminant models at 60%. This low result is disconcerting, but these two taphonomic agents have been difficult to differentiate in past studies. For instance, Yravedra et al. (2018) used 3D confocal microscopy and multivariate analysis to differentiate hammerstone percussion marks and carnivore tooth pits with a classification accuracy of 70%. The 10% difference in classification accuracy between this thesis and Yravedra et al. (2018) is probably due to the different variables used for agent classification between studies. For this thesis, percussion marks were measured using numeric variables (i.e. max length, max width, mean depth etc.). Whereas Yravedra et al. (2018) measured percussion marks using 17 coordinate landmarks on the exterior and interior surfaces of toothmark and percussion pits. These landmarks contain size and shape information of the pit in the form of Cartesian coordinates. Ultimately, the low classification accuracies acquired between this thesis and Yravedra et al. 2018 could be an indication that carnivores produce small tooth pits and scratches that can be easily misclassified as percussion marks.

The classification accuracies reported by the cutmark vs toothmark, cutmark vs percussion mark and tooth vs percussion mark discriminant models are comparable to other taphonomic studies trying to identify and differentiate BSM types by their micromorphological measurements. For example, Blumenshine et al. (1996) use a hand lens and low-power microscope to qualitatively differentiate cutmarks from tooth and hammerstone percussion

marks. This method provided a 99% classification accuracy when experts are diagnosing a BSM type of known origin. Even novices with less than 3 hours of training were able to correctly classify BSM types with an accuracy of 86%, the highest classification accuracy produced by this study. However, the results of Blumenschine et al. (1996) are qualitative and therefore not analogous to this thesis. Reexamination of the replicability and accuracy of using a hand lens to model mark morphology found that qualitative descriptions are subjective to the researcher and tend to lead to disagreement between researchers (Njau and Blumenschine 2006, James and Thompson 2014, Harris et al 2017). Nevertheless, there is a reduction in model accuracy reported in this thesis compared to the Blumenschine et al. (1996) study. However, regardless of the reduction in model accuracy in this thesis compared to Blumenschine et al. (1996), the methodology presented in this study is more objective and replicable even among non-experts. Additionally, the relatively higher classification accuracy of the paired QDA and random forest models indicates the fractal variables added to the micromorphological measurements already presented in Pante et al. (2017) can aid in correct BSM identification for previously difficult taphonomic agent comparisons such as cut vs trample marks.

## **5.2) Random Forest Analysis**

The random forest models made to complement the discriminant analysis show similar results when classifying the scanned marks by their micromorphological and fractal variables. Indeed, the random forest model comparing all four BSM types has a high classification error rate of 48%, which, like the “All 4” QDA model does not support H1, but does support the null hypothesis (H<sub>0</sub>). Examination of the confusion matrix for the random forest model comparing all 4 BSM types (see table 12 in the previous chapter) indicates random forest analysis has more difficulty than the comparable “all 4” QDA model in using the measured variables to classify

trample and tooth marks. For instance, the “All 4” random forest model is 4% and 12% respectively less accurate in distinguishing trample and tooth marks by their measured variables. Additionally, the “all 4” random forest model is 32% less accurate when classifying cutmarks. This significant drop in accuracy appears to be due to the random forest models’ inability to distinguish cutmarks from trample marks (62.5% of cutmark misclassifications are misattributed to trample marks). However, the “All 4” random forest model can distinguish percussion marks from the other three BSM types with much greater accuracy (31% increase) than the “all 4” QDA model. This drastic classification increase between statistical methods is peculiar but is probably just due to the different calculations each type of analysis entails.

The inability of random forest machine learning to distinguish between cut and trample marks carries over to the sub - grouped models. Indeed, the only model to show a significant drop in classification accuracy from QDA to random forest analysis is the cutmark vs trample mark random forest model which resulted in a 42% error rate for classification. As stated above, this high classification error rate could be due to the inherent difficulty in differentiating cut from trample marks. Therefore, the higher classification error indicates that the random forest model is not as adept at distinguishing cut and trample marks as the parallel discriminant models.

Regardless, most of the sub - grouped random forest models result in classification accuracies which support the results of the sub - grouped QDA models. For instance, when BSM types are sub - grouped into models classifying marks between only two BSM groupings at a time, the classification error decreases to the 28% – 14% range (excluding the cutmark vs trample model). Indeed, the classification accuracy/error rate is exactly the same between the QDA and random forest models comparing cut vs percussion marks (both 86% accurate) and trample vs toothmarks (both 74% accurate). Additionally, both random forest analysis and QDA

show small classification disagreement (within 6%) for the models comparing all 4 BSM types (QDA =58% accuracy, RF = 52% accuracy) and cut vs toothmark models (QDA = 86%, RF= 80% accurate). The strikingly similar classification accuracies between the QDA and random forest models are encouraging, as it verifies the veracity of the QDA results which generally support H1.

Lastly, the trample vs percussion mark and tooth vs percussion mark random forest models show a significant difference ( $\geq 10\%$ ) with their QDA counterparts. In both cases, the random forest shows a higher degree of competence in classifying the BSM by the 11 micromorphological and fractal variables. It is likely the large increase in classification accuracy is due to the random forest being more adept at classifying percussion marks. Interestingly, the results of the tooth vs percussion mark random forest model are even more similar to the results of Yravedra et al. (2018) than the sub - grouped QDA model. As stated above, they found that 70% of their sample of percussion marks could be statistically differentiated from carnivore toothmarks. This accuracy may be relatively average, but it is comparable to the 72% accuracy in distinguishing tooth from percussion marks in the random forest model of this study. Ultimately, the sub - grouped random forest machine learning models classifying experimental marks by their 11 measured variables agrees with the QDA results and mostly supports H1.

### **5.3) Limitations of Study**

This study relied on the ability of multivariate discriminant and random forest machine learning models to classify BSM into specific taphonomic groupings by their micromorphological and fractal measurements. The accuracy levels achieved by the discriminant and random forest models were relatively average, and low compared to Blumenschine et al. (1996) and Pante et al. (2017). Efforts to achieve higher classification accuracies were hampered

by a few factors, namely the sample size of the dataset, (maybe) the use of molds, and the magnification used to measure within-mark fractality. Indeed, the models in the study had a small sample size ( $n=100$  and  $n=50$  for paired models), which is inadequate to train a statistical classifier. Likewise, the use of molds may have influenced the accurate identification of taphonomic effectors from trace mark morphology and fractal measurements. All 100 experimental BSM of known origin were molded to expedite the scanning process. Molds speed up data collection by having a much less reflective surface compared to bone. Less surface reflectivity requires fewer scanning attempts to acquire a competent scan. Fortunately, the replication of BSM micromorphology using molding has previously been shown to provide an accurate representation of the original surface and resulting marks (Bello 2011). Furthermore, using the quantitative scanning methodology outlined by Pante et al. (2017), Muttart (2017) compared the morphology of BSM on the original bone surface to its molded copy and found no statistical differences. Therefore, it is safe to assume that molded BSM provides an accurate representation of the marks and does not influence the classifications of the feeding traces in this thesis. Lastly, the use of 3 marks from each bone specimen may have biased the sample, future BSM studies should only collect a single mark from each bone specimen to completely eliminate bias from a single bone specimen.

However, the critical limitation of this study is the use of 5x magnification during data collection. A 5x objective on the s-neox was used because increasing the objective means drastically increasing the scan time per mark and it isn't feasible to scan an entire mark at higher magnifications. Additionally, 5x objective was used so the results of this thesis can be comparable to other studies in the 3D imaging and analysis laboratory at Colorado State University which also used a 5x objective. However, when comparing the results of this thesis to

analogous studies using SSFA to differentiate diet from microwear or behavior from stone tool use wear, it is clear other authors used much higher magnifications between 10x and 200x to distinguish surfaces by their fractal measurements (Stemp & Stemp 2001; 2003, Ungar et al. 2003, Scott et al. 2005, Stemp et al. 2008, Stemp et al. 2009, Stemp et al. 2010, Merceron et al. 2010, Lesnik 2011, Scott 2012, Stemp et al. 2013; 2014, Krueger 2015, Watson & Gleason 2016, Ranjitkar et al. 2017). The reasons for using the higher magnifications are usually given as needed to reach the scales at which the fractal dimension is active and thus where surfaces can be differentiated using fractal variables. Therefore, it is likely that the 5x objective used in this study is too low a magnification to adequately detect the fractal dimension and thereby differentiate BSM types by their fractal measurements.

This conclusion is supported by the fact that while ideal mathematical fractals display scale-free properties over all possible scales, real-world fractals are scale-free only over a limited range of scales (Jesnik 2005, Brown 2005). For instance, Stemp et al. 2013 found that accurate discrimination of microwear on the surface of quartzite scrapers depends on the scale being used for analysis. They use two different objectives (50x and 100x) to distinguish between two types of quartzite scrapers used on fresh and dry deer hide. Fresh hide scrapers were discriminated from the dry hide scrapers at lower magnifications (50x), whereas the unused surfaces of the scrapers made from different types of quartzite were successfully discriminated with 100x magnification. Therefore, indicating the fractal behavior of stone tools were material and use-dependent. Furthermore, Stemp et al. (2013) state the ability to discriminate between the quartzite scrapers becomes increasingly possible as the scale of measurement decreases (and magnification increases). At the finest scales (10–1  $\mu\text{m}^2$ ), surface roughness can be discriminated with measurable differences between tools used on dry hide when compared to

those used on fresh hide, as well as for each of the two quartzite tools used on the same contact material.

Therefore, it is possible that higher classification accuracies could be obtained by increasing the magnification used for data collection. However, increasing the objective presents more methodological problems. Namely, raising the objective from 5x to 20x or higher would exponentially increase the time needed to scan the entirety of each individual mark. Unlike analogous studies of stone tool use-wear and teeth microwear, which only scan a relatively small, contained area of a tooth or stone tool, 3D BSM studies require scans of *entire* marks which are considerably larger in size and require more time to completely scan at high magnifications. It may be possible to bypass this issue by taking a single fractal measurement from a single part of each mark, however, there is the prospect that different parts of the same mark have different readings for the same fractal measurement, thereby making comparisons of fractal measurements between multiple marks very difficult. These questions can only be answered with future research and experimentation.

#### **5.4) Future Research Prospects**

Based on the limitations of this thesis and the results obtained, there are many related areas of study that require further investigation to provide a methodology that produces more accurate classifications of BSM agents. Methodologically, optical profilometry has the potential to develop into a more reliable quantitative method for studying BSMs. Its potential in diagnosing tool effectors from trace marks can even be applied to taphonomic studies of fossil assemblages in sites where there are no associated artifacts or known taphonomic agents such as Dikika, Ethiopia (McPherron et al. 2011). To achieve a higher degree of classification accuracy, there is a need for further inter-analyst studies dedicated to improving optical profilometry

measurement and analysis protocols (Pante et al. 2017). Additionally, the creation of a much larger experimental BSM database would provide an adequate dataset to train a statistical classifier. Lastly, for SSFA to be successfully used to classify BSM types, a higher objective is probably needed, however, this would require more time devoted to data collection on the part of the researcher to scan each mark. While this method could be laboriously time-consuming, it could lead to a more informed understanding of early hominin subsistence strategies.

## CHAPTER 6 CONCLUSION

This thesis describes the first study to use confocal microscopy paired with Scale-Sensitive Fractal Analysis (SSFA) to differentiate bone surface modifications (BSM) by their micromorphological and fractal measurements. The methodology used in this study expands upon previous work by Pante et al. (2017) which quantitatively characterizes BSM micromorphology according to a replicable protocol. The results provide detailed information regarding the relationship between within-mark surface complexity and the taphonomic agents creating the marks. Ultimately, the full potential of pairing SSFA and 3D microscopy to classify BSM agents can only be realized through future research building upon this dataset. Further development of the methodology used in this study could provide a more accurate identification of taphonomic agents from their resulting feeding traces in archaeological contexts. Creating stronger inferential connections between the marks found on fossilized bone surfaces to the taphonomic actors creating said marks would provide a more holistic understanding of the behavioral and ecological context within which our hominin ancestors operated when acquiring carcass resources. This study internalized this perspective by modeling the measurable fractal features of BSM experimentally created by known actors in the present to shed light on analogous prehistoric hominin butchery behavior.

Although this study was limited by sample size and the scale of observation, the results of both the QDA and random forest models demonstrate 3D microscopy paired with SSFA can be applicable to the identification of taphonomic effectors from their feeding traces. However, the degree of accuracy provided by this methodology depends upon the manner in which the BSM types are sub - grouped and compared. For instance, the quadratic discriminant and random forest model classifying cut, tooth, trample and percussion marks together results in low

classification accuracies between 52% - 58%, therefore supporting the null hypothesis (Ho). Conversely, sub - grouping the dataset into models discriminating between only pairs of BSM types (i.e., cutmark vs trample mark) increases the classification accuracy of the QDA and random forest models to the 60% - 86% range. The improved classification accuracy of the paired BSM models may indicate comparisons between feeding traces of different taphonomic agents should only be conducted between two BSM types at a time. Nevertheless, the higher accuracies resulting from sub - grouped discriminate and random forest models indicate the metrological measurements used in Pante et al. (2017), when paired with the 3 fractal variables asfc, SRC and smfc can distinguish between BSM types with average to high levels of accuracy. Therefore, when sub - grouped into pairs, the QDA and random forest results support H1, which states the fractal measurements of mark surface complexity are reflective of the actors creating BSM.

This thesis creates a new avenue for understanding the subsistence strategies of early hominins through the development of a new method for distinguishing hominin from non-hominin taphonomic traces. Indeed, the ability to distinguish hominin-induced cutmarks from other taphonomic traces is the foundational component of taphonomic inferential hierarchies used by archaeologists to understand hominin behavioral ecology (Blumenschine et al. 1988, Gifford Gonzalez 1991, Blumenschine et al. 1994; 1996, Pante et al. 2012; 2014, Merrit et al. 2019). The confusion resulting from qualitative mark mimicry has been addressed through the use of confocal microscopy (Archer and Braun, 2013; Pante et al., 2017; Otárola-Castillo et al. 2017; Gümrükçü and Pante, 2018) and statistical approaches capable of differentiating between BSM actors based on standardized ‘archetype’ marks by using 3D scanning equipment, and the statistical evaluation of overlap between mark types using 3D morphometrics (Bello et al 2008;

2009; 2011, Boschini and Crezzini 2012, Pante et al. 2017, Yrevedra et al 2018, Meijer et al. 2019, Francisco et al. 2020). This thesis has striven to build upon this body of work by utilizing the ability of fractals to mathematically describe and document irregular shapes at multiple scales to distinguish taphonomic agents. Indeed, even with the low 5x objective, the fractal variables assisted in discriminating between taphonomic agents (particularly cutmarks and trample marks), therefore highlighting the applicability of using high-resolution scanning to accurately model and interpret the fractal and micromorphological features of BSM. This point is crucial because developing an objective and standardized method of differentiating feeding traces provides a platform for more scientific, i.e. *testable* assumptions about hominin behavior in archeological sites.

Future research should seek to expand upon this research by increasing the sample size of all BSM types to where the dataset can be considered a statistical classifier. Additionally, future studies using SSFA to distinguish BSM types should increase the objective used for data collection to the 20x-100x range where within-mark fractal characteristics can distinguish between the worn surfaces of BSM left by different taphonomic agents. These measures would provide higher accuracies in agent classification and allows for a more holistic understanding of how and when early *homo* used stone tools for meat procurement. This dietary shift toward partial carnivory is considered by many paleoanthropologists as a key milestone in human evolution due to possibly enabling the emergence of adaptations associated with our genus (Aiello and Wells 2002, Milton 1999; 2003, Antón and Snodgrass 2012, Wrangham 2017). Therefore, this thesis strove to make a small contribution to our understanding of hominin behavioral and biological evolution.

## REFERENCES

- Aiello, Leslie & Wells, Jonathan. (2002). Energetics and the Evolution of the Genus HOMO. *Annu. Rev. Anthropol.* 31. 323-338. 10.1146/annurev.anthro.31.040402.085403.
- Antón, Susan & Snodgrass, Josh. (2012). Origins and Evolution of Genus Homo: New = Perspectives. *Current Anthropology*. 53. 10.1086/667692.
- Archer, Will, and David R Braun. "Investigating the signature of aquatic resource use within Pleistocene hominin dietary adaptations." *PLoS one* vol. 8,8 e69899. 21 Aug. 2013, doi:10.1371/journal.pone.0069899
- Behrensmeier, Anna K., Gordon, K. D., and Yanagi, G. T. 1989. "Non-human Bone Modification in Miocene Fossils from Pakistan." In *Bone Modification (Proceedings of First International Conference on Bone Modification)*. Bonnicksen, R. and Sorg, M. H., editors. 99–120. Orono, Maine: Center for the Study of the First Americans.
- Bello SM, Soligo C. 2008. A new method for the quantitative analysis of cutmark micromorphology. *Journal of Archaeological Science* 35(6):1542–1552 DOI 10.1016/j.jas.2007.10.018.
- Bello SM, Parfitt SA, Stringer CB. 2009. Quantitative micromorphological analyses of cut marks produced by ancient and modern handaxes. *Journal of Archaeological Science* 36(9):1869–1880 DOI 10.1016/j.jas.2009.04.014.
- Bello SM. 2011. New results from the examination of cut-marks using three-dimensional imaging. In: Ashton N, Lewis SG, Stringer C, eds. *The ancient human occupation of Britain*. Amsterdam: Elsevier, 249–262.
- Benito Calvo, Alfonso & Arroyo, Adrian & Sánchez-Romero, Laura & Pante, Michael & Torre, I. (2017). Quantifying 3D Micro-Surface Changes on Experimental Stones Used to Break Bones and Their Implications for the Analysis of Early Stone Age Pounding Tools. *Archaeometry*. 60. 10.1111/arcm.12325.
- Binford, L.R. (1981). *Bones: ancient men and modern myths*. Academic Press, New York.
- Blumenschine RJ. 1988. An experimental model of the timing of hominid and carnivore influence on archaeological bone assemblages. *J Archaeol Sci* 15:483–502.
- Blumenschine RJ, Selvaggio MM. 1988. Percussion marks on bone surfaces as a new diagnostic of hominid behavior. *Nature* 333: 763–765. [59]
- Blumenschine, J.A. Cavallo and S.D. Capaldo. (1994) Competition for carcasses and early hominid behavioral ecology: a case study and a conceptual framework. *Journal of Human Evolution*, 27, 197-213.

- Blumenschine RJ. 1995. Percussion marks, tooth marks and experimental determinations of the timing of hominid and carnivore access to long bones at FLK Zinjanthropus, Olduvai Gorge, Tanzania. *J Hum Evol* 29:21–51.
- Blumenschine, R.J., Marean, C., Capaldo, S.D., 1996. Blind tests of inter-analyst correspondence and accuracy in the identification of cut marks, percussion marks, and carnivore tooth marks of bone surfaces. *Journal of Archaeological Science*. 23, 493–507.
- Blumenschine RJ, Prassack KA, Kreger CD, Pante MC. Carnivore tooth-marks, microbial bioerosion, and the invalidation of Domínguez-Rodrigo and Barba's (2006) test of Oldowan hominin scavenging behavior. *Journal of Human Evolution*. 53: 420-6. PMID 17727916 DOI: 10.1016/J.jhevol.2007.01.011
- Blumenschine, Robert & Pobiner, Briana. (2007). Zooarchaeology and the ecology of Oldowan hominin carnivory. *Evolution of the Human Diet*. 167-190.
- Boschin F, Crezzini J. 2012. Morphometrical analysis on cut marks using a 3D digital microscope. *International Journal of Osteoarchaeology* 22(5):549–562 DOI 10.1002/oa.1272
- Brain, C. K. (1967). *Bone weathering and the problem of bone pseudo-tools*. Pretoria: s.n
- Brain, C. K. (1983). *The hunters or the hunted?: an introduction to African cave taphonomy*. University of Chicago Press.
- Braun David R., Pante Michael and Archer William 2016 Cut marks on bone surfaces: influences on variation in the form of traces of ancient behaviour *Interface Focus*.62016000620160006
- Brown, C.T., Witschey, W.R.T. & Liebovitch, L.S. The Broken Past: Fractals in Archaeology. *J Archaeol Method Theory* 12, 37–78 (2005). <https://doi.org/10.1007/s10816-005-2396-6>
- Brown C.A., Hans N. Hansen, Xiang Jane Jiang, François Blateyron, Johan Berglund, Nicola Senin, Tomasz Bartkowiak, Barnali Dixon, Gaëtan Le Goïc, Yann Quinsat, W. James Stemp, Mary Kathryn Thompson, Peter S. Ungar, E. Hassan Zahouani, Multiscale analyses and characterizations of surface topographies, *CIRP Annals*, Volume 67, Issue 2, 2018, Pages 839-862, ISSN 0007-8506, <https://doi.org/10.1016/j.cirp.2018.06.001>.
- Bunn, H.T., 1981. Archaeological evidence for meat-eating by Plio-Pleistocene hominids from Koobi Fora and Olduvai Gorge. *Nature* 291, 574–577.
- Bunn, H.T., Kroll, E.M. 1986. Systematic butchery by Plio/Pleistocene hominids at Olduvai Gorge, Tanzania. *Current Anthropology* 27: 431-452.

- Courtenay LA, Yravedra J, Mate-Gonzalez MA, Aramendi J, González-Aguilera D. 2017. 3D analysis of cut marks using a new geometric morphometric methodological approach. *Journal of Archaeological Anthropological Sciences* Epub ahead of print Nov 10 2017 DOI 10.1007/s12520-017-0554-x.
- Courtenay, Lloyd & Yravedra, José & Huguet, Rosa & Ollé, Andreu & Aramendi, Julia & González, Miguel Ángel & González-Aguilera, Diego. (2018). New taphonomic advances in 3D digital microscopy: A morphological characterisation of trampling marks. *Quaternary International*. 517. 10.1016/j.quaint.2018.12.019.
- COURTENAY, L., HUGUET, R. and YRAVEDRA, J. (2020), Scratches and grazes: a detailed microscopic analysis of trampling phenomena. *Journal of Microscopy*, 277: 107–117. <https://doi.org/10.1111/jmi.12873>
- Delaney-Rivera C., Plummer T.W., Hodgson J.A., Forrest F., Hertel F., Oliver J.S. 2009. Pits and pitfalls: taxonomic variability and patterning in tooth mark dimensions *Journal of Archaeological Science* 26:2597-2608
- Desnoyers, J. 1863a. Réponse à des objections faites au sujet de stries et d'incisions constatées sur des ossements de mammifères fossiles des environs de Chartres. Institut Imperial de France Academie des Sciences Extrati des Comptes rendus des seances de 'Academie des Sciences tome LV1 seance du 29 juin 1863
- Domínguez-Rodrigo, M. and Barba, R. 2006. New estimates of tooth mark and percussion mark frequencies at the FLK Zinj site: the carnivore–hominid–carnivore hypothesis falsified. *Journal of Human Evolution* 50(2), 170–94.
- M. Domínguez-Rodrigo, R. Barba, Five more arguments to invalidate the passive scavenging version of the carnivore-hominid-carnivore model: a reply to Blumenschine et al. (2007a), *Journal of Human Evolution*, Volume 53, Issue 4, 2007, Pages 427-433, ISSN 0047-2484, <https://doi.org/10.1016/j.jhevol.2007.05.010>.
- Domínguez-Rodrigo, M. and Yravedra, J. 2009. Why are cut mark frequencies in archaeofaunal assemblages so variable? A multivariate analysis. *Journal of Archaeological Science* 36(3), 884–94.
- Dominguez-Rodrigo, Manuel & Juana, S. & Galán, A. & Martín Rodríguez, Patricia. (2009). A new protocol to differentiate trampling marks from butchery cut marks. *Journal of Archaeological Science*, 36, 2643-2654. *Journal of Archaeological Science – J ARCHAEOLOG SCI.* 36. 2643-2654. 10.1016/j.jas.2009.07.017.
- Domínguez-Rodrigo, M., Mabulla, A. Z. P., Bunn, H. T., DiezMartin, F., Baquedano, E., Barboni, D., Barba, R., Domínguez-Solera, S., Sánchez, P., Ashley, G. M. and Yravedra, J. 2010a. Disentangling hominin and carnivore activities near a spring at FLK North (Olduvai Gorge, Tanzania). *Quaternary Research* 74(3), 363–75

- Domínguez-Rodrigo, Travis Rayne Pickering, Henry T. Bunn, Experimental study of cut marks made with rocks unmodified by human flaking and its bearing on claims of ~3.4 million-year-old butchery evidence from Dikika, Ethiopia, *Journal of Archaeological Science*, Volume 39, Issue 2, 2012, Pages 205-214, ISSN 0305-4403, <https://doi.org/10.1016/j.jas.2011.03.010>.
- Evans Adrien, A., Randolph E. Donahue, Laser scanning confocal microscopy: a potential technique for the study of lithic microwear, *Journal of Archaeological Science*, Volume 35, Issue 8, 2008, Pages 2223-2230, ISSN 0305-4403, <https://doi.org/10.1016/j.jas.2008.02.006>.
- Fernandez-Jalvo, Y. & Andrews, P. 2011. When Humans Chew Bones. *Journal of Human Evolution*. **60** (1): 117-123.
- J. Ferré, 3.02 - Regression Diagnostics, Editor(s): Steven D. Brown, Romá Tauler, Beata Walczak, *Comprehensive Chemometrics*, Elsevier, 2009, Pages 33-89, ISBN 9780444527011, <https://doi.org/10.1016/B978-044452701-1.00076-4>.
- Francisco, Cécile Blondel, Noël Brunetière, Anusha Ramdarshan, Gildas Merceron. Enamel surface topography analysis for diet discrimination. A methodology to enhance and select discriminative parameters. *Surface Topography: Metrology and Properties*, IOP Publishing 2018, 6 (1), pp.015002. [ff10.1088/2051-672X/aa9dd3ff](https://doi.org/10.1088/2051-672X/aa9dd3ff). [ffhal-03042216](https://doi.org/10.1088/2051-672X/aa9dd3ff)
- Fisher, J. J. W. 1995. Bone surface modifications in zooarchaeology. *Journal of Archaeological Method and Theory* 2(1), 7–68.
- Fleagle JG (1999) *Primate Adaptation and Evolution* (Academic, New York), 2nd Ed.
- Genuer, & Poggi, J.-M. (2020). *Random Forests with R* (p. 98–). Springer International Publishing AG. <https://doi.org/10.1007/978-3-030-56485-8>
- Gifford-Gonzalez, D. (1991). Bones are not enough: Analogues, knowledge, and interpretive strategies in zooarchaeology. *Journal of Anthropological Archaeology*, 10(3), 215–254.
- Stephen J Gould. Is Uniformitarianism Necessary. *American Journal of Science* 263:223-228.
- Griffith, S. J., Thompson, C. E. L., Thompson, T., & Gowland, R. L. (2016). Experimental abrasion of water submerged bone: the influence of bombardment by different sediment classes on microabrasion rate. *Journal of Archaeological Science: Reports*, 10, 15–29. <https://doi.org/10.1016/j.jasrep.2016.09.001>
- Grine, F.E., 1981. Trophic differences between “gracile” and “robust” australopithecines: a scanning electron microscope analysis of occlusal events. *South African Journal of Science* 77, 203–230
- Grine, F.E., Ungar, P.S., Teaford, M.F., 2002. Error rates in dental microwear quantification using scanning electron microscopy. *Scanning* 24, 144–153.

- Gumrukcu Uslu, Merve & Pante, Michael. (2018). Assessing the effects of fluvial abrasion on bone surface modifications using high-resolution 3-D scanning. *Journal of Archaeological Science: Reports*. 21. 10.1016/j.jasrep.2018.06.037.
- Harris, J.A., Marean, C.W., Ogle, K., Thompson, J., 2017. The trajectory of bone surface modification studies in paleoanthropology and a new Bayesian solution to the identification controversy. *Journal of Human Evolution*. 110, 69–81.
- Henri-Martin, L. 1907–1910. *Recherches sur l'évolution du Moustérien dans le gisement de la Quina (Charente)*, fascicule 1 (1907), Ossements utilisés; fascicule 2 (1909), Ossements utilisés; fascicule 3 (1910), Industrie osseuse. Paris: Schleider.
- Hyde, Joyce & Cadet, Lionel & Montgomery, J & Brown, Christopher. (2014). Multi-scale areal topographic analysis of surfaces created by micro-EDM and functional correlations with discharge energy. *Surface Topography: Metrology and Properties*. 2. 045001. 10.1088/2051-672X/2/4/045001
- ISO 25178-2:2012 Geometrical Product Specifications (GPS). *Surface Texture: Areal Part 2: Terms, Definitions and Surface Texture Parameters*. ISO, 2012.
- ISO/FDIS 25178-2 2021 Geometrical Product specifications (GPS)—surface texture: areal—Part 2: Terms, definitions and surface texture parameters(Geneva: International Organization for Standardization)
- James, E. C., & Thompson, J. C. (2014). On bad terms: Problems and solutions within zooarchaeological bone surface modification studies. *Environmental Archaeology*, 20(1), 89–103. doi: 10.1179/1749631414y.0000000023
- Jelinek, Herbert & Jones, Cameron & Warfel, Matthew & Lucas, Cecile & Depardieu, Cecile & Aurel, Gaëlle. (2006). Understanding Fractal Analysis? The Case of Fractal Linguistics. *Complexus*. 3. 66-73. 10.1159/000094189.
- Keeley LH. 1980. *Experimental determination of stone tool uses: a microwear analysis*. Chicago: University of Chicago Press.
- Keevil, T., Pante, M., Glantz, M., & Lacy, M. (2018). *Inferring Early Stone Age Tool Technology and Raw Material from Cut Mark Micromorphology Using High-Resolution 3-D Scanning with Applications to Middle Bed II, Olduvai Gorge, Tanzania* (ProQuest Dissertations Publishing). Retrieved from <http://search.proquest.com/docview/2055364067/>
- Kristin L. Krueger, *Reconstructing diet and behavior in bioarchaeological groups using incisor microwear texture analysis*, *Journal of Archaeological Science: Reports*, Volume 1, 2015, Pages 29-37, ISSN 2352-409X,

- Lartet, M. E. 1860. On the coexistence of man with certain extinct quadrupeds, proved by fossil bones from various Pleistocene deposits, bearing incisions made by sharp instruments. *The Quarterly Journal of the Geological Society of London* 16, 471–9.
- Lesnik, Julie J.. “Bone Tool Texture Analysis and the Role of Termites in the Diet of South African Hominids.” (2011).
- Lupo KD, O’Connell JF. 2002. Cut and tooth mark distributions on large animal bones: ethnoarchaeological data from the Hadza and their implications for current ideas about early human carnivore. *Journal of Archaeological Science* 29(1):85–109 DOI 10.1006/jasc.2001.0690.
- Lyell, Charles, Sir. (1830). *Principles of geology : being an attempt to explain the former changes of the earth's surface, by reference to causes now in operation* (v. 3). John Murray .... Retrieved from <https://library.si.edu/digital-library/book/principlesgeolov3lyel>
- Mandelbrot, Benoit B. "Form, chance and dimension." *Chance and Dimension*. Freeman, San Francisco (1977): 1-234.
- Mandelbrot, Benoit B.. *The fractal geometry of nature*. Vol. 1. New York: WH freeman, 1982.
- Maté-González, M.Á.; Yravedra, J.; González-Aguilera, D.; Palomeque-González, J.F.; Domínguez-Rodrigo, M. Micro-photogrammetric characterization of cut marks on bones. *J. Archaeol. Sci.* 2015, 62, 128–142
- Maté-González, M.Á., Palomeque-González, J.F., Yravedra, J. *et al.* Micro-photogrammetric and morphometric differentiation of cut marks on bones using metal knives, quartzite, and flint flakes. *Archaeol Anthropol Sci* 10, 805–816 (2018). <https://doi.org/10.1007/s12520-016-0401-5>
- McPherron, S. P., Alemseged, Z., Marean, C. W., Wynn, J. G., Reed, D., Geraads, D., ... & Béarat, H. A. (2010). Evidence for stone-tool-assisted consumption of animal tissues before 3.39 million years ago at Dikika, Ethiopia. *Nature*, 466(7308), 857-860
- Meijer, H. J.M., d’Errico, F., Queffelec, A., Kurniawan, I., Setiabudi, E., Sutisna, I., Brumm, A. & van Den Bergh, G. D. (2019). Characterization of bone surface modifications on an Early to Middle Pleistocene bird assemblage from Mata Menge (Flores, Indonesia) using multifocus and confocal microscopy. *Palaeogeography, Palaeoclimatology, Palaeoecology*, 529 1-11
- Merritt, S.R. 2016. Cut mark cluster geometry and equifinality in replicated Early Stone Age butchery. *International Journal of Osteoarchaeology* 26:585–598. <https://doi.org/10.1002/oa.2448>
- Merritt, S.R., Michael C. Pante, Trevor L. Keevil, Jackson K. Njau, Robert J. Blumenschine, Don't cry over spilled ink: Missing context prevents replication and

- creates the Rorschach effect in bone surface modification studies, *Journal of Archaeological Science*, Volume 102, 2019, Pages 71-79, ISSN 0305
- Gildas Merceron, Emilia Hofman-Kamińska, Rafał Kowalczyk, 3D dental microwear texture analysis of feeding habits of sympatric ruminants in the Białowieża Primeval Forest, Poland, *Forest Ecology and Management*, Volume 328, 2014, Pages 262-269, ISSN 0378 1127, <https://doi.org/10.1016/j.foreco.2014.05.041>.
- Metcalf, L., William Casey, Chapter 4 - Introduction to data analysis, Editor(s): Leigh Metcalf, William Casey, *Cybersecurity and Applied Mathematics*, Syngress, 2016, Pages 43-65, ISBN 9780128044520
- Milton K. 1999. A hypothesis to explain the role of meat-eating in human evolution. *Evol Anthropol* 8:11–21.
- Milton, K. (2003). The Critical Role Played by Animal Source Foods in Human (Homo) Evolution. *The Journal of Nutrition*, 133(11). Doi: 10.1093/jn/133.11.3886s
- Molinaro, Annette M., Richard Simon, Ruth M. Pfeiffer, Prediction error estimation: a comparison of resampling methods, *Bioinformatics*, Volume 21, Issue 15, , Pages 3301 3307, <https://doi.org/10.1093/bioinformatics/bti499>
- Muttart, M., Pante, M., Boone, R., & LaBelle, J. (2017). Taxonomic Distinctions in the 3D Micromorphology of Tooth Marks with Application to Feeding Traces from Middle Bed II, Olduvai Gorge, Tanzania [ProQuest Dissertations Publishing]. <http://search.proquest.com/docview/1961606316/>
- Mwakyoma, Ipyana F. *New Insights into Pleistocene Hominin Butchery and Tool Choice from a 0.9 Ma Fossil Assemblage from the HEB Site, Olduvai Gorge, Tanzania*. Colorado State University. Libraries, 2021. Print.
- Myers, Well, A., & Well, A. (Arnold). (2003). *Research design and statistical analysis* (2nd ed.). Lawrence Erlbaum Associates.
- Njau, J.K. & R.J. Blumenshine, 2006. A diagnosis of crocodylian damage to larger vertebrate bones. *For J. Human Evol.*, 50, 142-162
- Olsen, S. L. and Shipman, P. 1988. Surface modification butchery on bone: trampling versus butchery. *Journal of Archaeological Science* 15, 535–53.
- Orlikoff, E., Keevil, T., Pante, M. (2018). Quantitative analysis of the micromorphology of trampling-induced abrasion and stone tool cut marks on bone surfaces In: Abstracts of the Paleoanthropology Society 2018 Meeting, Austin, TX, 10–11 April 2018

- Otárola-Castillo, E., Torquato, M.G., Hawkins, H.C., James, E., Harris, J.A., Marean, C.W., et al., 2018. Differentiating between cutting actions on bone using 3D geometric morphometrics and Bayesian analyses with implications to human evolution. *J. Archaeol. Sci.* 89, 56–67. <https://doi.org/10.1016/j.jas.2017.10.004>
- Pante, M., & Capaldo, S. (2012). Validation of bone surface modification models for inferring fossil hominin and carnivore feeding interactions, with reapplication to FLK 22, Olduvai Gorge, Tanzania. *Journal of Human Evolution*.
- Pante, Michael & Scott, Robert & Blumenschine, Robert & Capaldo, Salvatore. (2014). Revalidation of bone surface modification models for inferring fossil hominin and carnivore feeding interactions. *Quaternary International*. 355. 10.1016/j.quaint.2014.09.007.
- Pante, M.C., Muttart, M.V., Keevil, T.L., Blumenschine, R.J., Njau, J.K., Merritt, S.R., 2017. A new high-resolution 3-D quantitative method for identifying bone surface modifications with implications for the Early Stone Age archaeological record. *Journal of human evolution*. 102, 1–11.
- Philpotts, Anthony R.; Ague, Jay J. (2009). *Principles of igneous and metamorphic petrology* (2nd ed.). Cambridge, UK: Cambridge University Press.
- Pobiner, B. L. (2015). New actualistic data on the ecology and energetics of hominin scavenging opportunities. *Journal of Human Evolution*, 80, 1–16.
- Pobiner BL, Higson CP, Kovarovic K, Kaplan RS, Rogers J, Schindler W III. 2018. Experimental butchery study investigating the influence of timing of access and butcher expertise on cut mark variables. *Int J Osteoarch* 28:377–387
- Pobiner, BL. The zooarchaeology and paleoecology of early hominin scavenging. *Evolutionary Anthropology*. 2020; 29: 68– 82. <https://doi.org/10.1002/evan.21824>
- Potts, R. B. and Shipman, P. 1981. Cutmarks made by stone tools on bones from Olduvai Gorge, Tanzania. *Nature* 291, 577–80.
- Ranjitkar, S et al. “Surface-Sensitive Microwear Texture Analysis of Attrition and Erosion.” *Journal of dental research* vol. 96,3 (2017): 300-307. doi:10.1177/0022034516680585
- Rebekić, Lončarić, Z., Petrović, S., & Marić, S. (2015). PEARSON’S OR SPEARMAN’S CORRELATION COEFFICIENT - WHICH ONE TO USE? *Poljoprivreda (Osijek, Croatia)*, 21(2), 47–54. <https://doi.org/10.18047/poljo.21.2.8>
- SAS Institute. *JMP Statistical Discovery from SAS Version 13: Predictive and Specialized Modeling*, 2nd ed., SAS Institute Inc., Cary, NC, 2016.

- Schmidt, C. W. (2010). On the relationship of dental microwear to dental macrowear. *American Journal of Physical Anthropology*, 142, 67–73.
- Scott R, Ungar P, Bergstrom T, Brown C, Grine F, Teaford M and Walker A 2005 Dental microwear texture analysis shows within-species diet variability in fossil hominins *Nature* 436 693–5
- Scott RS, Ungar PS, Bergstrom TS, Brown CA, Childs BE, Teaford MF, Walker A. 2006. Dental microwear texture analysis: technical considerations. *J Hum Evol* 51:339–349.
- Scott, Robert S et al. “Dental microwear texture and anthropoid diets.” *American journal of physical anthropology* vol. 147,4 (2012): 551-79. doi:10.1002/ajpa.22007
- Shipman, P. 1981. Applications of scanning electron microscopy to taphonomic problems. *Annals of the New York Academy of Sciences* 376, 357–85.
- Shipman, P. 1983. Early hominid lifestyle: hunting and gathering or foraging and scavenging?, pp. 31–49 in Clutton-Brock, J. and Grigson, C. (eds.), *Animals and Archaeology*, Vol. 1. Oxford: British Archaeological Reports International Series, no. 163.
- Shipman, P. and Rose, J. 1983a. Early hominid hunting, butchering, and carcass-processing behaviors: approaches to the fossil record. *Journal of Anthropological Archaeology* 2(1), 57–98.
- Shipman, P. and Rose, J. 1983b. Evidence of butchery and hominid activities at Torralba and Ambrona: an evaluation using microscopic techniques. *Journal of Archaeological Science* 10(5), 465–74
- Shipman, Pat, and Jennie J. Rose. “Cutmark Mimics on Modern and Fossil Bovid Bones.” *Current Anthropology*, vol. 25, no. 1, 1984, pp. 116–117., <https://doi.org/10.1086/203091>.
- Srivastava, S., Gupta, M. R., & Frigyik, B. A. (2007). Bayesian quadratic discriminant analysis. *Journal of Machine Learning Research*, 8(Jun), 1277-1305.
- Stemp W J, Michael Stemp, UBM Laser Profilometry and Lithic Use-Wear Analysis: A Variable Length Scale Investigation of Surface Topography, *Journal of Archaeological Science*, Volume 28, Issue 1, 2001, Pages 81-88, ISSN 0305-4403, <https://doi.org/10.1006/jasc.2000.0547>.
- Stemp W J and Stemp M 2003 Documenting stages of polish development on experimental stone tools: surface characterization by fractal geometry using UBM laser profilometry *J. Archaeol. Sci.* 30 287–96

- Stemp, W.J., Childs, B.E., Vionnet, S., Brown, C.A., 2008. The quantification of microwear on chipped stone tools: assessing the effectiveness of root mean square roughness (Rq). *Lithic Technol.* 33, 173e189.
- Stemp, W.J., Childs, B.E., Vionnet, S., Brown, C.A., 2009. Quantification and discrimination of lithic use-wear: surface profile measurements and lengthscale fractal analysis. *Archaeometry* 51, 366e382.
- Stemp, W.J., Childs, B.E., Vionnet, S., 2010a. Laser profilometry and length-scale analysis of stone tools: second series experiment results. *Scanning* 32, 233e243.
- Stemp W J, Lerner H J and Kristant E H 2013 Quantifying microwear on experimental Mistassini quartzite scrapers: preliminary results of exploratory research using LSCM and scale-sensitive fractal analysis *Scanning* 35 28–39
- Stemp W J, A review of quantification of lithic use-wear using laser profilometry: a method based on metrology and fractal analysis, *Journal of Archaeological Science*, Volume 48, 2014, Pages 15-25, ISSN 0305 4403, <https://doi.org/10.1016/j.jas.2013.04.027>
- Teaford, M. F., & Walker, A. (1984). Quantitative differences in dental microwear between primate species with different diets and a comment on the presumed diet of *Sivapithecus*. *American Journal of Physical Anthropology*, 64, 191–200.
- Jessica C. Thompson, J. Tyler Faith, Naomi Cleghorn, Jamie Hodgkins, Identifying the accumulator: Making the most of bone surface modification data, *Journal of Archaeological Science*, Volume 85, 2017, Pages 105-113, ISSN 0305-4403, <https://doi.org/10.1016/j.jas.2017.06.013>.
- Tolley, A., Pante, M., Arroyo, A., Torre, I. (2018). A Quantitative Assessment of Percussion-Induced Modification to Bone Surfaces. In: Abstracts of the Paleoanthropology Society 2018 Meeting, Austin, TX, 10–11 April 2018
- Ungar, P.S., Grine, F.E., 1991. Incisor size and wear in *Australopithecus africanus* and *Paranthropus robustus*. *Journal of Human Evolution* 20, 313–340.
- Ungar, P.S., 1994. Incisor microwear of Sumatran anthropoid primates. *American Journal of Physical Anthropology* 94, 339–363
- Ungar, P.S., Brown, C.A., Bergstrom, T.S., Walker, A., 2003. Quantification of Dental Microwear by Tandem Scanning Confocal Microscopy and Scale-Sensitive Fractal Analyses. *Scanning*. 25, 185–193.
- Ungar, Peter & Sponheimer, Matt. (2011). The Diets of Early Hominins. *Science* (New York, N.Y.). 334. 190-3. 10.1126/science.1207701.

- Ungar PS, Berger LR. Brief communication: Dental microwear and diet of *Homo naledi*. *Am J Phys Anthropol*. 2018 May;166(1):228-235. doi: 10.1002/ajpa.23418. Epub 2018 Feb 5. PMID: 29399788.
- Walker AC, Hoeck HN, Perez L: Microwear of mammalian teeth as an indicator of diet. *Science* 201, 808–810 (1978)
- Walker A: Functional anatomy and taphonomy. In *Fossils in the Making*. (Eds. Behrensmeyer AK, Hill AP). University of Chicago, Chicago (1980) 182–196
- Watson, Adam & Gleason, Matthew. (2016). A comparative assessment of texture analysis techniques applied to bone tool use-wear. *Surface Topography: Metrology and Properties*. 4. 024002. 10.1088/2051-672X/4/2/024002.
- Wrangham, Richard. (2017). Control of Fire in the Paleolithic: Evaluating the Cooking Hypothesis. *Current Anthropology*. 58. S000-S000. 10.1086/692113
- Wylie, A. (1985). The Reaction against Analogy. *Advances in Archaeological Method and Theory*, 8, 63–111. <http://www.jstor.org/stable/20170187>
- Yravedra J, Aramendi J, Mate'-Gonza'lez MA', Austin Courtenay L, Gonza'lez-Aguilera D (2018) Differentiating percussion pits and carnivore tooth pits using 3D reconstructions and geometric morphometrics. *PLoS ONE* 13(3): e0194324

## APPENDIX A- TABLE OF EXPERIMENTSL BSM SAMPLE

| Picture | ID          | Bone            | BSM Type | Mark Position             | Location                 |
|---------|-------------|-----------------|----------|---------------------------|--------------------------|
| 1       | CM1         | Femur           | Cutmark  | Anterior Midshaft         | KTBM 2 (KW - 02)         |
| 2       | CM2         | Femur           | Cutmark  | Medial Midshaft           | KTBM 2 (KW - 02)         |
| 3       | CM3 MarkA   | Radius          | Cutmark  | Anterior/Distal           | KTBM 2 (KW - 02)         |
| 3       | CM3 MarkB   | Radius          | Cutmark  | Anterior/Distal           | KTBM 2 (KW - 02)         |
| 3       | CM3 MarkC   | Radius          | Cutmark  | Anterior/Distal           | KTBM 2 (KW - 02)         |
| 4       | CM4         | Ulna            | Cutmark  | Anterior/Proximal         | KTBM 2 (KW - 02)         |
| 5       | CM5         | Humerus         | Cutmark  | Medial/Proximal           | KTBM 2 (KW - 02)         |
| 6       | CM6         | Tibia           | Cutmark  | Medio-proximal midshaft   | KTBM 2 (KW - 02)         |
| 9       | CM9         | Femur           | Cutmark  | Medio - Proximal midshaft | KTBM 2 (KW - 02)         |
| 12      | CM12 MarkA  | Radius          | Cutmark  | Anterior Midshaft         | KTBM 2 (KW - 02)         |
| 12      | CM12 MarkB  | Radius          | Cutmark  | Anterior Midshaft         | KTBM 2 (KW - 02)         |
| 13      | CM13        | Humerus         | Cutmark  | Dorsal and Distal         | KTBM 2 (KW - 02)         |
| 15      | CM15        | Femur           | Cutmark  | Located Medially on Shaft | KPTBM1                   |
| 16      | CM16        | Long Bone Frag. | Cutmark  | NA                        | TLK MA Thesis Cutmarks 2 |
| 17      | CM17 MarkA  | Long Bone Frag. | Cutmark  | NA                        | TLK MA Thesis Cutmarks 2 |
| 17      | CM17 MarkB  | Long Bone Frag. | Cutmark  | NA                        | TLK MA Thesis Cutmarks 2 |
| 17      | CM17 MarkC  | Long Bone Frag. | Cutmark  | NA                        | TLK MA Thesis Cutmarks 2 |
| 18      | CM18        | Long Bone Frag. | Cutmark  | NA                        | TLK MA Thesis Cutmarks 2 |
| 19      | CM19 MarkA  | Long Bone Frag. | Cutmark  | NA                        | TLK MA Thesis Cutmarks 2 |
| 19      | CM19 MarkB  | Long Bone Frag. | Cutmark  | NA                        | TLK MA Thesis Cutmarks 2 |
| 20      | CM20 MarkA  | Long Bone Frag. | Cutmark  | NA                        | TLK MA Thesis Cutmarks 2 |
| 20      | CM20 MarkB  | Long Bone Frag. | Cutmark  | NA                        | TLK MA Thesis Cutmarks 2 |
| 20      | CM20 MarkC  | Long Bone Frag. | Cutmark  | NA                        | TLK MA Thesis Cutmarks 2 |
| 21      | CM21        | Long Bone Frag. | Cutmark  | NA                        | TLK MA Thesis Cutmarks 2 |
| 25      | CM25        | Long Bone Frag. | Cutmark  | NA                        | TLK MA Thesis Cutmarks 2 |
| 29.5    | TRM4 MarkA  | Long Bone Frag. | Trample  | NA                        | ERO-R1                   |
| 29.5    | TRM4 MarkB  | Long Bone Frag. | Trample  | NA                        | ERO-R1                   |
| 29      | TRM4 MarkC  | Long Bone Frag. | Trample  | NA                        | ERO Sand 13 - 34         |
| 30      | TRM5 MarkA  | Long Bone Frag. | Trample  | NA                        | ERO Sand 13 - 34         |
| 30      | TRM5 MarkB  | Long Bone Frag. | Trample  | NA                        | ERO Sand 13 - 34         |
| 32      | TRM7 MarkA  | Long Bone Frag. | Trample  | NA                        | ERO Sand 13 - 34         |
| 32      | TRM7 MarkB  | Long Bone Frag. | Trample  | NA                        | ERO Sand 13 - 34         |
| 32      | TRM7 MarkC  | Long Bone Frag. | Trample  | NA                        | ERO Sand 13 - 34         |
| 34      | TRM9 MarkA  | Long Bone Frag. | Trample  | NA                        | ERO Sand 13 - 34         |
| 34      | TRM9 MarkB  | Long Bone Frag. | Trample  | NA                        | ERO Sand 13 - 34         |
| 34      | TRM9 Mark C | Long Bone Frag. | Trample  | NA                        | ERO Sand 13 - 34         |

|      |             |                 |            |                              |                 |
|------|-------------|-----------------|------------|------------------------------|-----------------|
| 38   | TRM13 MarkA | Long Bone Frag. | Trample    | NA                           | ERO Gravel 12   |
| 38   | TRM13 MarkB | Long Bone Frag. | Trample    | NA                           | ERO Gravel 12   |
| 39   | TRM14 MarkA | Long Bone Frag. | Trample    | NA                           | ERO Gravel 12   |
| 39   | TRM14 MarkB | Long Bone Frag. | Trample    | NA                           | ERO Gravel 12   |
| 40   | TRM15 MarkA | Long Bone Frag. | Trample    | NA                           | ERO Gravel 12   |
| 40.5 | TRM15 MarkB | Long Bone Frag. | Trample    | NA                           | ERO-R1          |
| 43   | TRM18 MarkA | Long Bone Frag. | Trample    | NA                           | ERO-R1          |
| 43   | TRM18 MarkB | Long Bone Frag. | Trample    | NA                           | ERO-R1          |
| 43   | TRM18 MarkC | Long Bone Frag. | Trample    | NA                           | ERO-R1          |
| 44   | TRM19       | Long Bone Frag. | Trample    | NA                           | ERO-R1          |
| 45   | TRM20       | Long Bone Frag. | Trample    | NA                           | ERO Gravel 12   |
| 47   | TRM22       | Long Bone Frag. | Trample    | NA                           | ERO Gravel 12   |
| 48   | TRM22       | Long Bone Frag. | Trample    | NA                           | ERO-R1          |
| 50   | TRM25       | Long Bone Frag. | Trample    | NA                           | ERO R1          |
| 53   | TOM3 MarkA  | Humerus         | Toothmark  | Anterior Midshaft            | MVM SHTM        |
| 53   | TOM3 MarkB  | Humerus         | Toothmark  | Anterior Midshaft            | MVM SHTM        |
| 54   | TOM4        | Femur           | Toothmark  | Anterior Midshaft            | MVM SHTM        |
| 55   | TOM5 MarkA  | Long Bone Frag. | Toothmark  | NA                           | MVM SHTM        |
| 55   | TOM5 MarkB  | Long Bone Frag. | Toothmark  | NA                           | MVM SHTM        |
| 55   | TOM5 MarkC  | Long Bone Frag. | Toothmark  | NA                           | MVM SHTM        |
| 62   | TOM12       | Humerus         | Toothmark  | Face of Humeral Head         | MG Wolf         |
| 63   | TOM13       | Humerus         | Toothmark  | Anterior/ Proximal Epiohyses | MG Wolf         |
| 64   | TOM14 MarkA | Rib             | Toothmark  | Dorsal/Distal Surface        | MG Wolf         |
| 64   | TOM14 MarkB | Rib             | Toothmark  | Dorsal/Distal Surface        | MG Wolf         |
| 65   | TOM15       | Rib             | Toothmark  | Anterior/Distal              | MG Wolf         |
| 67   | TOM17 MarkA | Rib             | Toothmark  | Dorsal/Distal Surface        | MG Wolf         |
| 67   | TOM17 MarkB | Rib             | Toothmark  | Dorsal/Distal Surface        | MG Wolf         |
| 67   | TOM17 MarkC | Rib             | Toothmark  | Dorsal/Distal Surface        | MG Wolf         |
| 68   | TOM18       | Rib             | Toothmark  | Anterior/Distal              | MG Wolf         |
| 69   | TOM19       | Rib             | Toothmark  | Dorsal/Medial                | MG Wolf         |
| 70   | TOM20 MarkA | Rib             | Toothmark  | Anterior face/ Medial        | MG Wolf         |
| 70   | TOM20 MarkB | Rib             | Toothmark  | Anterior face/ Medial        | MG Wolf         |
| 70   | TOM20 MarkC | Rib             | Toothmark  | Anterior face/ Medial        | MG Wolf         |
| 71   | TOM21       | Rib             | Toothmark  | Anterior/Distal              | MG Wolf         |
| 74   | TOM24 MarkA | Rib Frag.       | Toothmark  | Dorsal Face                  | MG Wolf         |
| 74   | TOM24 MarkB | Rib Frag.       | Toothmark  | Dorsal Face                  | MG Wolf         |
| 75   | TOM25       | Rib Frag.       | Toothmark  | NA                           | MG Wolf         |
| 75   | TOM25       | Rib Frag.       | Toothmark  | NA                           | MG Wolf         |
| 75   | TOM25       | Rib Frag.       | Toothmark  | NA                           | MG Wolf         |
| 76   | PM1         | Long Bone Frag. | Percussion | NA                           | AMT 35 - L6, L7 |
| 77   | PM2 MarkA   | Long Bone Frag. | Percussion | Anterior face/ Near Head     | AMT 35 - L6, L7 |

|    |            |                 |            |                          |                |
|----|------------|-----------------|------------|--------------------------|----------------|
| 77 | PM2 MarkB  | Long Bone Frag. | Percussion | Anterior face/ Near Head | AMT 35 - L6,L7 |
| 80 | PM5        | Long Bone Frag. | Percussion | NA                       | AMT 37 - 6     |
| 82 | PM7 MarkA  | Long Bone Frag. | Percussion | NA                       | AMT 35 - L6,L7 |
| 82 | PM7 MarkB  | Long Bone Frag. | Percussion | NA                       | AMT 35 - L6,L7 |
| 84 | PM9 MarkA  | Long Bone Frag. | Percussion | NA                       | AMT 37 - L6    |
| 84 | PM9 MarkB  | Long Bone Frag. | Percussion | NA                       | AMT 37 - L6    |
| 84 | PM9 MarkC  | Long Bone Frag. | Percussion | NA                       | AMT 37 - L6    |
| 86 | PM11 MarkA | Long Bone Frag. | Percussion | NA                       | AMT 35 - 3     |
| 86 | PM11 MarkC | Long Bone Frag. | Percussion | NA                       | AMT 35 - 3     |
| 87 | PM12       | Long Bone Frag. | Percussion | NA                       | AMT 37 - L3,L4 |
| 88 | PM13 MarkA | Long Bone Frag. | Percussion | Anterior Midshaft        | AMT 37 - L3,L4 |
| 88 | PM13 MarkB | Long Bone Frag. | Percussion | Anterior Midshaft        | AMT 37 - L3,L4 |
| 88 | PM13 MarkC | Long Bone Frag. | Percussion | Anterior Midshaft        | AMT 37 - L3,L4 |
| 90 | PM15       | Long Bone Frag. | Percussion | NA                       | AMT 37 - L3,L4 |
| 91 | PM16       | Long Bone Frag. | Percussion | Anterior Midshaft        | AMT 35 - L5    |
| 92 | PM17       | Long Bone Frag. | Percussion | NA                       | AMT 35 - L5    |
| 93 | PM18 MarkA | Long Bone Frag. | Percussion | NA                       | AMT 35 - L5    |
| 93 | PM18 MarkB | Long Bone Frag. | Percussion | NA                       | AMT 35 - L5    |
| 94 | PM19       | Long Bone Frag. | Percussion | NA                       | AMT 35 - L5    |
| 96 | PM21 MarkA | Long Bone Frag. | Percussion | NA                       | AMT 37 - L5    |
| 96 | PM21 MarkC | Long Bone Frag. | Percussion | NA                       | AMT 37 - L5    |
| 98 | PM23 MarkA | Long Bone Frag. | Percussion | Along fracture Edge      | AMT 35 - L3    |
| 98 | PM23 MarkB | Long Bone Frag. | Percussion | Along fracture Edge      | AMT 35 - L3    |

**APPENDIX B - HISTOGRAM DISTRIBUTIONS OF UNIVARIATE BSM DATA**

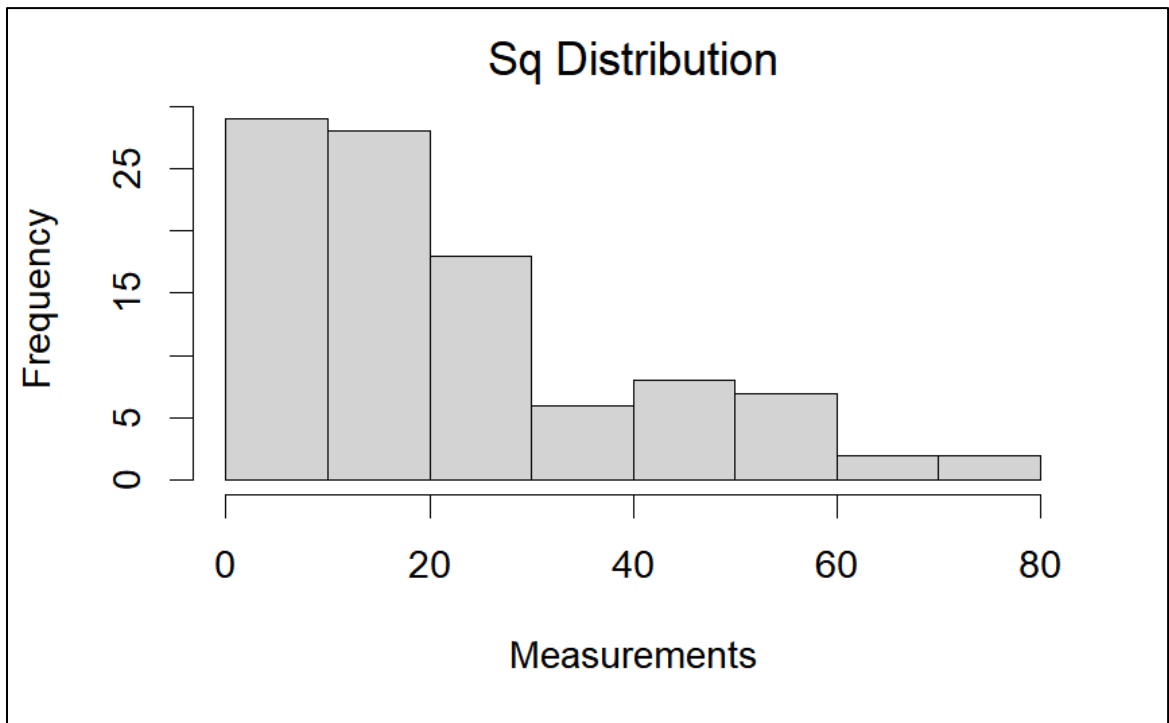


**Figure B.1)** Histogram of Sq measurements across all BSM types.

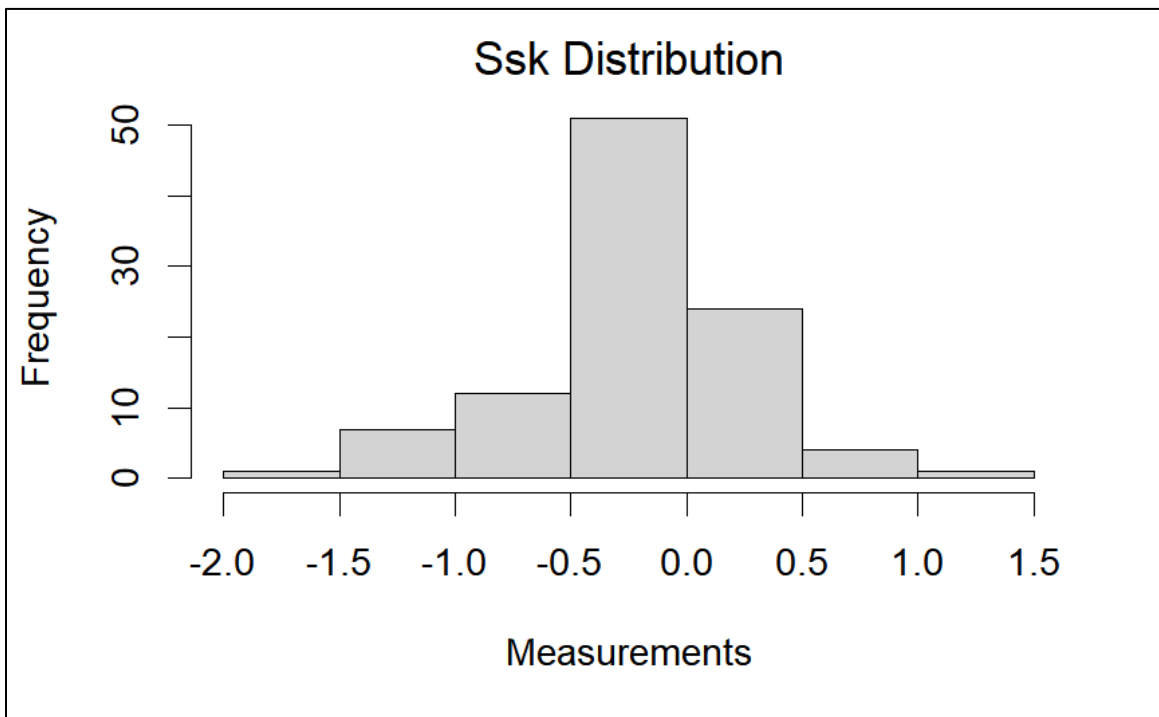


**Figure B.2)** Histogram of Ssk measurements across all BSM types.

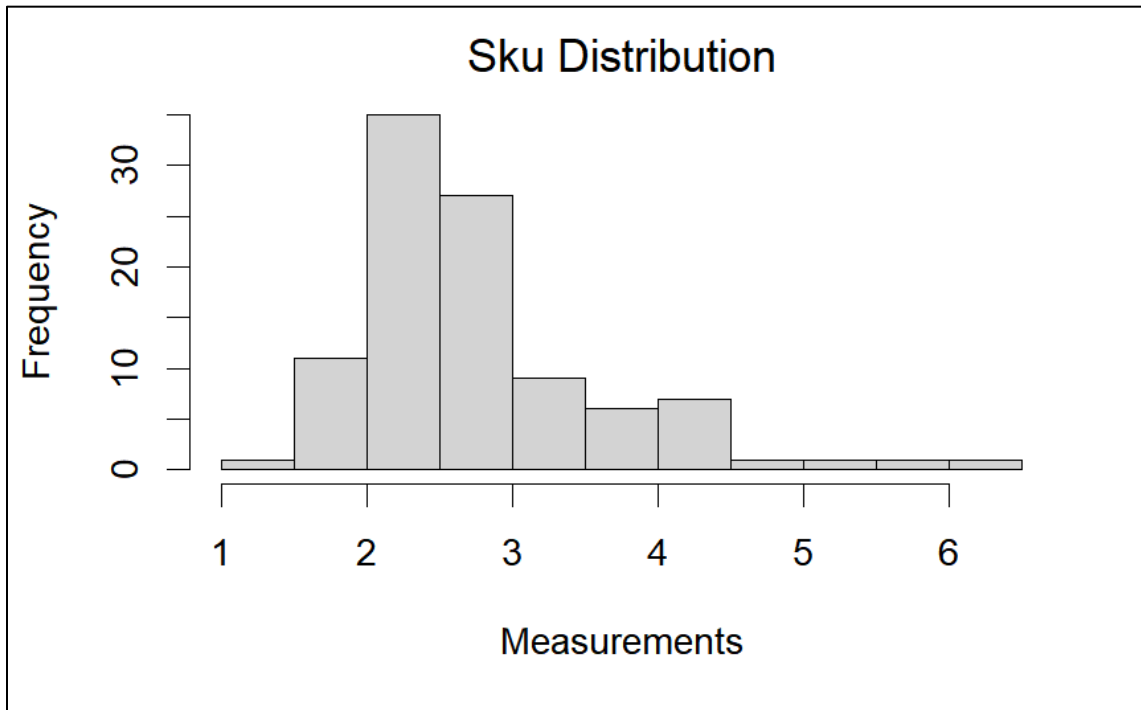


**Figure B.3)** Histogram of Sku measurements across all BSM types.

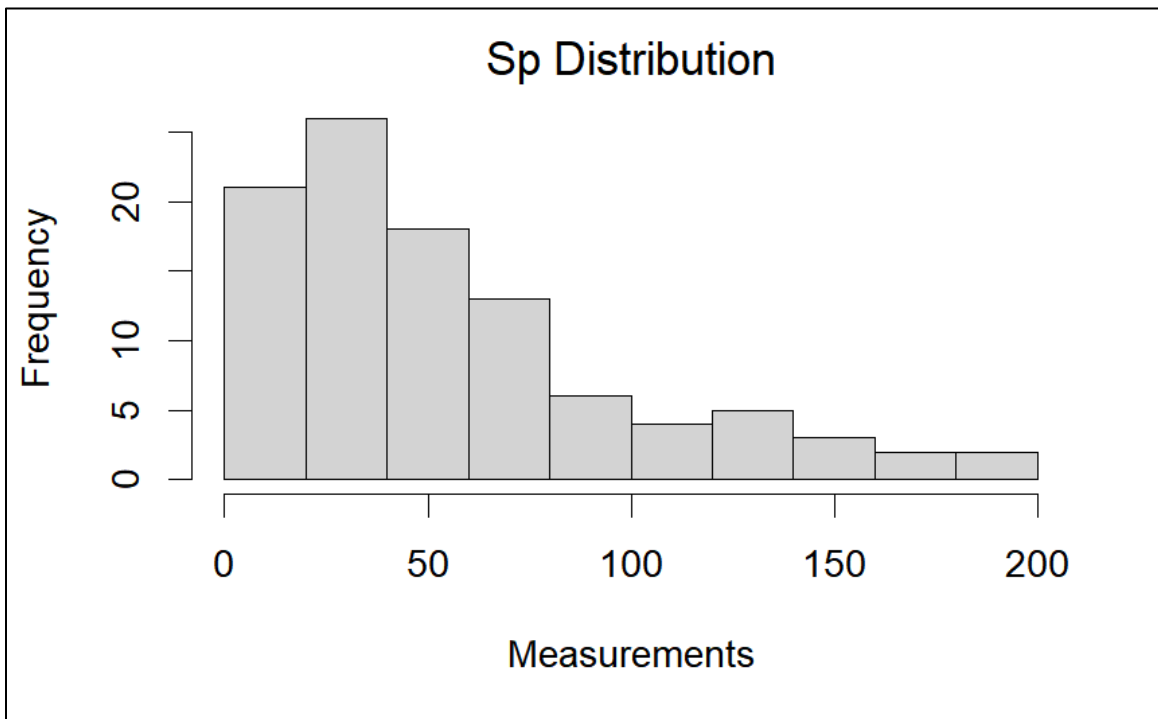


**Figure B.4)** Histogram of Sp measurements across all BSM types.

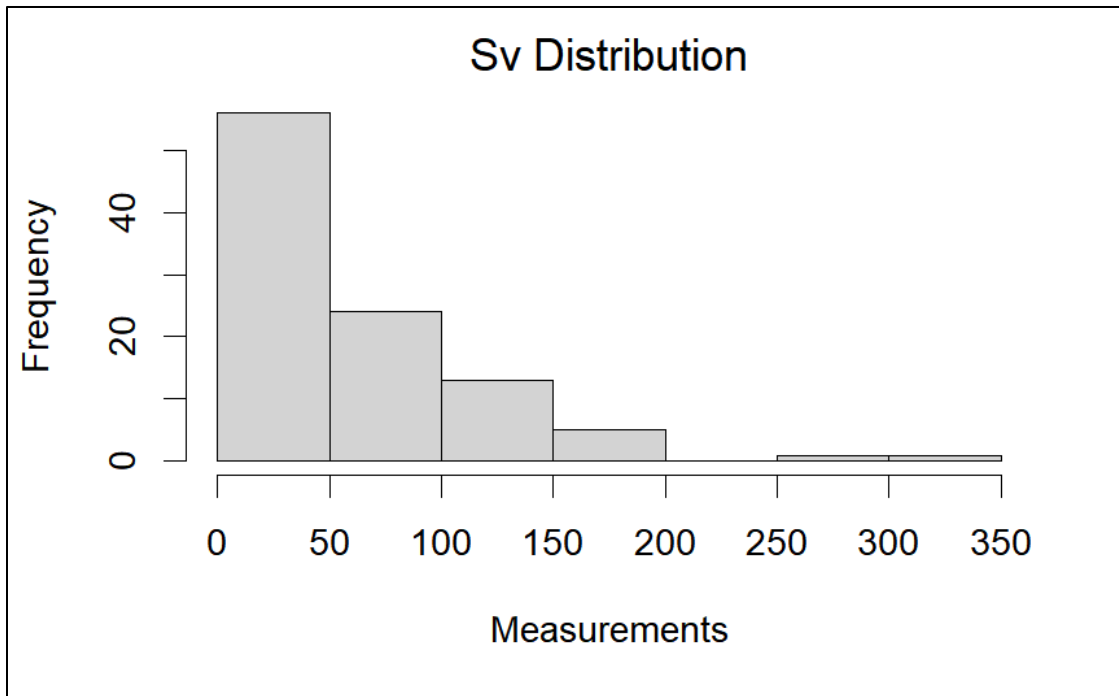


**Figure B.5)** Histogram of Sv measurements across all BSM types.

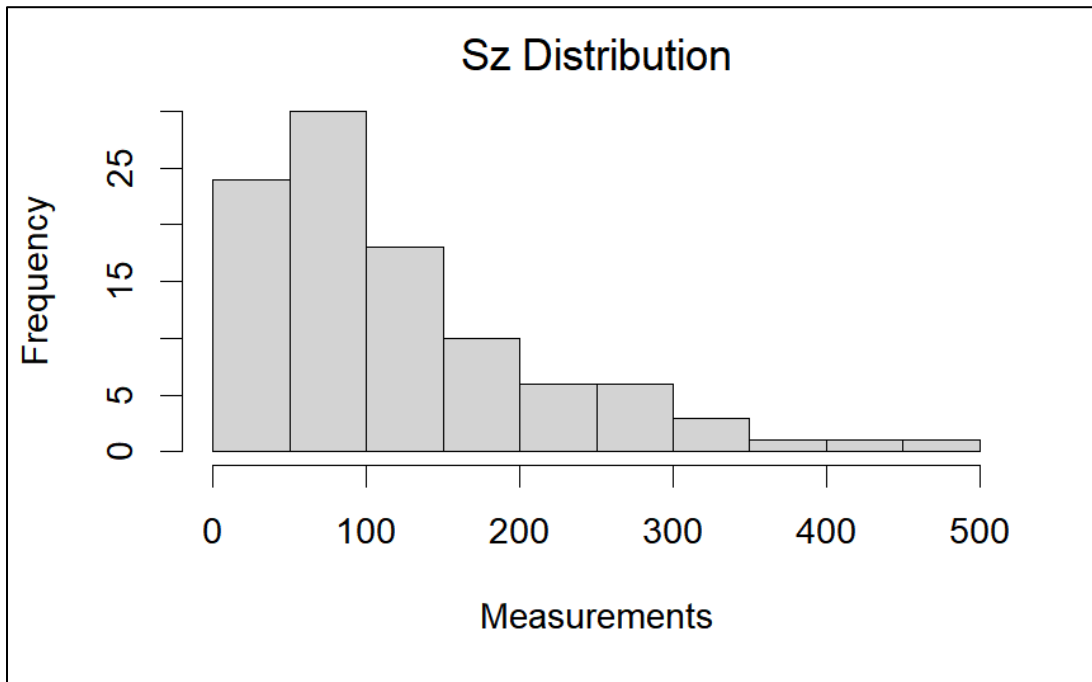


**Figure B.6)** Histogram of Sz measurements across all BSM types.

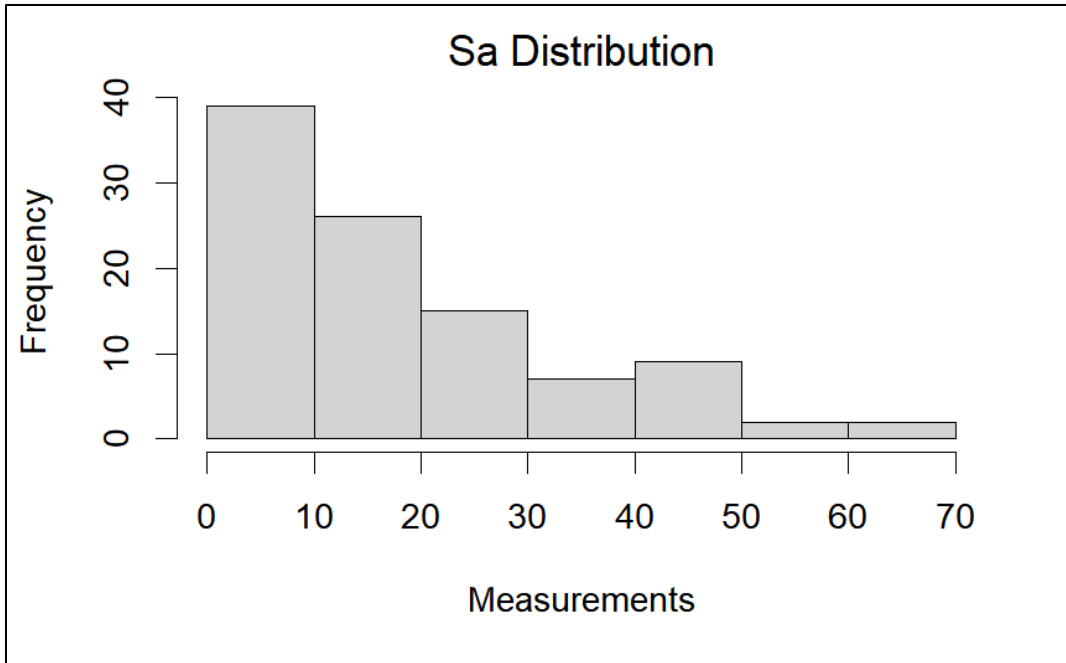


**Figure B.7)** Histogram of Sa measurements across all BSM types.

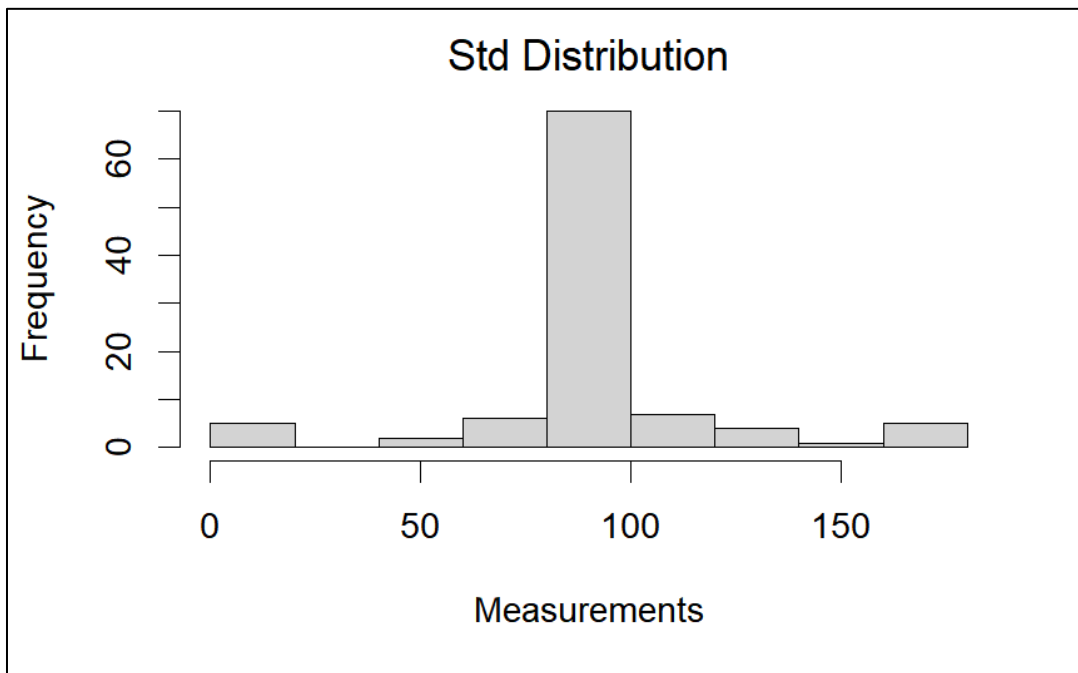


**Figure B.8)** Histogram of Std measurements across all BSM types.

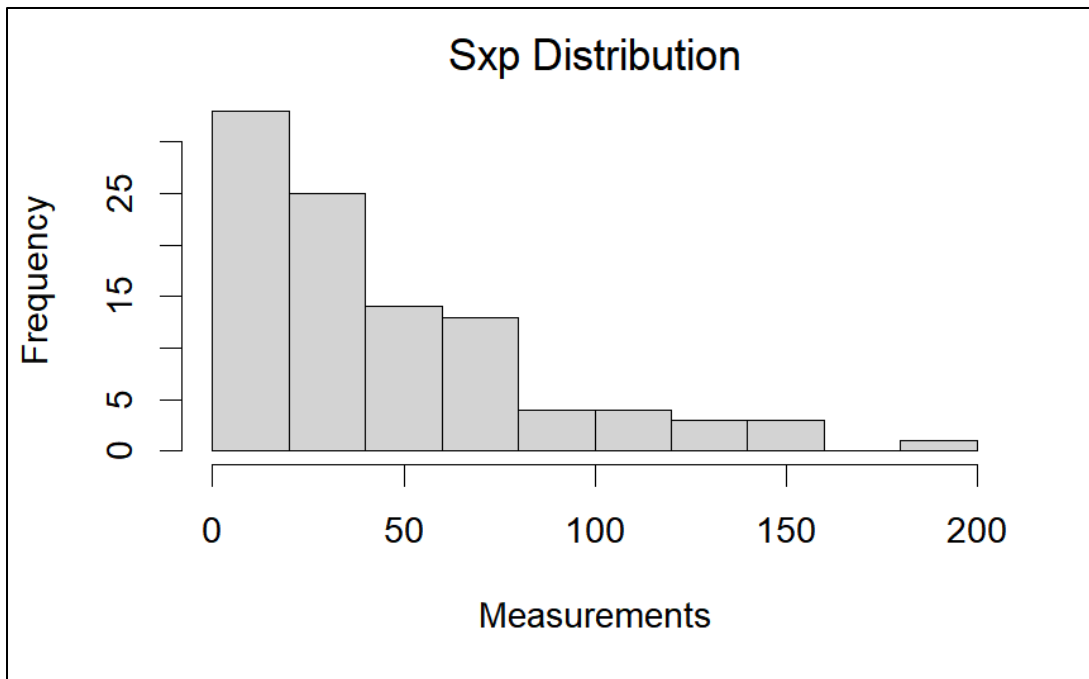


**Figure B.9)** Histogram of Sxp measurements across all BSM types.

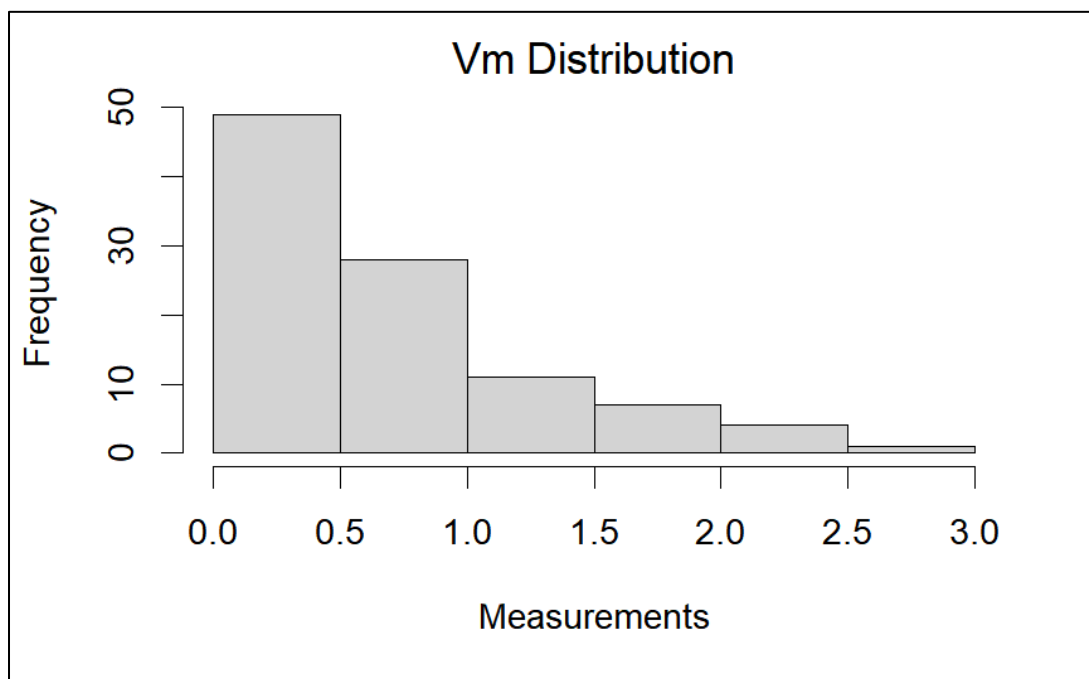


**Figure B.10)** Histogram of Vm measurements across all BSM types.

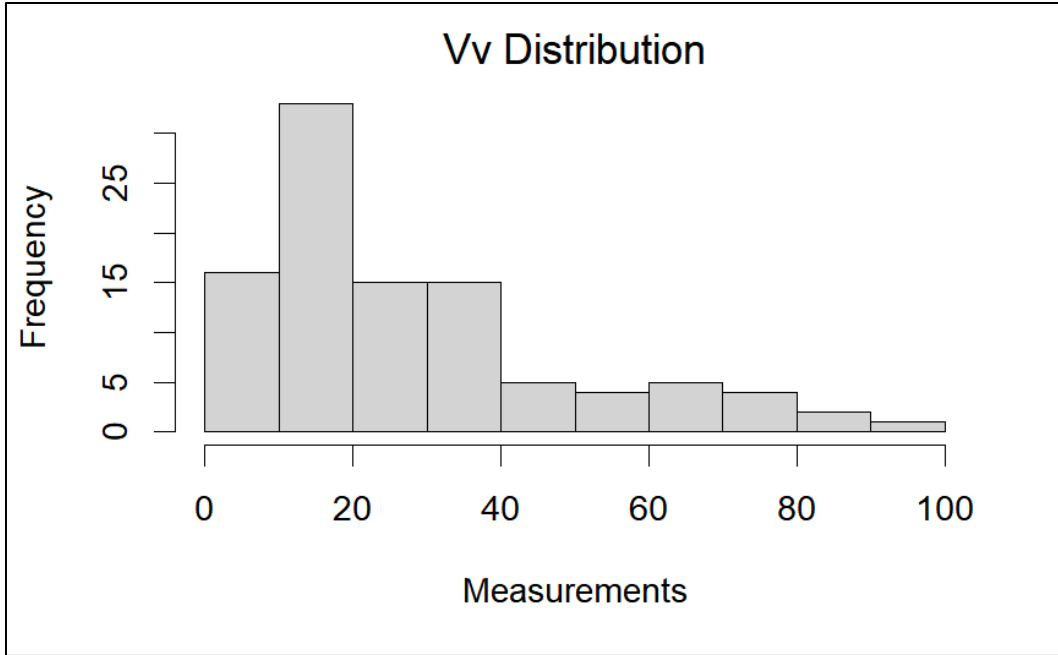


**Figure B.11)** Histogram of Vv measurements across all BSM types.

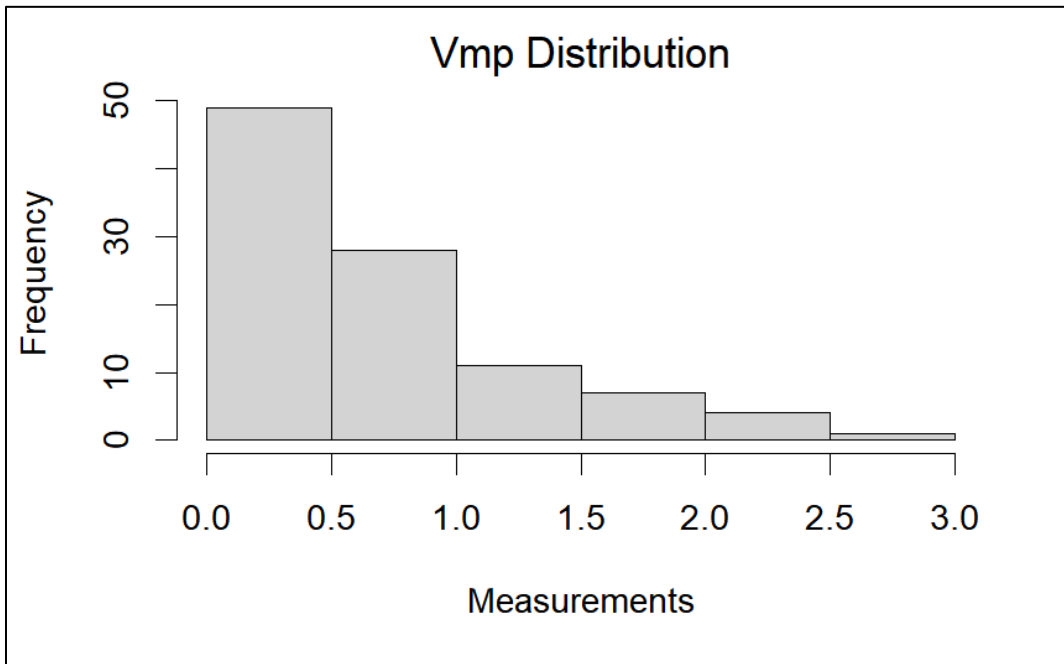


**Figure B.12)** Histogram of Vmp measurements across all BSM types.

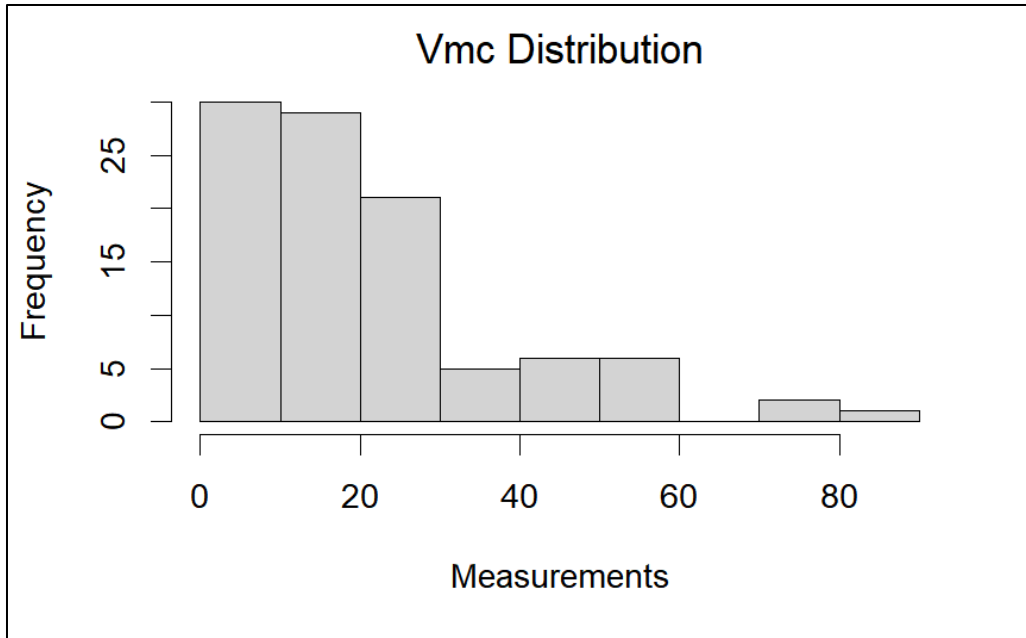


**Figure B.13)** Histogram of Vmc measurements across all BSM types.

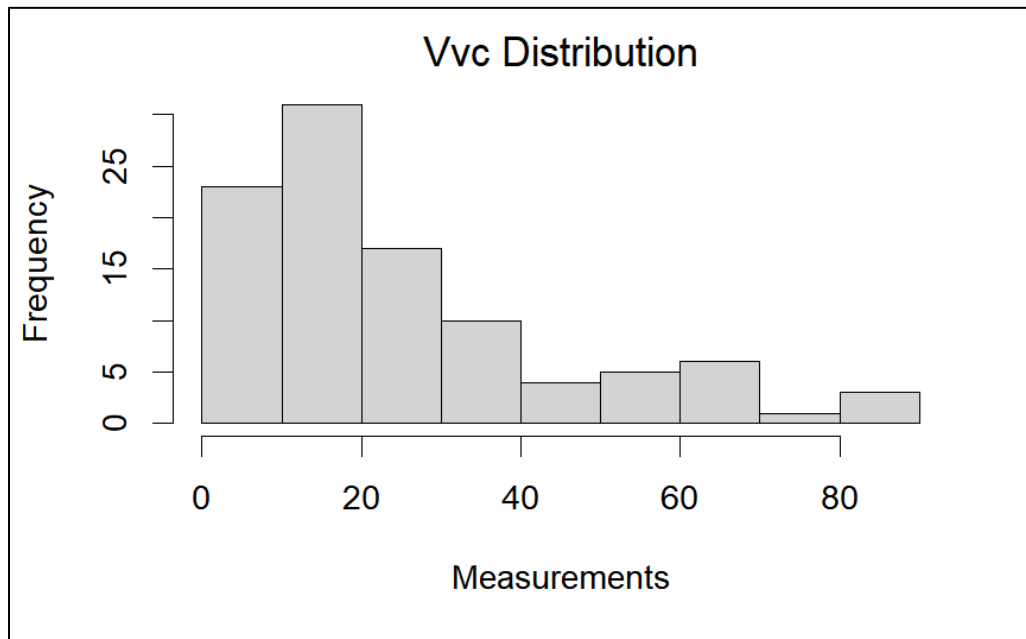


**Figure B.14)** Histogram of Vvc measurements across all BSM types.

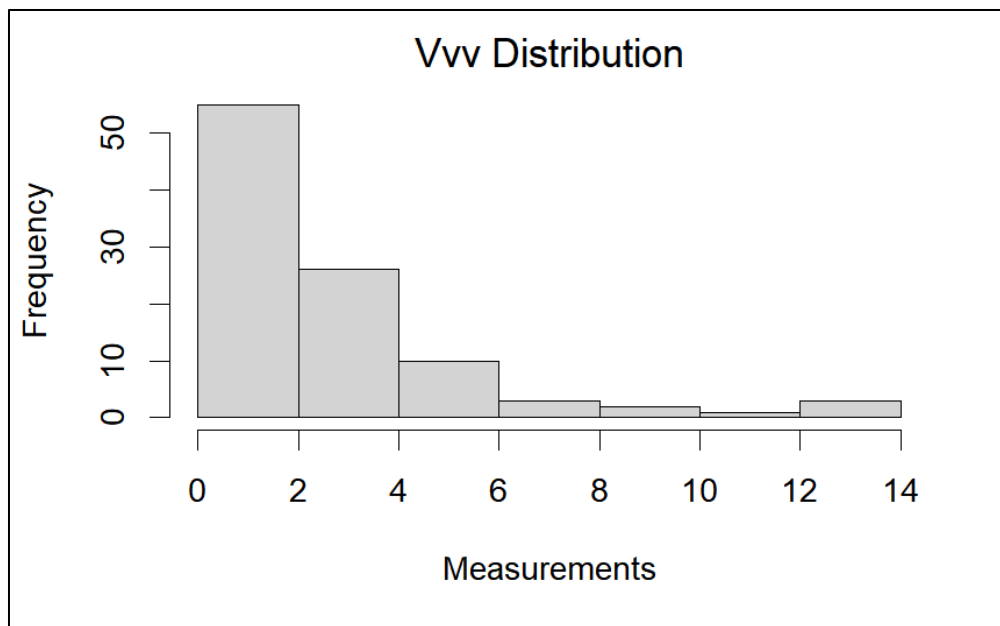


**Figure B.15)** Histogram of Vv measurements across all BSM types.

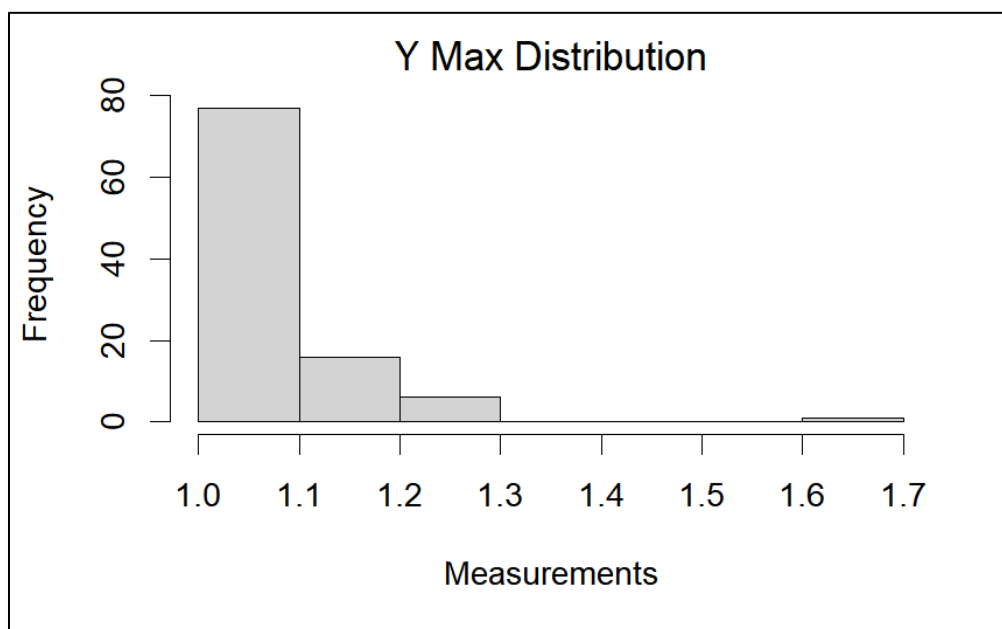


**Figure B.16)** Histogram of Y Max measurements across all BSM types.

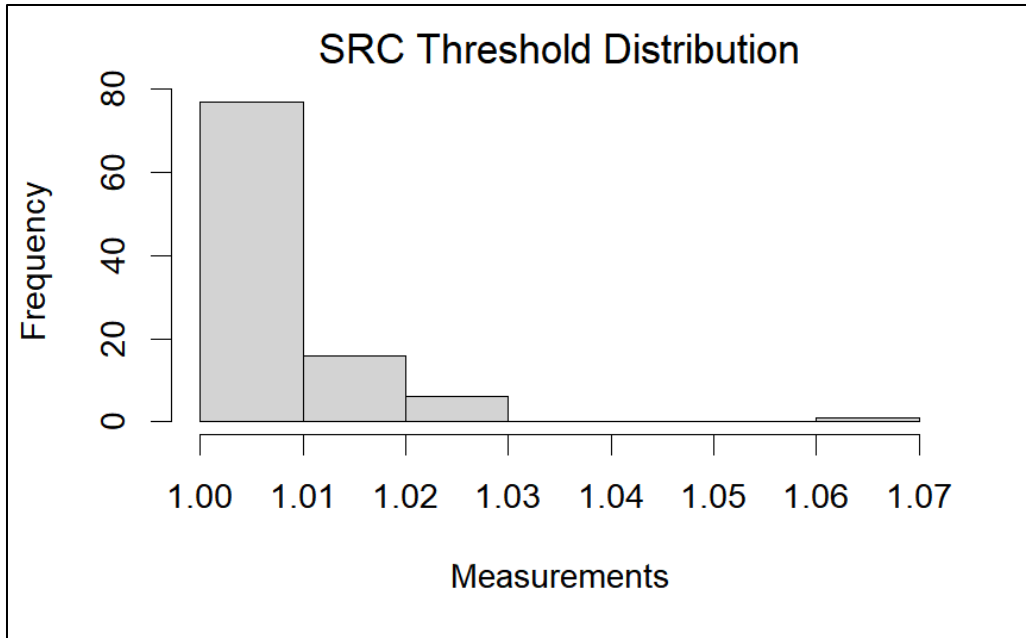


**Figure B.17)** Histogram of SRC Threshold measurements across all BSM types.

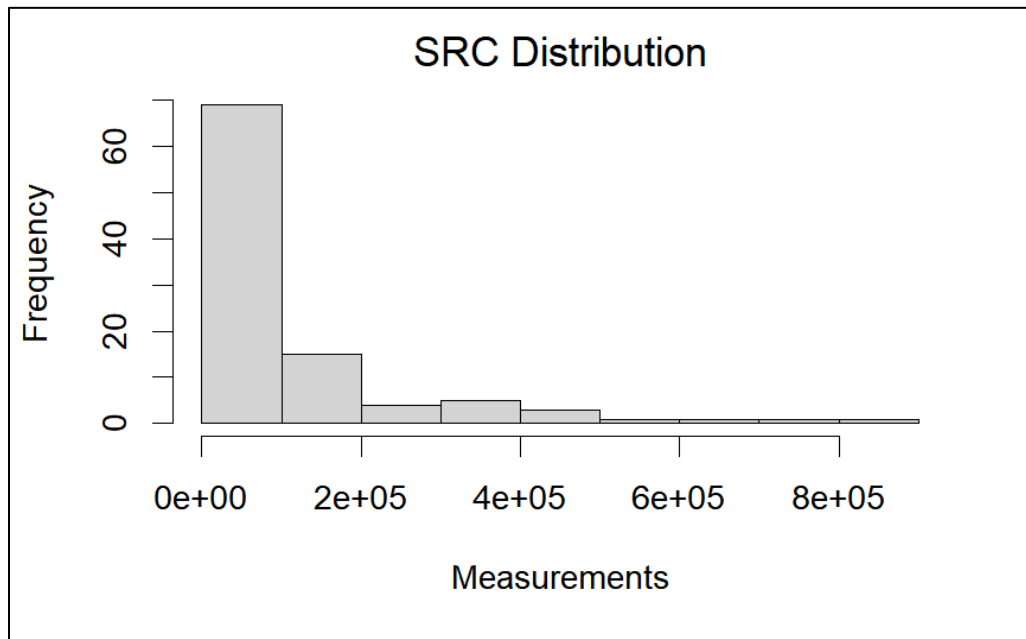


**Figure B.18)** Histogram of SRC measurements across all BSM types.

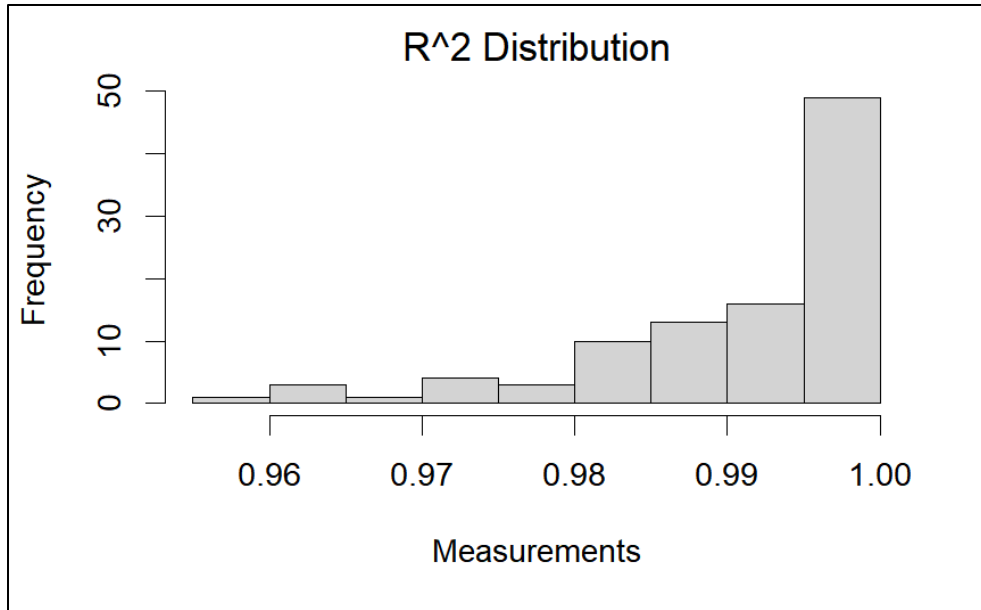


**Figure B.19)** Histogram of R-Squared measurements across all BSM types.

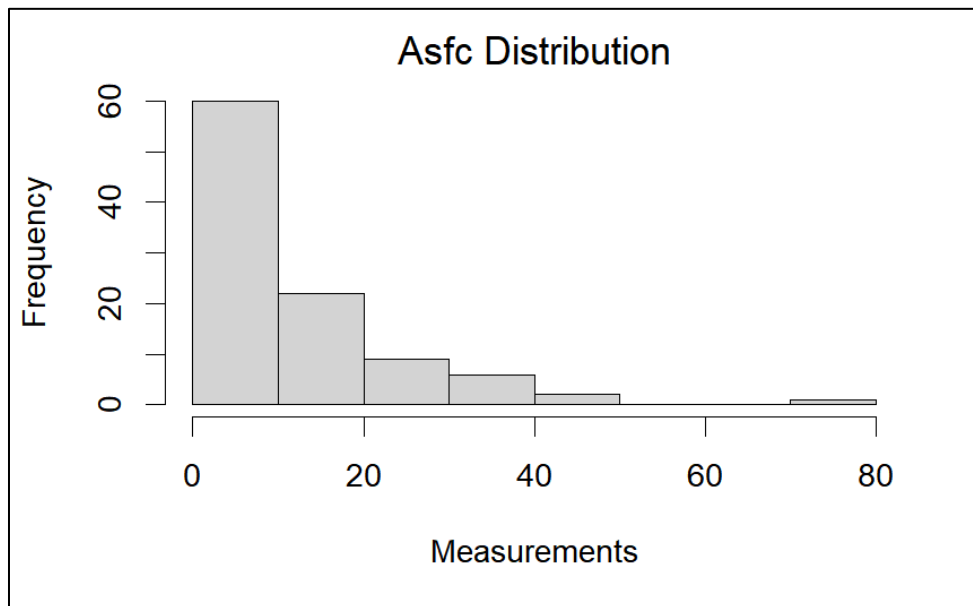


**Figure B.20)** Histogram of Asfc measurements across all BSM types.

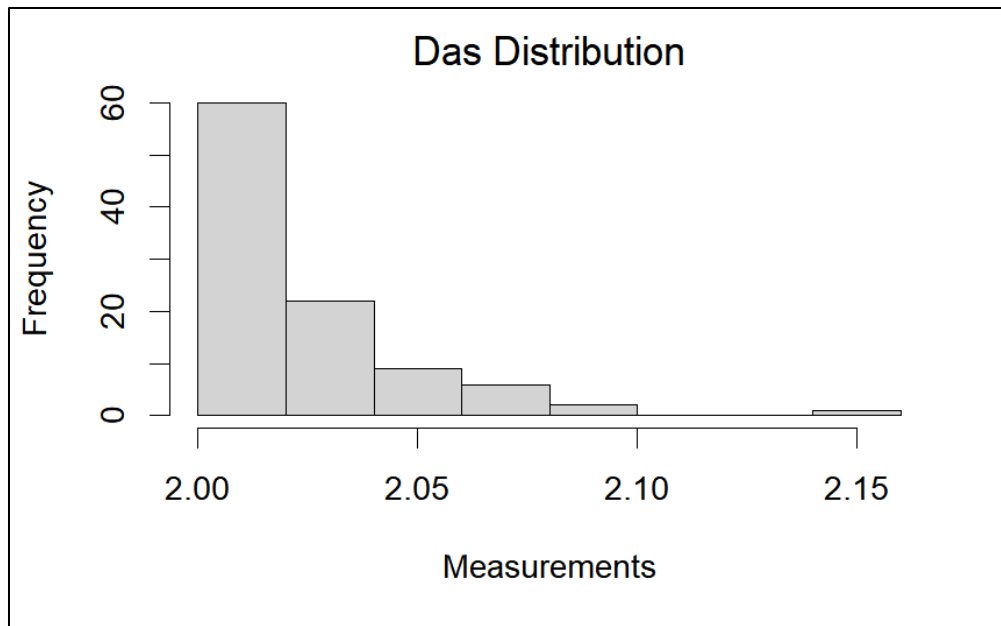


**Figure B.21)** Histogram of Das measurements across all BSM types.

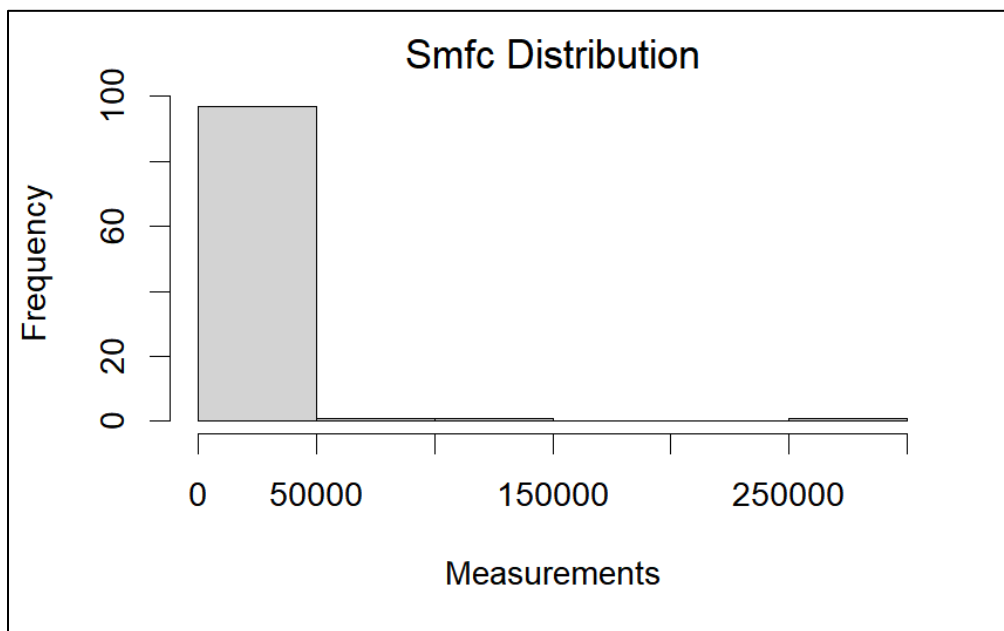


**Figure B.22)** Histogram of Smfc measurements across all BSM types.

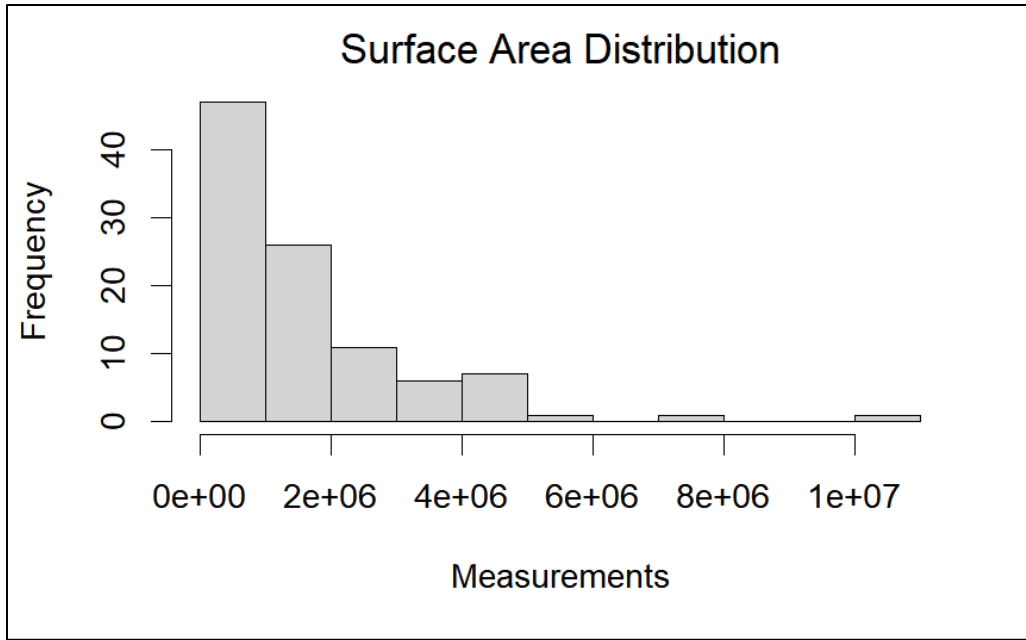


**Figure B.23)** Histogram of Surface Area (3D) measurements across all BSM types.

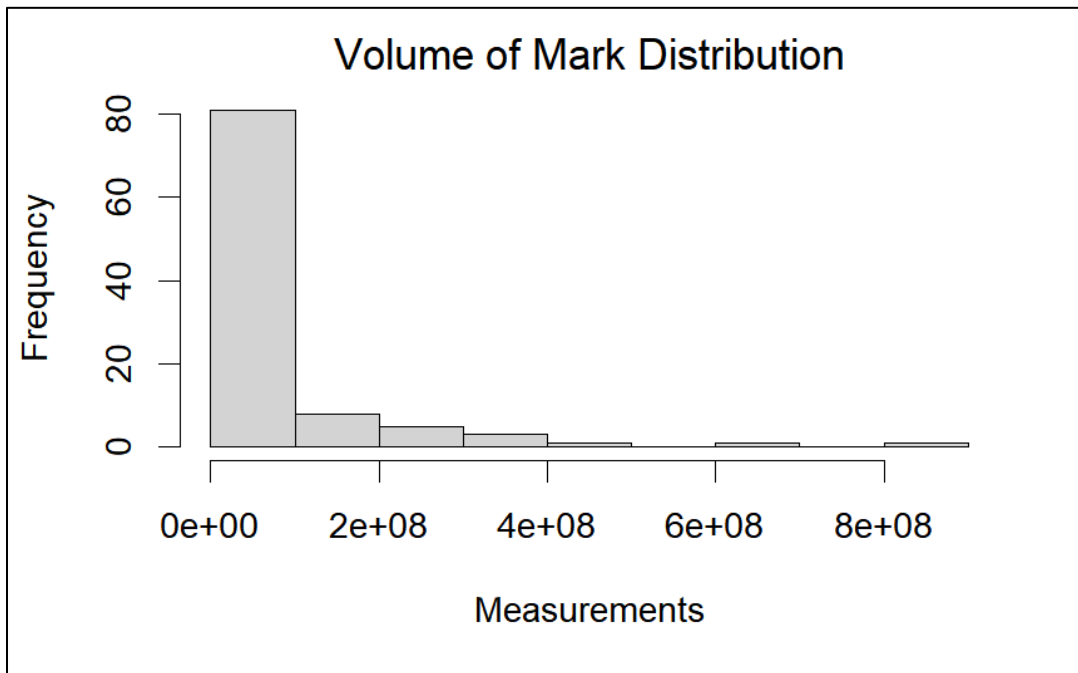


**Figure B.24)** Histogram of Volume of Mark (3D) measurements across all BSM types.

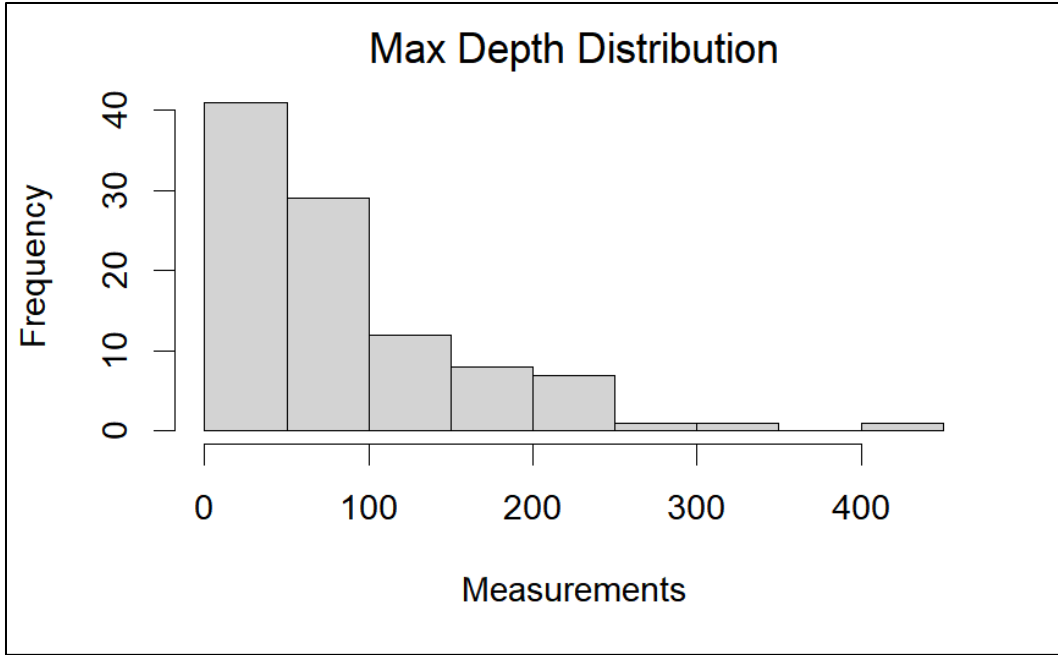


**Figure B.25)** Histogram of Max Depth (3D) measurements across all BSM types.

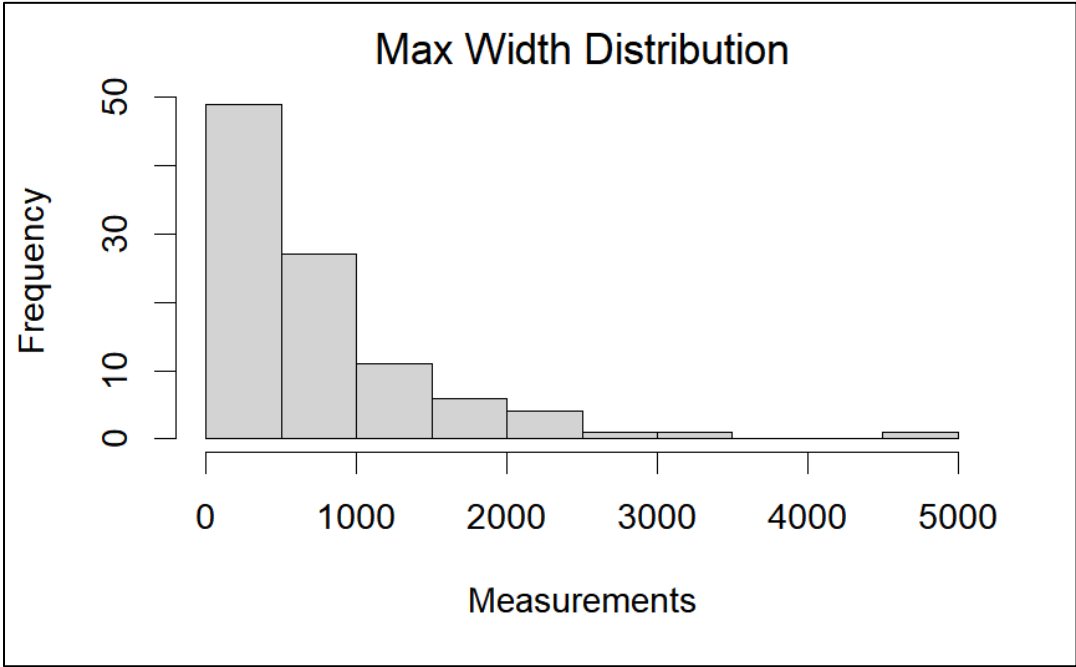


**Figure B.26)** Histogram of Max Width (3D) measurements across all BSM types.

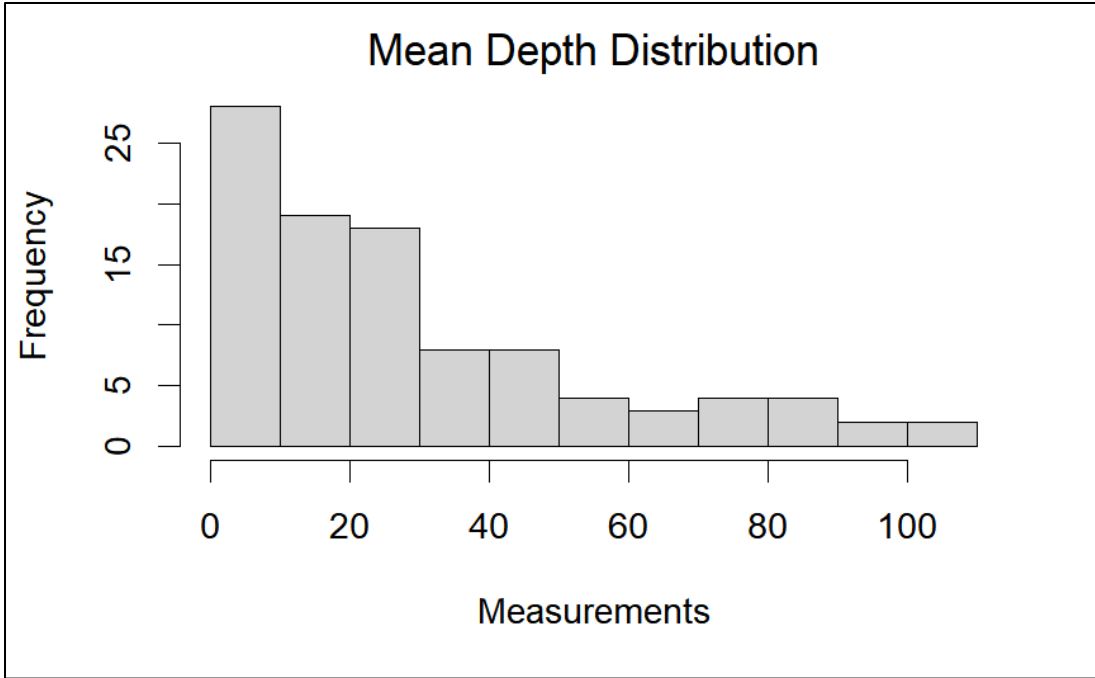


**Figure B.27)** Histogram of Mean Depth (3D) measurements across all BSM types.

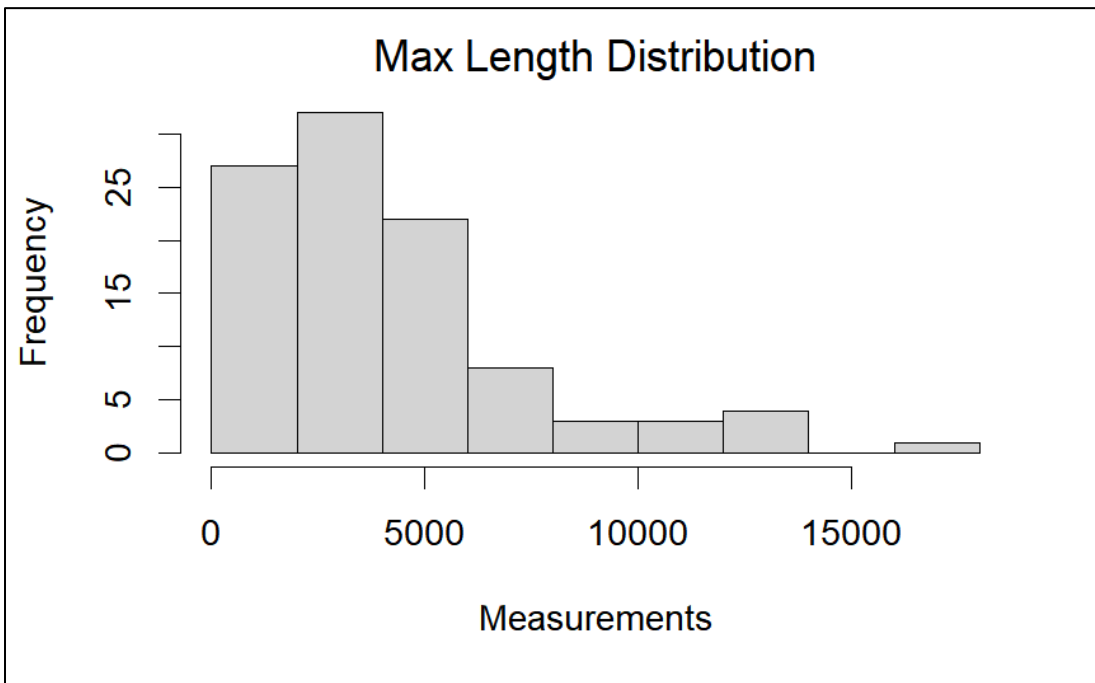


**Figure B.28)** Histogram of Max Length (3D) measurements across all BSM types.